Marine Research Institute. Report no. 108

SATELLITE ALTIMETRY AND CIRCULATION IN THE DENMARK STRAIT AND ADJACENT SEAS

John MORTENSEN

Department of Geophysics
Niels Bohr Institute
University of Copenhagen

___

Marine Research Institute
Reykjavík, Iceland

Reykjavík 2004

PREFACE

This publication on Satellite Altimetry and Circulation in the Denmark Strait and adjacent Seas by John Mortensen is based on a revised version of his Ph.D. Thesis from the Niels Bohr Institute at the University of Copenhagen 1997. The supervisor was Professor Carl Christian Tschern-ing. The present representation is revised with respect to notes by referees as the thesis was forwarded to be published in Rit Fiskideildar of the Marine Research Institute in Reykjavík. As this series is not anymore to be continued it was decided to publish the thesis in another publication of the Marine Research Institute, Hafrannsóknastofnunin, Fjölrit. As mentioned above, attention was paid to remarks by referees both as regards length and content. The thesis includes valuable information on both new techniques as satellite altimetry in oceanographic research as well as on modelling of ocean circulation in Icelandic and near-by waters. The presentation is based on two updated manuscripts by John Mortensen with some necessary editorial amendments in structure of text, figures and references.

A historical and traditional background of Danish Research in Iceland and Icelandic waters is their excellent work on geodesy and hydrography in the 18^{th}, 19^{th} and into the 20^{th} century. Thus it was of an utmost great pleasure to experience further investigations were geodesy and hydrography in Icelandic waters were considered together by a Danish scientist. Dr. John Mortensen was involved in oceanographic work at the Marine Research Institute in Reykjavík for some years both on behalf of the Institute prior to 1997 as well as the EU-MAST project VEINS in the years 1997-2000. Sincere thanks are forwarded to Dr. John Mortensen for his valuable work at the Institute and his kind appearance.

Eiríkur Þ. Einarsson, the librarian at the Marine Research Institute, Reykjavík, and the secretaries Eydís Cartwright and Sigurborg Jóhanns-dóttir helped by preparing the manuscript for printing.

Svend-Aage Malmberg
Editor

Contents

ABSTRACT

In this paper, ocean circulation derived by using measurements obtained from the European Remote Sensing satellite ERS-1, was investigated. Focus was placed in the Denmark Strait and adjacent Seas ($59°N<\varphi<71°N$, $10°W<\lambda<45°W$), including part of the Iceland Sea to the north, the Irminger Sea and part of the Iceland Basin to the south. ERS-1 derived 35 days mean dynamic topography relative to the best available geoid model of the region, GGEOID93B, was compared with different kinds of in situ measurements. The altimetric solution using the geostrophic assumption shows its capability of reproducing many of the observed surface current features in the region, and is in remarkable agreement with recent near surface drifter results. The altimetry even shows evidence of a cyclonic circulation in the Iceland Basin just south of Iceland which has lately been indicated in a schematic circulation pattern of the northern North Atlantic. However, unsolved problems associated with the north Icelandic shelf and the high velocities observed in the East Greenland Current still exist.

In order to increase the knowledge of the circulation and transports in the layers below the surface layer, state-of-the-art experiments were conducted integrating dynamic heights derived from altimetry at open lateral boundaries in the limited area model MIKE 3. MIKE 3 is a non-hydrostatic primitive equation model set up with a 50×60×20 grid with a resolution of 20 km horizontally and 50 m vertically. The resolution is sufficient to resolve mesoscale topographic structures, which are known to be of importance in controlling the circulation of the region. During the numerical experiments, improved temperature and salinity fields were used. The experiments show reasonable agreement with observations in the East Greenland Current and Iceland Sea. They indicate that the Denmark Strait Overflow is influenced by far-field barotropic currents. However, the experiments also show that many unresolved modelling issues still remain which may be a consequence of both poorly known parameters and the initialization of the model. In particular the integration of open lateral boundary conditions which makes use of sea surface elevations needs further investigation.

INTRODUCTION

The northern North Atlantic plays a key role in determining long-term changes in the climate system (Sy *et al.*, 1992), through its northward transport of heat and subsequent formation of intermediate and deep water masses due to heat loss to the atmosphere. Our present knowledge of the North Atlantic Ocean circulation can be characterized as a mosaic composed of a lot of bricks, which over the last few decades have been gathered in combination within numerical ocean circulation models. This combination has improved our understanding of its circulation but it still lacks to a high degree both spatial and temporal resolution in describing the flow field.

With the introduction of measurements of the sea surface from space, a number of parameters are now obtained on routinely basis which have a high spatial and temporal resolution. A relatively new field, which has experienced an enormous progress in recent years, is satellite radar altimetry. The first altimeter was launched with Skylab as early as 1973. Since then both instruments, computers and satellite tracking systems technology have developed rapidly, especially in most recent years. Consequently with the present accuracy of altimetric products delivered by e.g. TOPEX/POSEIDON or ERS-1/ERS-2 (ESRIN, 1992; Knudsen *et al.*, 1992a,b; Fu *et al.*, 1994; Fu and Cheney, 1995) valuable measurements of the sea surface are now accessible. The user groups are mainly geodesists, space engineers, modellers, glaciologists and oceanographers. Since these user groups of scientists are interested in different parts of the signal, improved versions of the data set are regularly released.

The altimetric products of interest for oceanography comprise sea surface height (SSH), significant wave height (SWH) and surface wind field. The data sets have proven to be capable of resolving sea surface height variability, eddy kinetic energy, fronts in oceanic regions and have contributed to the tremendous recent advance in the global tidal modelling (e.g. Andersen *et al.*, 1995). Little attention has, however, been given to the use of altimetry in the investigation of the near surface circulation, more specifically the determination of the dynamic (sea surface) height/topography and to the combination of numerical circulation models with dynamic height derived from altimetry. The main reason for this was found in the existing geoid models, which went into the calculation of the dynamic height. The geoid is defined as a gravitational equipotential surface, to which the ocean sea surface would conform if it were at rest and no other forces were acting other than gravity. Until recently the geoid models had an accuracy, which were less than the ocean signal to be determined. Preliminary studies of the surface circulation in the area between Greenland and Iceland derived from altimetry revealed that the used global geoid model OSU91A (Ohio State University) was on the brink of yielding satisfactory results. The relatively good agreement can partly be explained by the dense coverage of gravity measurements from the area, which went into the calculations of the geoid model. This means that global geoid

models are highly dependant on direct gravity measurements and their accuracy therefore varies from place to place depending upon the density of gravity measurements for the particular area. A more accurate geoid model will thus give rise to a more precise determination of the dynamic topography, which in turn will give a

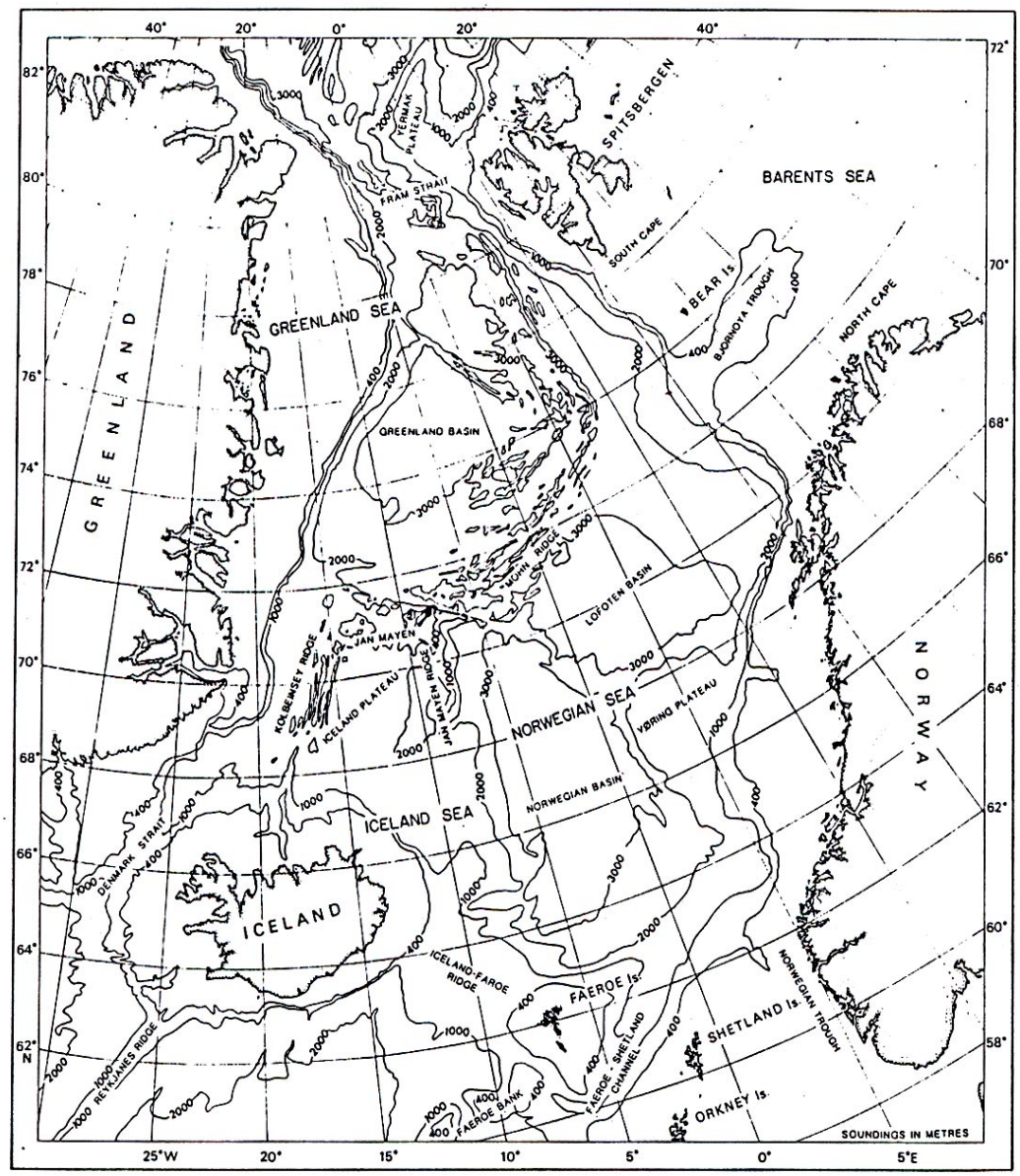

Fig. 1. Bathymetry and nomenclature in Icelandic waters and the Nordic Seas. Depth conturs are in meters. (From Hopkins, 1988).

better view of the circulation system in the region under investigation. Satellite altimetry will thus with an accurate geoid in future give us the opportunity to derive nearly synoptic surface circulation field and the possibility to detect major and minor variations in the circulation patterns, which are of great importance, not only in climate studies but also in a number of other fields.

With the recent development in the field of satellite altimetry and geoid models it is feasible to test their ability to estimate near-surface circulation and height variations in a limited oceanic area. The present work is limited to Icelandic waters and adjacent ocean

areas (59°-71.5°N, 10°-45°W), located at the boundary between the Nordic Seas (i.e. Greenland, Iceland and Norwegian Seas) and the northern North Atlantic. Here there exist in addition to global geoid models a number of local geoid models, which are under continuous development. In order to increase our knowledge of the circulation and transports in the layers below the surface layer, a state-of-the-art experiment have been conducted integrating dynamic heights derived from altimetry at open lateral boundaries in a limited area model.

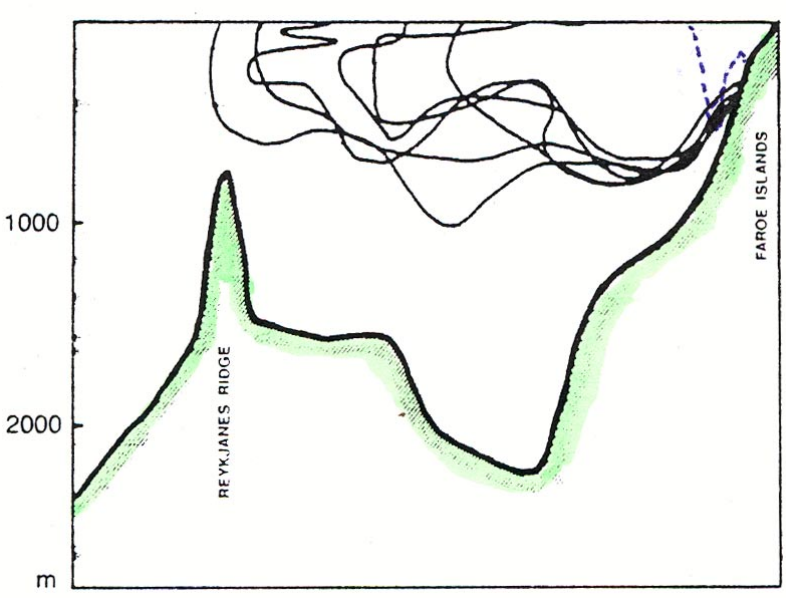

Fig. 2. Extension and depth of the 35.2 isohaline along the 62°N latitude across the Iceland Basin from the Faroes to the Reykjanes Ridge in June-July 1948-58 and in May 1988 (dotted). Adapted from Hansen (1985), based on contributions by F. Hermann and K.P. Andersen in Ann.Biol., for the years 1948-1958, Krauss (1995), and the Marine Research Institute, Reykjavik, database.

The region discussed within this work is shown in Figure 1 showing the bottom topography and nomenclature of the major features. As is well known and mentioned by e.g. Hopkins (1988), the bathymetry of a region plays a vital role in the dynamics of its circulation. The thermohaline characteristics are determined by the geographical settings and the bathymetric connection with other oceanic regions, and the circulation is directed and limited by the geomorphology. The most conspicuous feature of the area is the ridge systems, dividing the deeper region into a number of more or less isolated basins.

GENERAL CIRCULATION

The northern North Atlantic and Nordic Seas are among the most monitored regions of all the world's oceans and include an extensive literature. However, a more comprehensive work is still needed before a qualitative and quantitative description of the circulation in the area is achieved.

The long-term variations of the water masses and their characteristics in the region have been discussed by numerous authors (e.g. Dickson *et al.*, 1988; Belkin *et al.*, 1998). These variations have perhaps a greater influence on the circulation than previously assumed. The variability of the region is exemplified by Figure 2 showing the extension and depth distribution of the 35.2 isohaline at the same season for six different years in the period 1948-1958 and 1988 along the 62°N latitude across the Iceland Basin from the Faroes to the Reykjanes Ridge.

Among other examples can be mentioned two intermediate water masses associated with the North Atlantic thermohaline circulation: the Labrador Sea Water (LSW) and Arctic Intermediate Water (more precisely lower Arctic Intermediate Water as defined by Swift and Aagaard (1981)). Observations in the Labrador Sea have revealed decade-long changes in the temperature, salinity, density and formation rate of LSW and the

changes in the source have been followed over most of the North Atlantic Ocean (Talley and McCartney, 1982; Sy *et al.,* 1997). New travel times have been estimated for the eastward transport of LSW, indicating a surprisingly high mean speed of 1.5-2 cm s^{-1} (Sy *et al.,* 1997). The lower Arctic Intermediate Water has been less studied than LSW and therefore little is known about its temporal and spatial changes. However observations from the Norwegian Sea (Blindheim, 1990, Blindheim *et al.,* 2000) indicate that this water mass has undergone a temporal and spatial change since the fifties. It was thus absent in the fifties and sixties in the Norwegian Sea but became a major water mass in the eighties and nineties, located between the Atlantic Water and Norwegian Sea Deep Water. According to Blindheim (1990) the water mass has its source area in the Arctic domain in the Greenland and Iceland Seas. He further states that if any fluctuations have occurred in the lower AIW during later decades (1974 to 1985), it has been in volume rather than in properties. A natural question is to what extent the general circulation is influenced by the long-term coordinated changes in the convective activity of the North Atlantic as discussed by Dickson *et al.* (1996). The answer will not be given here but the question should be kept in mind.

A review of the literature on the general circulation of the North Atlantic north of 50°N reveals a number of leading circulation schemes, which have been proposed and refined by others during the last century. The descriptions ranged from qualitative to semi-quantitative ones. Of trendsetters for the oceanographic community can be mentioned Helland-Hansen and Nansen (1909), Nansen (1912), Hermann and Thomsen (1946), Dietrich *et al.* (1975), Worthington (1970), and Ellett and Blindheim (1992).

With their publication in 1909, Helland-Hansen and Nansen (1909), a comprehensive work was published on the Norwegian Sea (the Nordic Seas). It was based upon the Norwegian researches 1900-1904 supplemented with the literature available at that time. Their map of the circulation of the Norwegian Sea, based on their observations (Figure 3), is perhaps the most quoted and influential map of the circulation in the Nordic Seas and the ridge areas between Greenland and Scotland. A puzzle in their map is the lack of a cyclonic circulation in the Iceland Sea, although in their discussion of cyclonic systems in the Nordic Seas they mentioned the possibility of a cyclonic system in the Iceland Sea. The question is, were they influenced by their contemporaries or did lack of data force them to state that nothing certain could be said about this cyclonic system. Three years later, however, the gyre of the Iceland Sea turns up in a map of the surface circulation of the

Fig. 3. The surface circulation in the Nordic Seas (Helland-Hansen and Nansen, 1909).

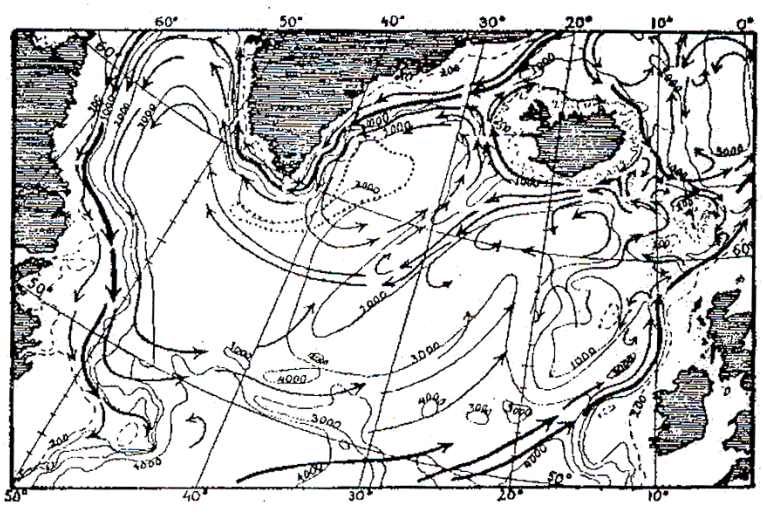

Fig. 4. Hypothetical circulation scheme of the Northern North Atlantic (Nansen, 1912)

northern North Atlantic by Nansen (1912) (Figure 4), during his discussion of bottom waters and cooling of the oceans. Together these two maps make the basis for maps published prior to the second world war north of 50°N and their influence is traceable today. The influence is clearly seen in a surface circulation map of the Atlantic Ocean published by Meyer (1923), which was later adapted by Wüst (1928) who added fronts and supposed bottom water formations sites to the map (Figure 5). Sixty years later Ivers (1975) (Figure 6), arrived at a result which was in striking resemblance with that of Nansen (1912). Ivers' result was obtained using geostrophic shear calculations for individual station pairs and a qualitative assessment of likely flow direction as a function of depth, based on water-mass distributions. The general circulation in the Iceland Sea was discussed in detail by Stefánsson (1962) who by means of dynamic methods verified the existence of the cyclonic gyre in the Iceland Sea. Later it was supported by results from satellite tracked surface drifters by Poulain *et al.* (1996).

The post war development in the field of general circulation can be characterized as the time where the schemes proposed by Helland-Hansen and Nansen for the northern North Atlantic and Nordic Seas were either refined or radically changed due to accumulation of new and more comprehensive data material. The changes in the Nordic Seas were of minor character although an important refine-

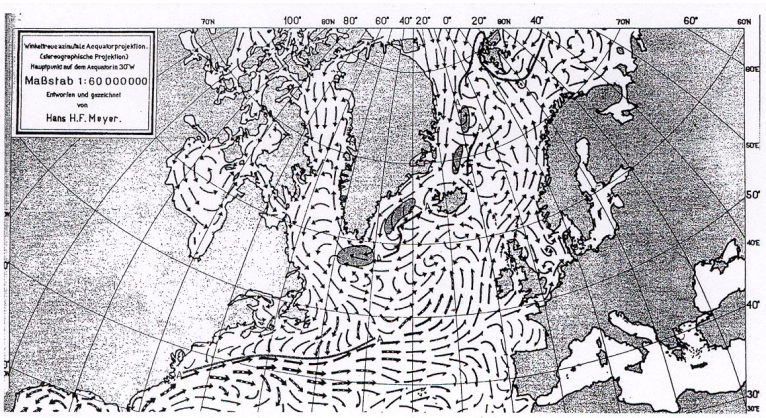

Fig. 5. Circulation scheme of the northern North Atlantic and Nordic Seas by H.F. Meyer (1923) published by Wüst (1928).

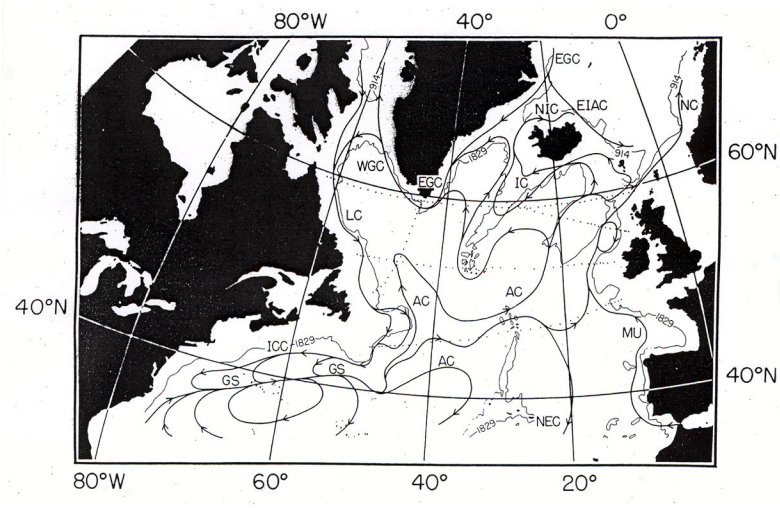

Fig. 6. Shallow circulation scheme of the northern North Atlantic (Ivers, 1975).

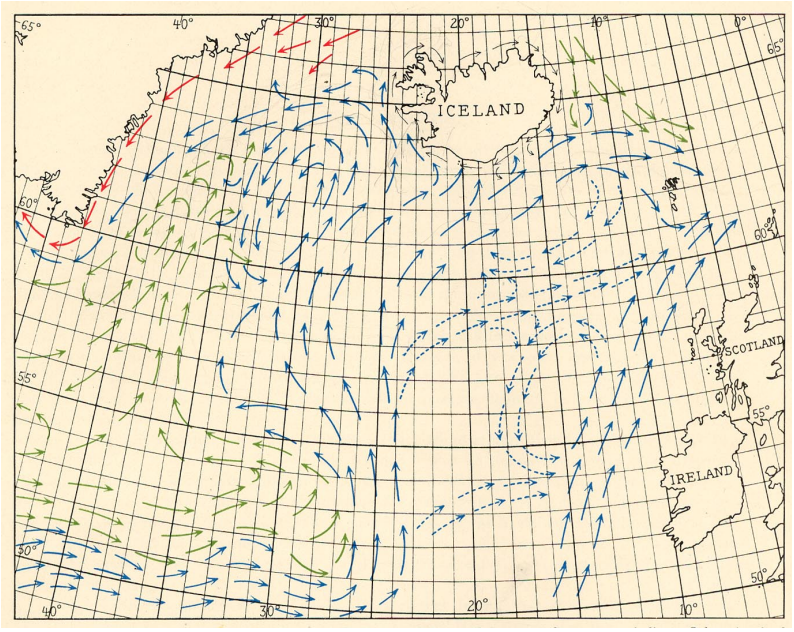

Fig. 7. Surface currents in Icelandic waters and adjacent seas as derived from drifting bottles (Hermann and Thomsen, 1946).

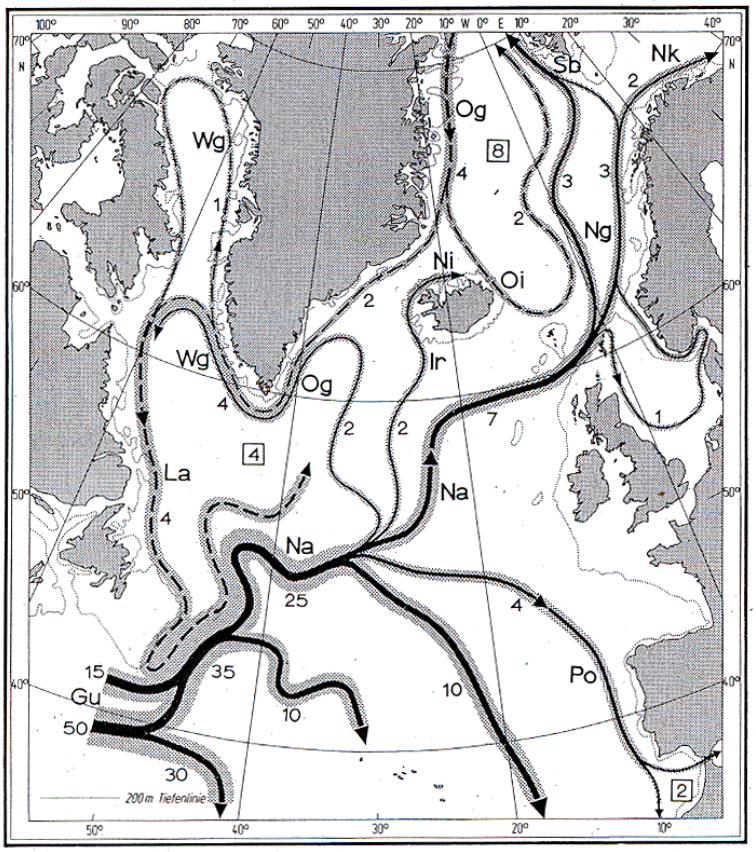

Fig. 8. Surface currents schematic flow and transports (Sv) in the northern North Atlantic and Nordic Seas. (From Dietrich et al., 1975).

ment and verification work took place as mentioned above for the Iceland Sea. The northern North-Atlantic on the other hand experienced radical changes especially in the Iceland Basin. Among the first to propose a new scheme for the northern North-Atlantic were Hermann and Thomsen (1946) (Fig. 7), by introducing an "anticyclonic" circulation in the Iceland Basin. The hitherto accepted idea of a southwest ward flow along the eastern flank of the Reykjanes Ridge was replaced by a northward flowing branch of the North-Atlantic Current. Although their scheme for the Iceland Basin was solely based on results from drift bottle experiments it was later supported by schemes based on dynamic calculations (*e.g.* Dietrich, 1957a, 1957b, 1963; Wegner, 1973; Dietrich *et al.*, 1975) though in modified versions just south of Iceland.

In the start of the seventies the description of the general circulation changed from being qualitative showing current as arrows to semi-quantitative described by transport lines (*e.g.* Dietrich *et al.*, 1975; Worthington, 1970; Ellett and Blindheim, 1992). The main difference between these schemes were observed in the area east of the mid-Atlantic Ridge system (*i.e.* in the Iceland Basin) connected to the northward transport of the North Atlantic Current. A frequently referred scheme is for example that of Dietrich *et al.* (1975) (Fig. 8), clearly showing that details of the general circulation have decreased on the expends of a transport estimate and budget between different parts of the ocean. For the present study is the recent development in the field of general circulation schemes a drawback. As Hansen (1985) states it "It is a rather depressing conclusion that in many respects the most reliable descriptions of the circulation pattern seem to be the older ones, and that numbers for transports are still not available to any great precision".

Summarizing our present knowledge of the general circulation in the study area is not a simple matter, as an attempt will have to be divided into more or less "well" established and disputable current features. With "well" established is not meant that the current or circulation are known in great detail with respect to transport magnitudes or variability, but only that it is a persistent feature. Of "well" established features are: the southward progress of the East Greenland Current along the east coast of Greenland; the cyclonic circulation in the Iceland Sea; the northward progress

of the Irminger Current west of Iceland and its continuation after bifurcation; the East Icelandic Current; and to some degree the cyclonic circulation in the Irminger Sea. Of disputable features are: the circulation of the Iceland Basin; and to some degree the circulation of the Irminger Sea.

Recent results utilizing satellite tracked surface drifters in the Iceland Basin (Otto and van Aken, 1996; Valdimarsson, 1998; Valdimarsson and Malmberg, 1999) reveal a mean circulation which is similar to the one proposed by Nansen (1912). However, a high level of variability are observed which indicates that more than one circulation mode are present.

PRINCIPLES OF SATELLITE ALTIMETRY

Satellite altimeters are radars which transmit short pulses towards the planetary surface and, by recording the return time of the pulse, measure the height of, e.g., the altimeter relative to the position of the sea surface. If the position of the altimeter can be fixed, it is possible to calculate the absolute height of the sea surface. Due to the favourable reflective properties of water, the method is especially suitable over the ocean. Oceanographic applications of this information include the studies of ocean circulation and tides. Through gravity field analysis it can reveal details of ocean bathymetry in remote areas. In addition, the deformation of the microwave pulse on reflection at the sea surface contains information about significant wave height (SWH).

The basic concept is very simple (Figure 9): Knowing the position of the satellite, i.e. its height above a reference ellipsoid (e.g. WGS84), *h*, everything necessary to obtain the sea surface height, *SSH*, is the distance between the satellite and the ocean surface, *a*, which is

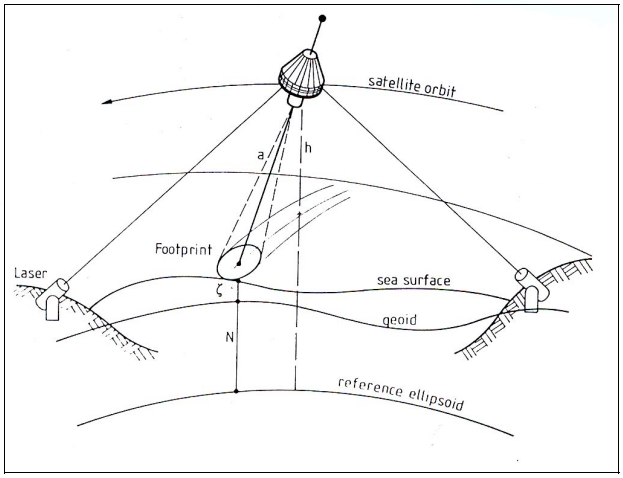

Fig. 9. Basic concept of satellite altimetry (Seeber, 1993).

$$SSH = h - a. \tag{1}$$

The derived *SSH* is of interest to both geodesists and physical oceanographers. Thus the data gives rise to a symbiotic relationship between the two fields. The altimeter derived observation of the sea surface height is composed of a number of terms which are

$$SSH = N + \zeta + \zeta_{tide} + \varepsilon \tag{2}$$

where

- N is the geoid height,
- ζ the time varying dynamic height,
- ζ_{tide} ocean tides, and
- ε is the sum of errors.

From the oceanographer's point of view, the knowledge of dynamic topography (derived from the dynamic heights) is of importance, to improve the understanding of the oceanic general circulation and its variability. From the geodetic point of view, the geoid is the important signal. To a first approximation the mean

SSH is the geoid with an accuracy in the order of 0.5 m, where the ocean signal is "in the noise level". With the increasing demand for more accurate global geoid models (future goal with an accuracy of the order 3 cm for wavelengths of 100 km, (ESA, 1996)), the ocean signal is no longer within the noise level, but must be removed. Under this condition the two research fields merge.

The principle behind the altimeter measurement is the information obtained in the shape and timing of the return radar pulse. For altimeters situated at a height of ~500 km a resolution of ~1 cm would require a time resolution of ~30 picosecond. Within this time span the leading edge of the emitted radar pulse should rise to full power. A radar pulse of this size would require an unrealistically wide frequency band of ~30 GHz to carry it. In addition the return pulse would be swamped by surface-wave noise, due to the reflection of the leading edge by waves.

Instead measurements are carried out with a much longer pulse of about 3 nanoseconds. For the altimeter situated on board the ERS-1 measurements are carried out using a 330 MHz (3 nanosecond; ocean mode) pulse centred at 13.8 GHz, with a pulse repetition frequency of 1020 Hz. By sampling the return pulse at a rate of approximately twice per nanosecond, the relatively long return pulse (waveform) can be analysed by curve fitting (Figure 10). Errors introduced by the curve fitting can be reduced by averaging over a certain number of samples to obtain the necessary accuracy. For ERS-1, the full data rate is 20 measurements per second, resulting from a smoothing process of the original observation onboard the satellite. For the user community data is normally distributed in the form of smoothed altimeter data with 1 second spacing, corresponding for the ERS-1, to a spacing of ~7 km along the sub-satellite track at the sea surface. When it comes to the "observation accuracy" for these products, they depend on the resolution of the altimeter and the applied smoothing algorithm. Estimates for the ERS-1 altimeter heights in ocean mode are significantly better than 10 cm for the 1 second products (ESA, 1992).

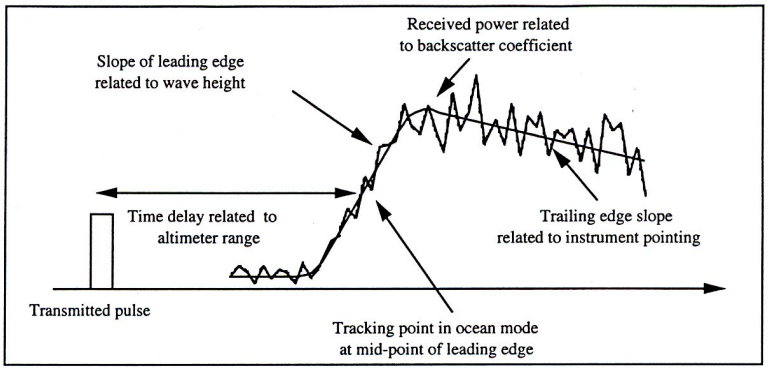

Fig. 10. Profile of the ocean return pulse (waveform; CERSAT, 1995).

Thus, the interest is connected to the shape of the return pulse. Over oceans it highly depends on the wave field where the effect is imposed as an additional slope on the leading edge of the return signal strength curve (Figure 10). The slope is related to the wave field as the significant wave height, while for the altimetry the timing of the midpoint of the leading edge slope is equivalent to the average position of the sea surface. In addition an estimate of the surface wind-field can be obtained from the power level of the return signal.

The area from which the altimetric measurement is representative is called the footprint. The return signal strength, which

depends on the reflecting surface area, grows rapidly when hit by the radar pulse until the "illuminated" area transit from a disk to an annulus. It is this transition which determines the footprint's size. For a calm sea the radius of the footprint is ~1.2 km, but for a rough sea it will increase according to the significant wave height (SWH). For the 1 second product this gives quite a high spatial resolution, with an elongate form with the length of ~9.4 km and width of ~2.4 km for a calm sea.

The altimeter measurement, *a*, is calculated from the time measurement on the assumption that the radar signal propagates with the speed of light. However, the signal propagation is slowed down by the influence of the ionosphere and troposphere, resulting in an overestimate of the measured distance. Thus, the altimeter range must be corrected for these effects. The different corrections are briefly described and discussed below, where special attention is assigned to the ERS-1 ocean product (OPR02) corrections in Icelandic waters. A similar analysis has recently been given by Fu *et al.* (1994) for TOPEX geophysical data records on a global scale.

Dry troposphere correction. The radar signals are delayed by the dry air mass of the troposphere, at a rate of ~0.2277 cm/ mbar of atmospheric sea level pressure. The magnitude of this correction is about 2.3 m and has a low variability (typically 10 cm), which varies slowly in both time and space. The correction

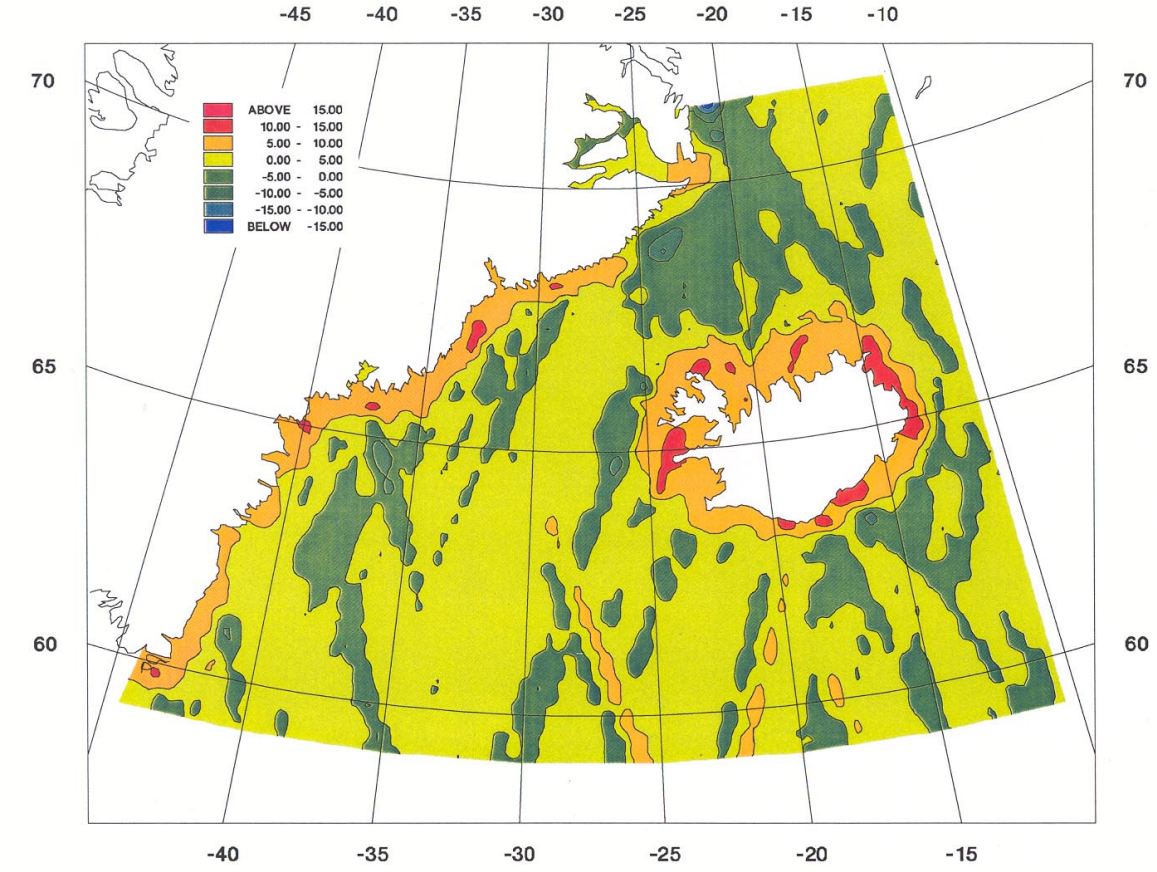

Fig. 11. MWS minus ECMWF wet trophospheric correction difference (cm) for ERS-1 repeat 5 (September 1992). Colour scale runs from -15 to 15 cm.

is made by using the sea level pressure product of the European Centre for Medium Range Weather Forecasts (ECMWF) provided every 6 hour by the French Meteorological Office. The root-mean-square (RMS) accuracy of the correction is estimated to be ~0.7 cm on an assumption of an RMS 3 mbar accuracy for the pressure product (Fu *et al.*, 1994). The area around the Iceland is known to be characterized by a high low-pressure activity and to the presence of the atmospheric Polar Front. A comparison made between the ECMWF model pressure and ground truth pressure observations made in Reykjavik reveal a RMS difference of 4 mbar. The comparison is made between a Topex/Poseidon crossover point and the pressure gauge in Reykjavik, located 100 km apart. Thus, a sufficiently high accuracy of the ECMWF model pressure is found in the area, taking into consideration the distance between the two comparison points. Three hours pressure observations from Reykjavik, Iceland, from the period January 1992 - December 1995 were kindly made available by the Icelandic Meteorological Office.

Wet troposphere correction. In addition to the dry air mass, the water vapour content in the path also cause delay in the radar signal. The correction is typically about 10 cm over Icelandic waters, thus much smaller than the dry troposphere correction. However, it varies rapidly from a few millimetres in dry and cold air to more than 40 cm in hot and humid air over short space and time scales, which weather models often cannot map (Stum 1994). ERS-1 ocean products (OPR02's) contain two different corrections. One correction makes use of the before mentioned ECMWF model outputs provided by the French Meteorological Office. The other makes use of simultaneous radiometer measurements performed onboard the satellite, where a microwave sounder (MWS) is used to measure the brightness temperatures in two frequency channels, to retrieve the correction in combination with the wind speed derived from the altimeter. Work done by Eymard *et al.* (1994) shows that the ERS-1 microwave radiometer correction estimates matches in-situ radiosonde estimates with no bias and a difference of 2 cm RMS. Comparison made by Stum (1994) between ERS-1 and TOPEX microwave radio-meters at crossover points showed good agreement, with no relative bias and a difference of 1 cm in standard deviation. He furthermore showed that the TOPEX microwave radiometer (TMR) is better at monitoring the water vapour variations than the ECMWF model, although the ECMWF derived correction could be used as a backup if the TMR fails. The above suggests that the wet troposphere correction derived from the MWS is to be preferred.

Figure 11 shows a map of the difference between MWS - and ECMWF wet troposphere correct-ions. The corrections are obtained from the multidisciplinary phase C repeat 5 (September 1 to October 6, 1992) and are quoted for the respective models as a negative value. The data set has not been subjected to averaging in latitude by longitude boxes. Compared with the results of Stum (1994) a good agreement is found. However, a major difference is found in the coastal areas off Iceland and Greenland where the MWS simply fails to work as indicated by positive values greater

than 5 cm in Figure 11. The reason is not fully understood, but is probably connected to the transition of the satellite track from ocean to land and vice versa. The RMS difference is calculated to 2.63 cm for the aerial box (59°-71.5°N, 45°-2°W), where points including MWS failures are not included in the statistics. There is a minor tendency for the ECMWF to give slightly higher values (i. e. a bias). In case of MWS failure, the ECMWF derived correction can be used as a backup. However, a direct replacement of MWS with ECMWF should be avoided due to the observed bias between the two data set.

Ionosphere correction. In the ionosphere, the delay of the radar signals is caused by free electrons. The effect varies from day to night, with season, and increases with the sunspot number. The corrections available in the ERS-1 altimeter product are model values, based on the monthly sunspot number ("R12") published by Centre Consultatif International des Radio communications (CCIR). This term is typically around 2 cm over Icelandic waters. According to CERSAT (1995) the accuracy of the correction is estimated to be about 2 cm RMS during low solar activity. However, during high solar activity it can reach 5 cm to 10 cm particularly in the tropical areas. No comprehensive work on the subject has been published. Higher accuracy can be obtained by using a multi-frequency altimeter, as the dual-frequency altimeter onboard TOPEX (Fu *et al.,* 1994).

Electromagnetic (EM) bias correction. This correction is related to the sea-state or more precisely to the fact that the radar backscatter cross section is asymmetric with respect to wave troughs and crests, with the troughs cross section being larger. Therefore the measured altimeter range will be biased toward wave troughs. The correction is roughly proportional to the height of waves and is expressed in terms of the significant wave height (CERSAT, 1994).

The electromagnetic bias should not be confused with the sea-state bias, which is the overall effect of the sea-state on the altimeter range measurement. An additional tracker bias is introduced by the algorithm which tracks the slope of the leading edge of the radar pulse. The tracker bias is a function of the significant wave height. Normally this correction is found among the instrumental corrections.

The EM correction is typically observed to be in the range of 2-8 cm for September month 1992 over Icelandic waters. Compared with the above corrections it varies rapidly in both time and space. An inspection of the correction values for repeat 5 (September, 1992) revealed major problems in coastal areas, where either the correction was absent or of a spurious magnitude, indicating that caution must be taken when applying the correction in coastal areas. In addition, a limited number of dubious values in the interior of the ocean could be eliminated by using an along track filter followed by a linear interpolation scheme.

It has not been possible to find an estimate of the RMS accuracy of the EM correction for ERS-1. Analysis of the correction for TOPEX between the altimeter range and significant wave height (SWH) suggest that there is a residual EM bias error

Altimeter		
Altimeter noise*	3.0	
EM bias	~2.0	
Ionosphere	~2.0	
Dry troposphere	0.7	
Wet troposphere	2.0	
Total altimeter range**	4.6	4.6
Precision orbit determination		
Radial orbit height	15.0***	6.0[+]
Sea surface height		
Single-pass surface height	15.7***	7.6[+]

One sigma values in cm
*Altimeter noise is based on 1-sec average at 2 m significant wave height
**Altimeter bias not included
***Generated DPAF
[+]Based on the DGM-E04 gravity model

Table 1. Assessment of measurement accuracies for ERS-1 (units cm).

of about 1% of the significant wave height in the geophysical data records (GDR) (Rodriguez and Martin 1994).

Precise orbit determination. The uncertainty in the radial component of the satellite orbit has for long been the largest error source in satellite altimetry. The precise orbit following the ERS-1 OPR02 products is generated at the German Processing and Archiving Facility (DPAF), which utilizes satellite laser ranging measurements and altimeter crossover data in their computations. Typical accuracy of the precise orbit for ERS-1 (OPR02) is about 12 to 15 cm in the radial component. Lately, these values have been improved considerably by the introduction of precise ERS-1 orbits produced with the Delft Gravity Model DGM-E04, based on satellite laser ranging measurements, altimeter residual and altimeter crossovers (R. Scharroo, personal comm., 1997). The radial precision of the new orbits is estimated to be between 4-6 cm. Unfortunately these new precise orbits were first accessible around January 1997. Therefore, orbits produced by DPAF are used in the following.

Table 1 shows an estimate of the error budget, based on the above, for the sea surface height (SSH) measured by ERS-1. The error is given in terms of root-sum-square for the 1/s data rate and 2 m significant wave height. The total measurement error, 15.7 cm for the ERS-1 OPR02 products, is higher than the mission requirement, which specifies a total error of <10.0 cm. With the newly released precise orbits this requirement is achieved. For comparison it can be remarked that the TOPEX altimeter has an estimated total error of 4.7 cm (Fu *et al.*, 1994) of which 3.5 cm is orbit error.

Tidal correction. When it comes to the study of ocean currents and their variability from altimetric measurements of sea level, one must consider the residual tidal signal. The tide sensed by the altimeter is composed of the ocean tide, the load tide and the body or solid tide. The tide corrections all make use of model predictions. According to Fu *et al.* (1994) the accuracy of the body tide models are better than 1 cm, whereas the main concern is the accuracy of the ocean tide models. Since the beginning of 1990

there has been a rapid development of global ocean tide models, mainly achieved in the field where models are based on high-precision altimetry from the TOPEX/POSEIDON (T/P) satellite. In 1994 this resulted in the release of not less than 12 new global ocean tide models, reviewed by Andersen *et al.* (1995), of which all were superior to the classical Cartwright and Ray (1990, 1991) and Schwiderski (1980a,b) models when compared to a global set of tide gauges. Many of the models derived from T/P altimetry are continuously updated and improved as more data becomes available. Thus, the continuous development in the field provides the opportunity to choose the currently "best" available model, which fits the area of interest. In this study the corrections applied for body tide were those supplied with the OPR02 data (CERSAT 1994), while the Andersen/Grenoble ocean tide model version AG95.1 was used for the correction of ocean tides and load tides. AG95.1 is a long-wavelength adjustment of the Grenoble model for the M_2 and S_2 constituents with the first two years T/P crossover data set (Andersen, 1995; Andersen *et al.*, 1995). The model turned out to be the best in an recent intercomparison of ocean tide models for the Atlantic Ocean and on the Northwest European shelf region (Andersen *et al.*, 1995). In the Atlantic RMS differences with 39 tide gauge observations were found with values of 1.41, 0.97, 0.96 and 0.50 cm for the M_2, S_2, K_1 and constituents respectively.

Geoid models

The discussions above have up to now been on the altimeter range measurement and the different corrections which are connected to this measurement. Thus, knowing the orbital height, the altimeter range and the different corrections, we are now, according to eq. (1), able to derive the sea surface height (*SSH*). The *SSH* or more precisely its temporal variations have attracted great interest, as it is a relatively simple quantity to handle when the satellite ground track is repeated over a longer time span. In oceanography it is widely used in the study of transient ocean variability phenomena. For example, it has been used in the determination of sea surface height variability ("mesoscale variability") (e.g. Cheney *et al.*, 1983), eddy kinetic energy (e.g. Heywood *et al.*, 1994), detection of fronts (e.g. Scott and McDowall, 1990), and seasonal sea level variability combined with sea surface temperature (e.g. Knudsen *et al.*, 1996),

When it comes to the use of dynamic heights or dynamic topography and its combination with general circulation models, the number of references become smaller (e.g Park and Gambéroni, 1995; Menemenlis *et al.*, 1997). The reason is found in eq. (2), where the troublesome term is the geoid height or simply the geoid, which with the exception of few areas, is only known to an accuracy of about 0.5 m.

The geoid is defined as a gravitational equipotential surface, to which the ocean sea surface would conform if it were at rest with no forces acting on it other than gravity. Departures of the sea level from the marine geoid result from local exchange of mass and heat with the atmosphere through the sea surface, ocean currents, tides,

waves and atmospheric pressure systems, and it may in places depart as much as 1-2 m. In general terms, the dynamic topography and its slopes provide a dynamical surface boundary condition on the ocean circulation. Variation in the gravity field produced by mass excesses and deficiencies within the earth, gives rise to an irregular shape of the geoid which departs from the reference ellipsoid. Globally, relative to the reference ellipsoid the geoid has a dynamic range of about 200 m, which is larger than the dynamic topography associated with ocean currents by about two orders of magnitude.

During the past 30 years there has been a tremendous development in the field of geoid modelling, due to the mathematical development in the field of spherical harmonic potential coefficient models, improved computer software and the introduction of earth orbiting satellites. Combination of terrestrial gravity data and satellite data (analysis of orbit variations and use of altimetry) led in 1991 to the introduction of the global Ohio State University OSU91A spherical harmonic model, complete to degree and order 360 (Rapp *et al.*, 1991). The accuracy of this model is in the ocean estimated to be ±10 cm on scales greater than 1000 km and for point undulation ±26 cm (Rapp, 1994).

Parallel to the development of global geoid models there has been a progress in the field of detailed regional geoid models. Here for example multi-band spherical FFT methods have been used in the determination of regional geoid models (Forsberg and Sideris, 1993), where the geoid prediction is based on a spherical harmonic reference model (e.g. OSU91A) and all available terrestrial gravity data (ship, land and air based) from the area on gridded form. An error estimate for a detailed geoid model is seldom achieved, as it is difficult to assess. Instead, oceanographic arguments must be used in the evaluation of the models. Four geoid models will be tested for their ability to derive the dynamic topography corresponding to the general circulation observed in Icelandic waters.

DATA AND METHODS

The data sets used in this work were gathered from many different sources, including satellite altimetry, hydrography, satellite tracked drifters, tide gauge and atmospheric pressure records.

Below is given a description of a hydrographic data set and the construction of a 35 days mean dynamic topography time series derived from ERS-1 satellite altimetry. The remaining data sets will be introduced as a natural part of the text.

Hydrographic data set

To facilitate the oncoming modelling work and evaluation of the dynamic topography derived from satellite altimetry, a hydrographic data set was needed for the study area. A natural choice would be the traditionally used climatological data set in ocean circulation model studies by Levitus (1982). The Levitus data set has been and still is of great help for the modelling community. However, many have noted its restricted use in

Table 2. Hydrographic data set composition.

Research Vessel/Origin	Programme	Date	No. stations
Poseidon (Krauss)	special cruise	13/5-24/5 1988	71
Johan Hjort (Blindheim)	monitoring	26/7-17/8 1988	96
Tyro (WOCE)	WOCE	11/7-12/7 1990	9
Tyro (WOCE)	WOCE	12/4-22/4 1991	40
Bjarni Sæmundsson	GSP 91	30/8-11/9 1991	56
Meteor (WOCE)	WOCE	5/9-10/9 1991	24
Johan Hjort (WOCE)	Nordic WOCE 92	15/7-21/7 1992	31
Valdivia (WOCE)	WOCE	15/9-21/9 1992	21
Bjarni Sæmundsson*	Nordic WOCE	18/9-25/9 1992	72
Bjarni Sæmundsson*	monitoring	18/5- 4/6 1993	79
Bjarni Sæmundsson*	special cruise	11/6-23/6 1993	155
Johan Hjort (WOCE)	Nordic WOCE 94	24/7-11/8 1994	94
Bjarni Sæmundsson*	special cruise	24/2 1995	2
ICES		1988-1990	68

* Hafrannsóknastofnunin (Marine Research Institute, Reykjavík)
World Ocean Circulation Experiment (WOCE)

Fig. 12. Location of CTD - stations used in the study; salinity and temperature data set, 1988-1995.

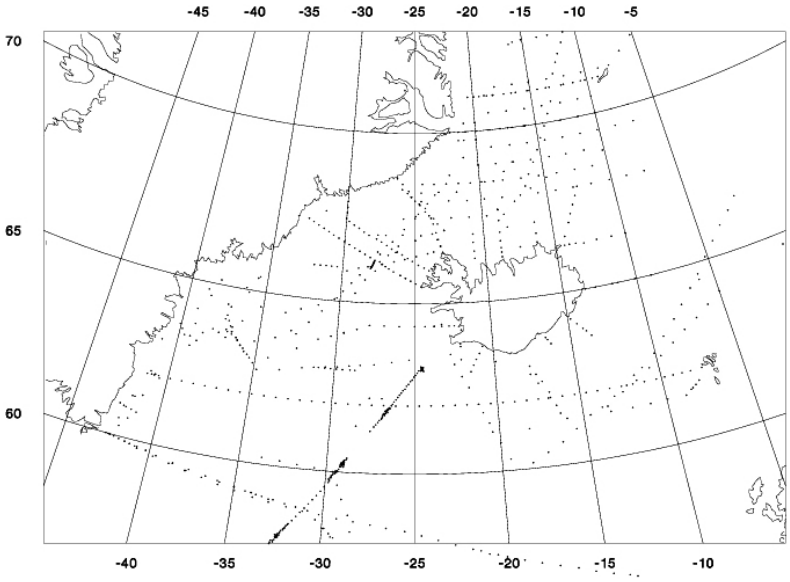

diagnostic modelling studies (e.g. Legutke, 1991), due to its time- and spatial-averaged nature. Thus, important features such as fronts and topographical effects on the density field have been smoothed out.

Using this fact, it was therefore decided to make a new hydrographic data set for the area (60°-72°N, 5°-45°W) representative for the year 1992. To compensate for low sampling rate in a single year high quality conductivity-temperature-depth (CTD) data from the period 1988-1994 (1995) were included in the new data set. The period was kept as short as possible to avoid the effect of interannual variations. In the case of repeated monitoring cruises the most representative cruise were included in the data set.

The data used in this analysis were collected during thirteen different cruises and from the International Council for the Exploration of the Sea (ICES) hydrographic data base (Table 2). The data set consists of 818 high quality CTD stations. The

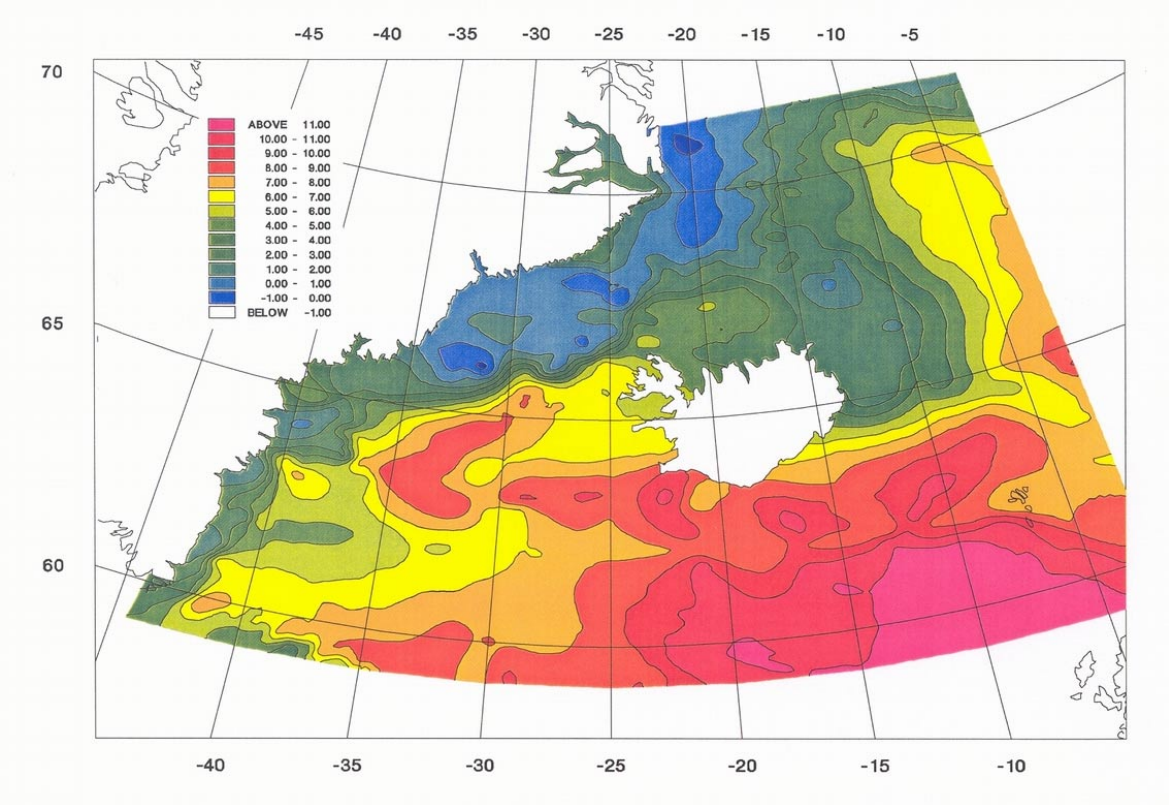

Fig. 13a. Average temperature, upper 50 m from the data set 1988-1995. Contour intervals 1°C.

Fig. 13b. Average salinity, upper 50 m from the data set 1988-1995. Contour interval 0.1.

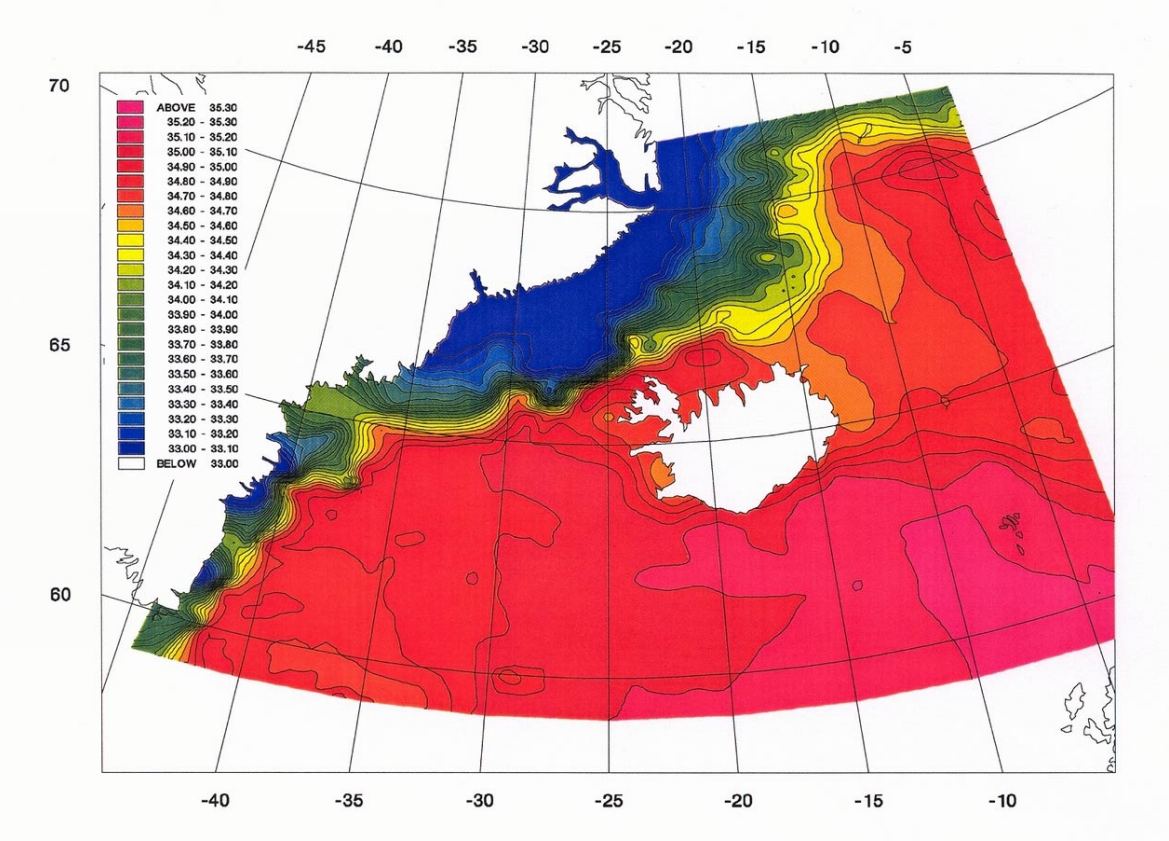

majority of the stations were collected during the months from May to September, making the data set representative for the spring-summer period. The vertical resolution of the single CTD-profiles varies between 1 dbar and 10 dbar, with an accuracy in salinity better than 0.006 psu and in temperature better than 0.006° C. All CTD-profiles were quality tested using an aerial TS-analysis. Errors in single values in the TS-profile were rejected from the profile, whereas for more serious problems the whole station was rejected and the source was notified. The stations which passed the quality test are shown in Figure 12. A reasonable station coverage is observed in most of the region, although a desirable coverage was not obtained in the Iceland Basin, Irminger Sea and near the coast off Greenland.

A description of the different water masses based on the data set have been given by Mortensen (1997).

Average temperature and salinity distributions of the upper 50 m, from the data set (1988-1995), are shown in Figure 13a,b. The most prominent features of the surface layer are the fronts which separates the warm and saline water of the northern North Atlantic from the cold and relative fresh waters of the Nordic Seas. The Polar Front is clearly seen in both variables following the coast of east Greenland from north to south, associated with the approximate outer limit of the East Greenland Current. Warm and saline Atlantic Water carried by the North Icelandic Irminger Current is apparent in the surface layer immediately north of Iceland, here characterized by salinities above 34.8. The Iceland-Faroe Front between Iceland and the Faroe Islands is best observed in the temperature map. Another distinct feature in the temperature map is the small scale variability which, to a high degree, is associated with the way the data set is constructed. Here mixing of observations from slightly different seasons, as in the present case, gives rise to different stages in seasonal heat exchange with the atmosphere. The atmospheric influence on the water column temperature decreases considerably with depth, and at 100 m depth, its influence is practically absent, giving rise to a more coherent temperature distribution in the deeper layers.

The hydrography data set (1988-1995) was subjected to dynamic height calculations with the purpose of checking its integrity and constructing surface current maps of the region for comparison with earlier studies (e.g. Stefánsson, 1962; Swift, 1980). In calculating the dynamic height of historical reasons, the 200 and 800 dbar surfaces were selected, as reference levels. The dynamic topography therefore indicates the sea surface elevation relative to the chosen reference level. No attempt was made to include those stations where the depth to the bottom is less than the reference depth. The most serious problem involved in the calculations is treating the data set as if it were synoptic. Treating the data set (1988-1995) as if it were simultaneous probably does not involve serious errors in areas with relatively low variability and where few cruises enters the calculations. However in regions with relatively high variability and where an increasing number of different cruises overlap serious errors can arise making an overall interpretation difficult.

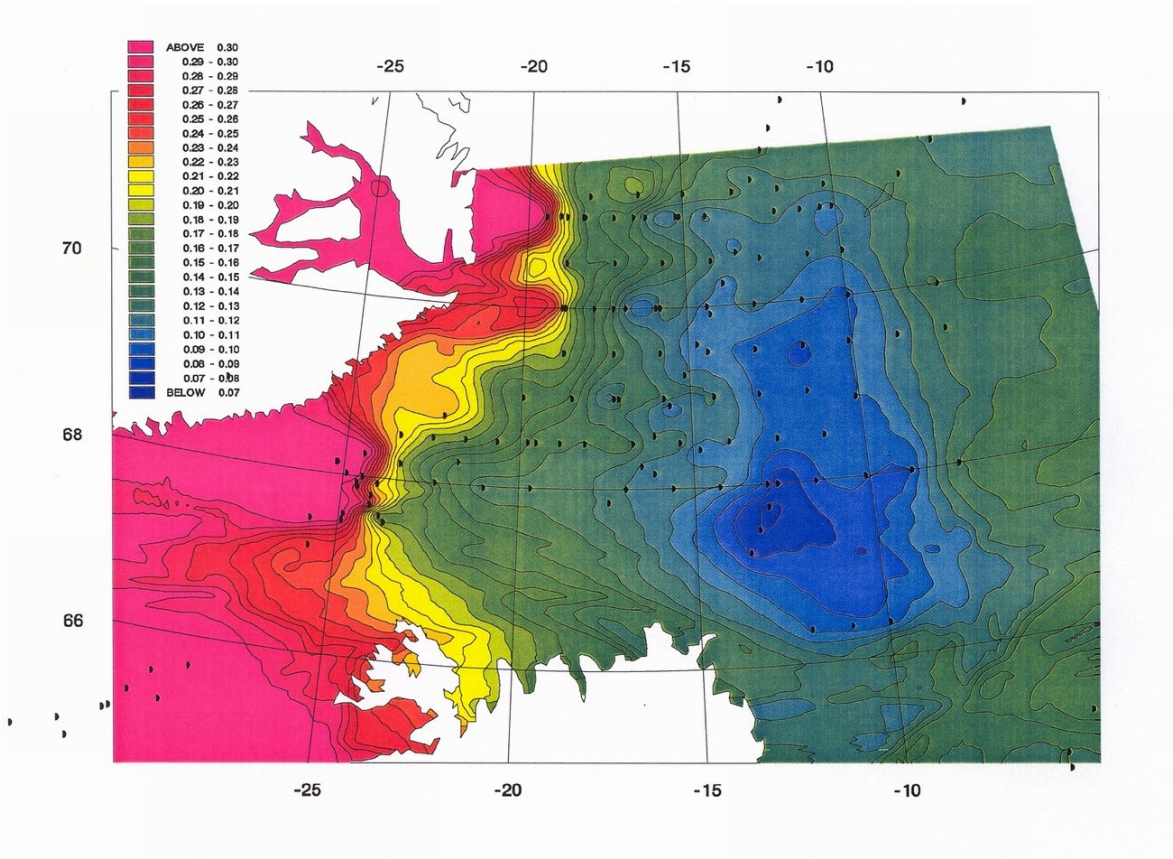

Fig. 14. Hydrographic derived dynamic topography relating to 800 dbar in the Iceland Sea from the data set 1988-1995. Units are in dynamic meters and contour interval 0.01 dyn.m. Dots represent observations which enter the calculations.

The dynamic topography of the sea surface relative to the 800 dbar in the Iceland Sea from the data set (1988-1995) is shown in Figure 14 (one dynamic meter is approximately equal to one metric meter). The question is now: Can the dynamic topography be treated as quasi synoptic? The calculations are in the present case mainly based on two cruises from 1988 and 1991. Hydrographic observations from the region shows that the variation between the two years is limited to the upper 50 meters (Malmberg *et al.*, 1996). In an extensive analysis in the Iceland Sea Stefánsson (1962) showed that dynamic topography of the 50 m level instead of the sea surface relative to the 800 dbar level gave nearly identical results. This suggests that in the case of the Iceland Sea the dynamic topography can be treated as quasi synoptic.

Highest gradients, in Figure 14, are associated with the southward flowing East Greenland Current, with decreasing gradient towards the centre of the Iceland Sea. In the central part of the Iceland Sea, the cyclonic gyre is well-resolved and indicating the closure of the northern contour lines for the first time. There is weak evidence of a weak secondary gyre at about 69°30'N, a similar gyre (~70°30'N) was observed by Swift (1980) in a single case, else it does not appear in other literature. A complex transition area is observed between the East Greenland Current and the cyclonic gyre in the Iceland Sea. The area is seen as meanders in the isopleths located immediately above the Kolbeinsey Ridge, suggesting that a complicated exchange takes place between the two current systems. A feature which is almost absent further south in Figure 14 is the East Icelandic Current. The explanation of the absent of the current is that it is normally observed to be strongest

near the continental slope off the northeast coast of Iceland in water depths less than 800 m, which are not included in this analysis.

Compared with earlier results from the beginning of the fifties (Stefánsson, 1962) and the middle of the seventies (Swift 1980) there is a remarkable resemblance. Only one major difference, and perhaps also the most interesting, is observed as a southward movement of the centre of the cyclonic gyre in the Iceland Sea. While the dynamic topography from the fifties to the middle of the seventies only showed slight differences (Swift, 1980), with the gyre centre located in both periods at about 68°30'N the present results indicate that the centre has moved to 67°30'N, in the beginning of the nineties. The movement of one degree, which is equivalent with 111 km, has not earlier been reported in the literature. It is interesting to note that at the same time the secondary gyre also moves southward by the same distance, suggesting that the entire gyre system has moved southward. An explanation can only be of speculative character, but is probably connected to changes of the wind stress curl in the region. A verification of the gyre centre movement has not been possible due to the lack of near synoptic hydrographic data far enough north in the region.

The circulation system described by Figure 14 also conforms with drift trajectories of drifters deployed in 15 m depth by the SACLANT Underwater Research Centre (Poulain *et al.*, 1996). Their results indicate speeds in the range of 10 cm/s - 40 cm/s in the cyclonic gyre in the Iceland Sea superimposed an eddy field. Whereas the results of the above mentioned analysis of hydrography indicate speeds in the range of 1 cm/s to 6 cm/s, suggesting that a considerable barotropic component is present in the Iceland Sea, as a choice of a different reference level will not alter the features seen in Figure 14 considerably according to Stefánsson (1962).

The dynamic topography of the sea surface relative to the 200 dbar in the investigation area of the data set (1988-1995) is shown in Figure 15, the 200 dbar chosen as reference level due to the shallow shelves in the region.

The overall circulation pattern in the Iceland Sea was observed to have changed only slightly compared with the results using 800 m as reference level. A feature not resolved by the data set (1988-1995) is the eastward flow over the shallow north Icelandic continental shelf and slope, which is apparent in all earlier studies. Earlier results all indicate a rising sea level towards the north coast of Iceland from the deeper parts of the continental slope (Stefánsson 1962; Swift 1980), a result not observed within the present data set. If this is a result of the non-synoptic character of the data set or due to the observed changes in hydrographic conditions in North Icelandic Waters since the earlier observations is not possible to determine with the present data set.

The surface circulation in the Irminger Sea and the Iceland Basin, Figure 15, is seen to be highly influent by the non-synoptic character of the data set. However the influence is observed to be reduced considerably if the dynamic topography of the sea surface

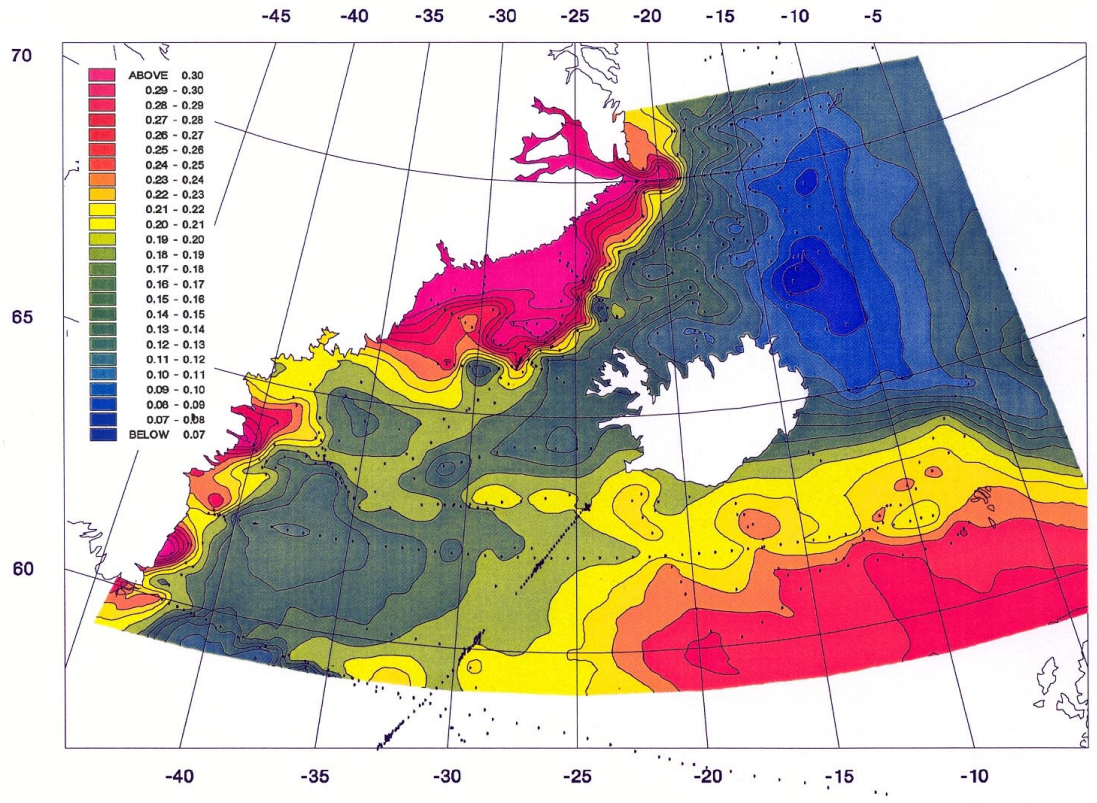

Fig. 15. Hydrographic derived dynamic topography relating to 200 dbar in the Danmark Strait area and adjacent seas from the data set 1988-1995. Units are in dynamic meters and contour interval 0.01 dyn.m. Dots represent observations which enter the calculations.

was calculated relative to the 1000 dbar pressure surface, not shown. The surface circulation is in both cases characterized by a broad northeastward flow in the Iceland Basin and a cyclonic circulation in the Irminger Sea with the East Greenland Current located near the coast of Greenland, in agreement with earlier observations (e.g. Wegner, 1973).

The above results indicate that the hydrographic data set (1988-1995) is of a reasonably coherent character, coherent enough to be used in the coming modelling works, even though it is composed of non-synoptic observations.

Altimeter Data Processing

Since its launch on July 17, 1991, the European remote sensing satellite, ERS-1, has provided a wealth of data of particular interest to oceanographers. The ERS-1 flight was divided into various mission phases. Where data from the 35-days repeat cycle mission (the multidisciplinary phase C) were selected for this study. Phase C was operated between April 14, 1992 and December 15, 1993. Beside the ERS-1 data set TOPEX geophysical data records (GDR-M) from the Archiving, Validation, and Interpretation of Satellite Data in Oceanography (AVISO) Center were selected for two cross-over points from repeat 1 to 86 covering the period October 1992 to January 1995.

ERS-1 data were obtained by principal investigators in Ocean Product Records (OPR02) format. All available 1/s mean altimetric measurements from the entire 35 days-repeat mission covering the area 59°-71.5°N, 10°-45°W were used, including all 18 repeat cycles. Figure 16 shows the stacked data points for repeat 1 to 18

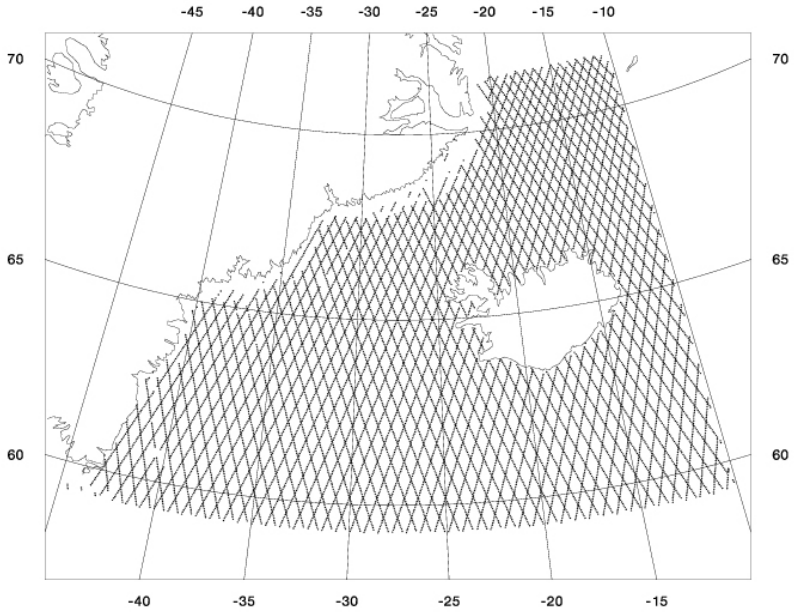

Fig. 16. ERS-1 35 days repeat mission tracks in the study area. Stacked data points for repeat 1-18.

corresponding to optimal data set obtained during one repeat cycle (35 days). The mean track spacing is around 30 km in the east-west direction and the 1/s along-track average values yields one point every ~7 km.

For each repeat the ERS-1 altimetric measurements of the sea surface height were corrected for geophysical effect applying geophysical corrections supplied with the OPR02 records (see introduction). Ocean tides and tidal loading were removed using the Andersen/Grenoble ocean tide model version AG95.1. In order to obtain the dynamic height (eq. 2) for each repeat four different geoids model were subtracted and the results are discussed later. An additional data set using the correction for inverse barometer effect were made, following the guide lines used by TOPEX (Callahan, 1993). The TOPEX data processing followed nearly the same lines as the ERS-1 data above though utilizing geophysical corrections supplied with the GDR-M. In the following it will be stressed when the data set including the inverse barometer effect corrections is used.

Construction of 35 days mean dynamic topography

The first steps in the construction of eighteen 35 days mean dynamic topography from ERS-1 data were to remove erroneous observations and reduce orbital errors.

Erroneous observations were identified by an along-track running ten points filter. For a point to be accepted nine neighbouring points had to be within a distance of 245 km (or 35 s) and fulfil the condition that no more than five of the nine points had an absolute height difference of greater than 30 cm. Further observations were removed if the standard deviation of the 20 height measurements within the 1/s average values in the OPR02 exceeded 0.3 m or if the absolute value of the dynamic height relative to the used geoid model exceeded 2.5 m.

Reduction of orbital errors and other long wavelength effects (wavelength greater than 2000 km), which are of no interest in this

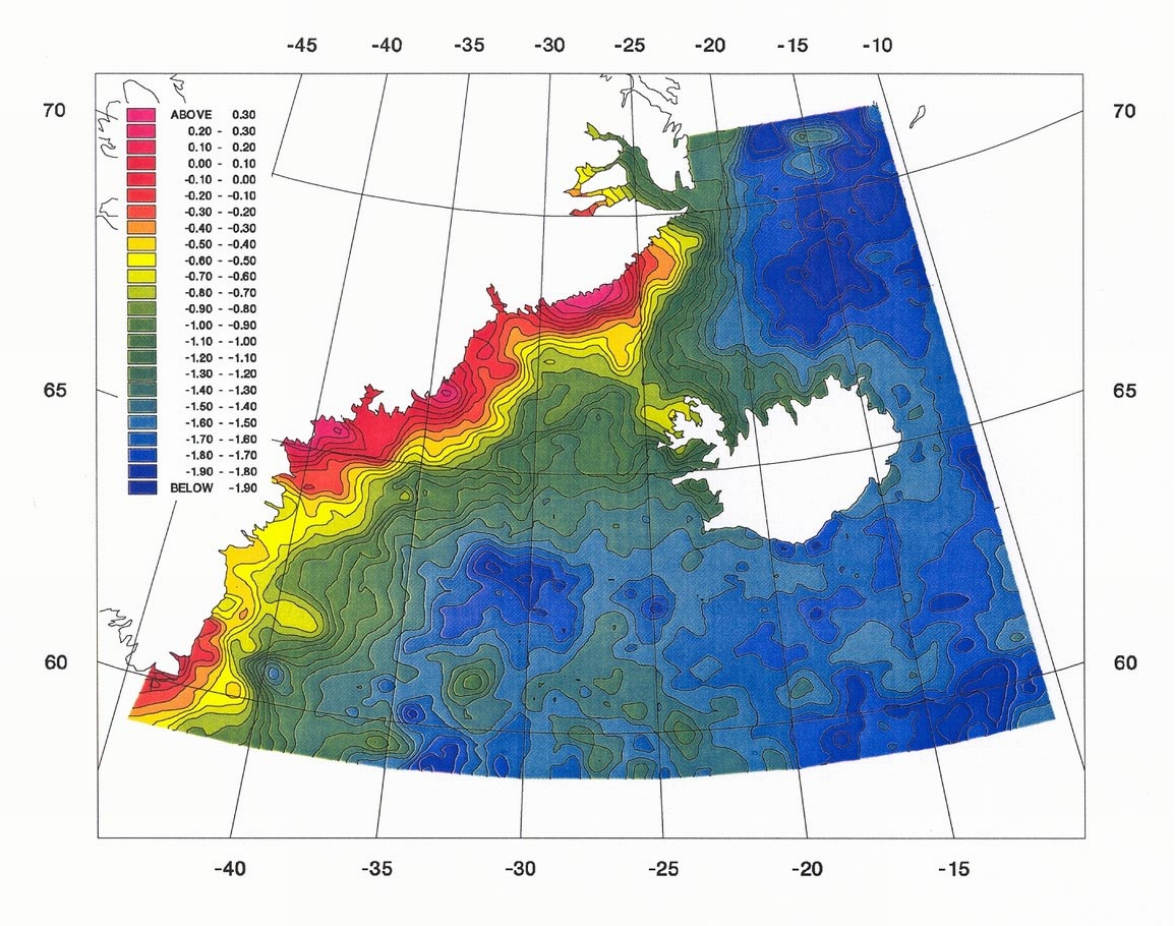

Fig. 17. 35 days mean dynamic topography from repeat 5 (Sept. 1992). Units are in meter and contours are every 0.1 m.

study, were performed using a bias/tilt cross-over adjustment analysis on the tracks from a single repeat (Knudsen, 1993). The orbit error spectrum for ERS-1 have been reported by Minster *et al.* (1992) showing dominant peaks at frequencies at 1 and 3 cycles per revolution, meaning that the errors will be observed as a bias between the ascending and descending tracks in the study area. In the cross-over adjustment analysis track related errors are estimated in order to minimize the track differences at the cross-over location using least squares adjustment. The result from the cross-over adjustment for repeat 5 using the Greenland geoid model GGEOID93B showed that the RMS of 681 cross-over differences was reduced from 0.242 m to 0.070 m. The removal of the estimated errors from 11671 observations resulted in a nearly unchanged mean sea surface (dynamic height) from -1.411 m to -1.417 m and in a reduction of the RMS value of the dynamic height from 0.445 m to 0.430 m.

Eighteen 35-days repeat raw mean dynamic topography maps were now ready for use. Unfortunately, large areas near the east coast of Greenland were covered by sea ice during most of the period the ERS-1 data were collected, resulting in low data coverage from this area. Unusual heavy ice conditions were observed in the area between Greenland and Iceland in fall 1993. In addition, a relatively high level of noise and small-scale features were observed in the raw mean dynamic topography. Figure 17 shows the 35 days raw mean dynamic topography relative to the

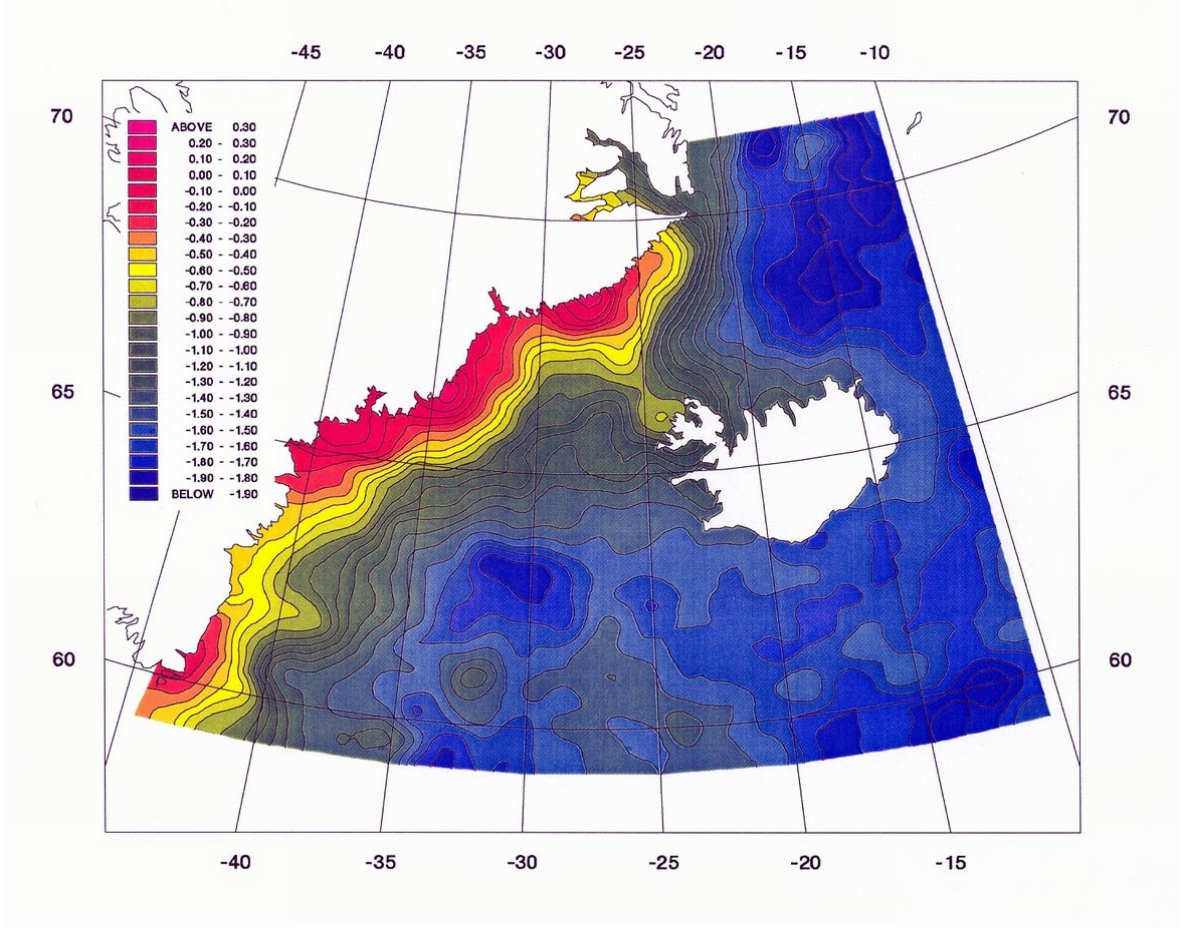

Fig. 18. 35 days mean "smoothed" dynamic topography from repeat 5 (September 1992). Units are in meter and contours are every 0.1 m.

geoid model GGEOID93B (see Chapter on choice of geoid model) for repeat 5 (September 1992).

For the coming discussions and modelling efforts it was therefore decided to reduce the noise level by smoothing and at the same time add extra points near Greenland. The choice was set by the altimeter and model constraints, the altimeter having difficulties resolving mesoscale eddies with size less than 60 km, in accordance with observations made by Le Traon *et al.* (1990) and Fu and Cheney (1995), and the numerical model's needs for dynamic heights estimates near Greenland. In order to smooth and add extra points to the single repeats the derived along-track values of the dynamic height were interpolated onto a 0.05×0.1 degree grid (ca. 5.5×5.5 kilometres) using local collocation including the 4×4 observations closest to the prediction point. The local collocation uses a homogenous and isotropic covariance model defined using the signal variance and the correlation length of the signal. A mean standard deviation of 10 cm and a correlation length of 250 km were used in the present case. The grid calculated were then interpolated onto a stacked data point set for repeat 1-18 (Figure 16) using spline interpolation involving the 4×4 observations closest to the predicted point.

Figure 18 shows the dynamic topography for repeat 5 after the smoothing process, which will be discussed in Chapter on Modelling. A much smoother field is obtained and mesoscale features and noise with length scale less than 50 km have been

removed by the smoothing process. In the following the resulting time series of 35 days mean "smoothed" dynamic topography will be used.

The programs used above during the calculation of the dynamic topography are all but one part of the GRAVSOFT package (Tscherning *et al.*, 1992).

RESULTS AND DISCUSSION/EVALUATION OF THE DYNAMIC TOPOGRAPHY DERIVED FROM SATELLITE ALTIMETRY

With the recent development in the fields of satellite altimetry and geoid models it has become feasible to test their ability to derive the dynamic topography and hereby the near surface circulation. For the present test altimeter data from the ERS-1 35 days repeat mission were used, due to its higher spatial resolution and northward extent compared to the more accurate TOPEX/-POSEIDON which turns at 66°N.

The ability of satellite altimetry to describe the near surface ocean circulation depends highly on the choice of geoid model. In the following four different geoid models are tested: OSU91A, GGEOID93B, GGEOID94A and GGEOID96A. OSU91A was briefly described above and the latter three are all later versions of the Greenland geoid model GGEOID92 described by Forsberg and Sideris (1993). In brief, the GGEOID92 is a detailed gravimetric geoid model of Greenland on a 5' x 10' (latitude, longitude) grid, where a 9-band fast Fourier transformation (FFT) has been used. The prediction is based on the OSU91A spherical harmonic

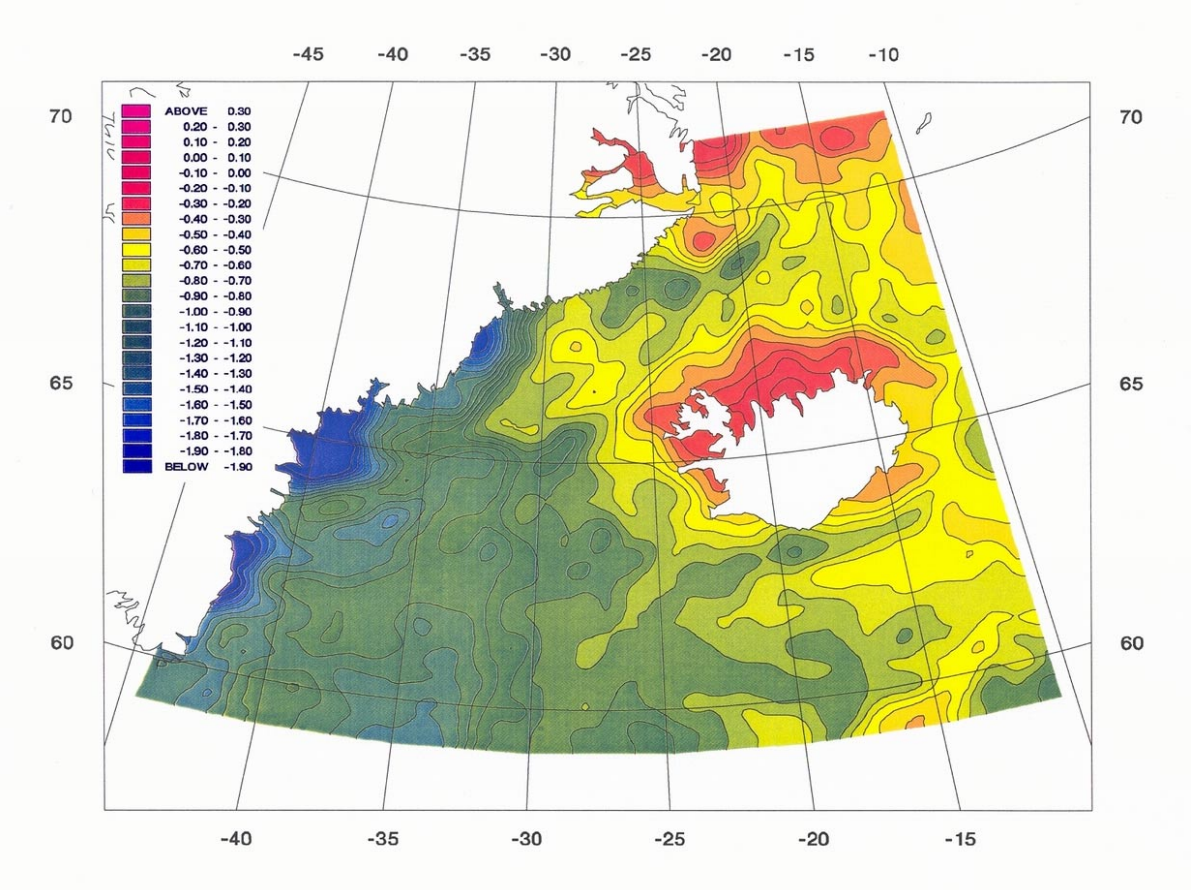

Fig. 19a Altimetric dynamic topography, derived with the use of OSU91A geoid model for repeat 5 (September 1992). Units are in meter and contours are every 0.1 m.

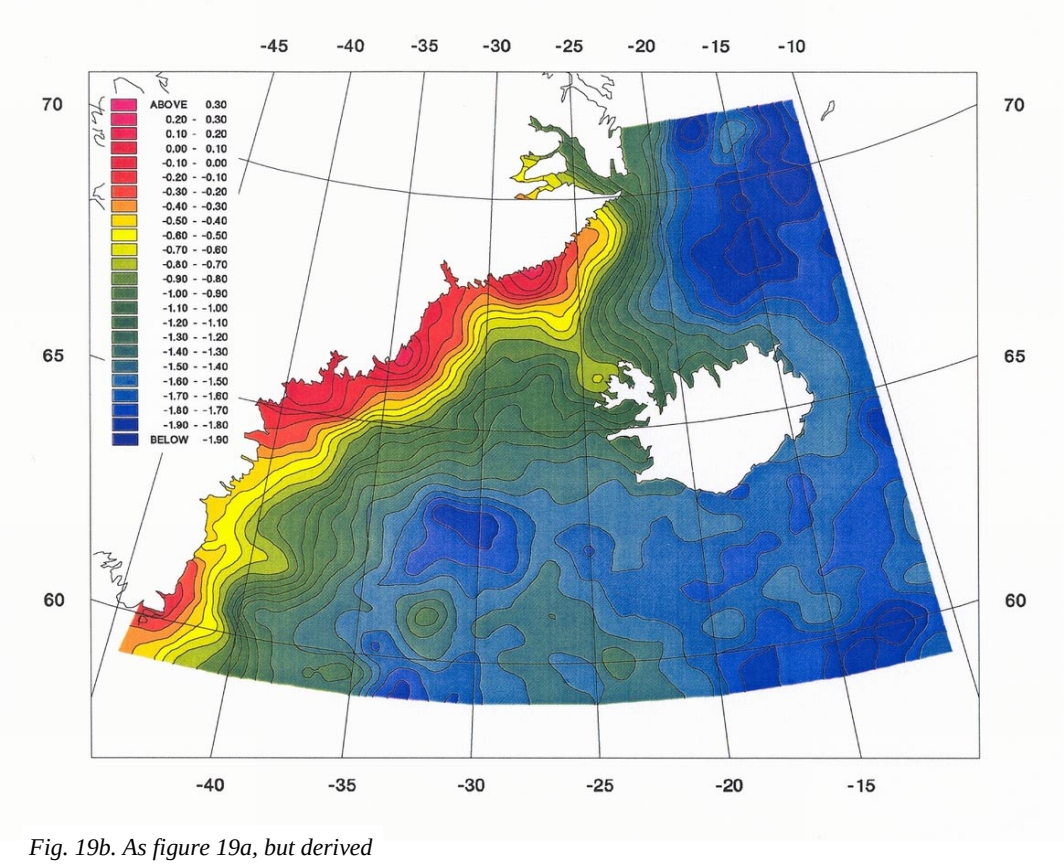

Fig. 19b. As figure 19a, but derived with the use of GGEOID 93B. Units are in meter and contours are every 0.1 m.

Fig. 19c. As figure 19a, but derived with the use of GGEOID 94A. Units are in meter and contours are every 0.1 m.

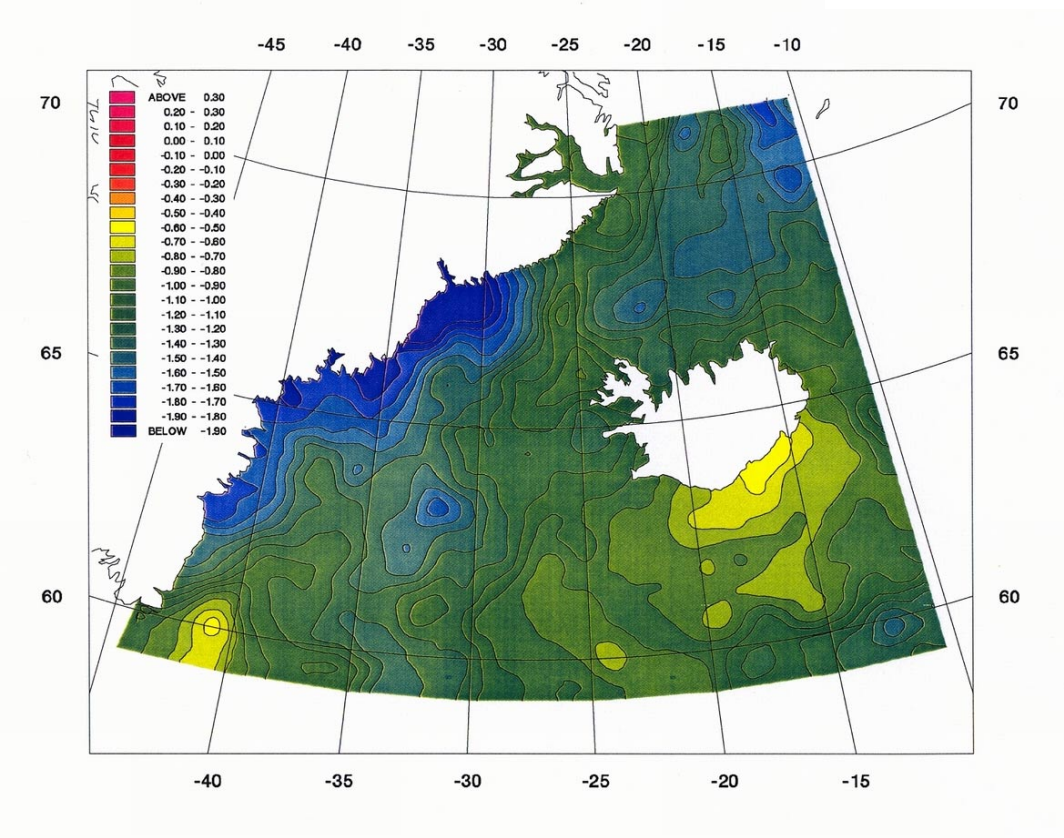

reference model, and all available gravity data gridded on a 5' X 10' grid, covering the area 59° - 84°N, 75° - 10°W. Over land there were additionally used a 5' Digital Terrain Model (DTM) of Greenland. The geoid model GGEOID93B is an updated version of GGEOID92, whereas GGEOID94A and GGEOID96A are later versions which both make use of additional data from airborne gravity surveys over Greenland in 1991-92 (Forsberg, personal communication 1996; Roman *et al.*, 1997).

Choice of geoid model

In the following an oceanographic argument will be given for the choice of the best geoid model, among the four models mentioned above. For the evaluation altimeter data from ERS-1 repeat 5 have been used as a reference data set, from which the dynamic topography is derived with use of the different geoid models, the calculations procedure are described above. Figures 19a,b,c show the altimetric derived dynamic topography for repeat 5 (September 1992) using OSU91A, GGEOID93B and GGEOID94A, respectively. The geoid model GGEOID96A is not drawn into the discussion, as it resembles the GGEOID94A to a high degree.

In order to get an first impression of the circulation, surface current speeds can be deduced from the slope of the dynamic topography using the geostrophic approximation. Where the magnitude of the current speed depends on the distance between the isolines and the direction is parallel to the isolines, having higher sea level to the right when looking in the flow direction, resembling the atmospheric flow around high and low pressure systems.

Comparing the satellite derived dynamic topography with in situ measurements in the interior of the ocean requires some consideration. It is clear, that the dynamic topography derived from hydrography yields only the baroclinic component connected to the density field, whereas altimetry (and also numerical models) yields the combined effect of the barotropic (connected to the surface elevation) and the baroclinic components. Utilizing the knowledge of the circulation compiled above it is possible to construct a first estimate of the sea surface topography. Direct current measurements in the Greenland Sea and on the border to the Iceland Sea (Fahrbach *et al.*, 1995; Mortensen *et al.*, 1991) all indicate that the barotropic mode dominates the flow in this area. Model studies of the Atlantic Ocean by Mellor *et al.* (1982) show similar results, however with a less dominating barotropic mode just south of Iceland, in the Irminger Sea and Iceland Basin. Making use of these observations, the geostrophic relation and the knowledge of the circulation, a coarse picture of the dynamic topography takes form. A distinct feature will be the East Greenland Current with its sea level sloping up towards the coast along Greenland, with its high speed core located above the continental slope. Two other, but weaker, features are supposed to be observed in the Irminger and Iceland Seas as local minima in the dynamic topography, indicating the cyclonic circulation in these Seas.

Inspection of the dynamic topography produced by the different geoid models in Figure 19 a,b,c, reveals that OSU91A and GGEOID94A are not able to reproduce the East Greenland Current, whereas GGEOID93B does. At the same time GGEOID93B shows evidence of cyclonic circulation in both the Irminger and Iceland Seas making it the most promising geoid model for the area at present time.

It is not surprising that the OSU91A fails to work in the area near Greenland, as very few gravity measurements existed from this area when it was produced. However, near Iceland where gravity measurements are dense the model seems to work surprisingly well, when compared with surface drifter tracks (Valdimarsson, 1998; Valdimarsson and Malmberg 1999). A finding which could be used when detailed studies are carried out in near Icelandic Waters.

GGEOID94A, an updated version of GGEOID93B, which includes new airborne gravity data over Greenland, was supposed to improve the geoid determination near Greenland significantly. Instead, as Figure 19c indicates, it was a major drawback. Probably a very small bias at the ~1 mgal level are inherent in the airborne gravity data set, giving rise to the distortion of the geoid model near Greenland.

The GGEOID93B derived dynamic topography reveals, as mentioned above, the large-scale current system of the region (Figure 19b), with the southward flowing East Greenland Current and the cyclonic gyres in the Iceland and Irminger Seas.

Evaluation of the dynamic topography derived with the use of the GGEOID93B geoid model

The dynamic topography derived by the geoid model GGEOID93B (Fig. 19b) will in the following be evaluated with existing observations and model results from the area. Due to the lack of quasi synoptic observations the evaluation will bear the impression of a quantitative analysis.

Compared with model derived dynamic topography by Mellor *et al.* (1982), Aukrust and Oberhuber (1995), and Heburn and Johnson (1995) a reasonably good agreement is found, although a number of characteristic differences are observed. The most pronounced differences are found in the spatial variation of the dynamic height associated with the East Greenland Current. There for example the models normally observe height variations in the ranges of 0.5 - 0.8 m from the interior of the Irminger Sea to the coast of Greenland, compared with ~1.4 m calculated by the altimeter in Figure 19b. Some of this discrepancy can probably be explained by the extrapolation routine (local collocation) used in the case of missing points near Greenland, which tends to overestimate the dynamic heights in these points. However, uncertainties in the geoid model cannot be ruled out. Neither can it be ruled out, that the models referred to above are giving a wrong picture of the circulation and thereby an underestimate in the range, depending on initialization and data used. Another distinct difference is observed south of Iceland in the Iceland Basin. Models often show a gentle slope of the sea surface upward to the

east in this area, whereas the altimeter derived sea surface is of a variable type with no tendency to slope upward to the east.

An indirect estimate of the dynamic topography derived from hydrography has not been possible due to the very complex bottom topography in the area, which makes it impossible to choose a reference level deep enough for a comparison. Instead dynamic topography relative to the 200 dbar level was calculated using hydrography, Figure 15. Compared with the altimetry there is a remarkable resemblance in the Denmark Strait, especially above the East Greenland continental shelf, although much lower sea surface slopes are observed in the case where the dynamic topography is derived from hydrography. Given the limited use of comparing the dynamic topography with model results and hydrography, as mentioned above, another method must be considered.

This method makes use of the geostrophic relation, current meter measurements and drift path of surface drifters. Using the geostrophic relation, the geostrophic surface velocities can be calculated from the spatial gradients of the dynamic topography (ζ) as:

$$u(\varphi,\lambda) = \frac{-\gamma}{f \cdot R}\frac{d\zeta}{d\varphi} \tag{3}$$

Fig. 20. Distiribution of geostrophic surface currents inferred from dynamic topography derived from altimetry in September 1992 (repeat 5), (50 cm/s at 64°N; 19°W).

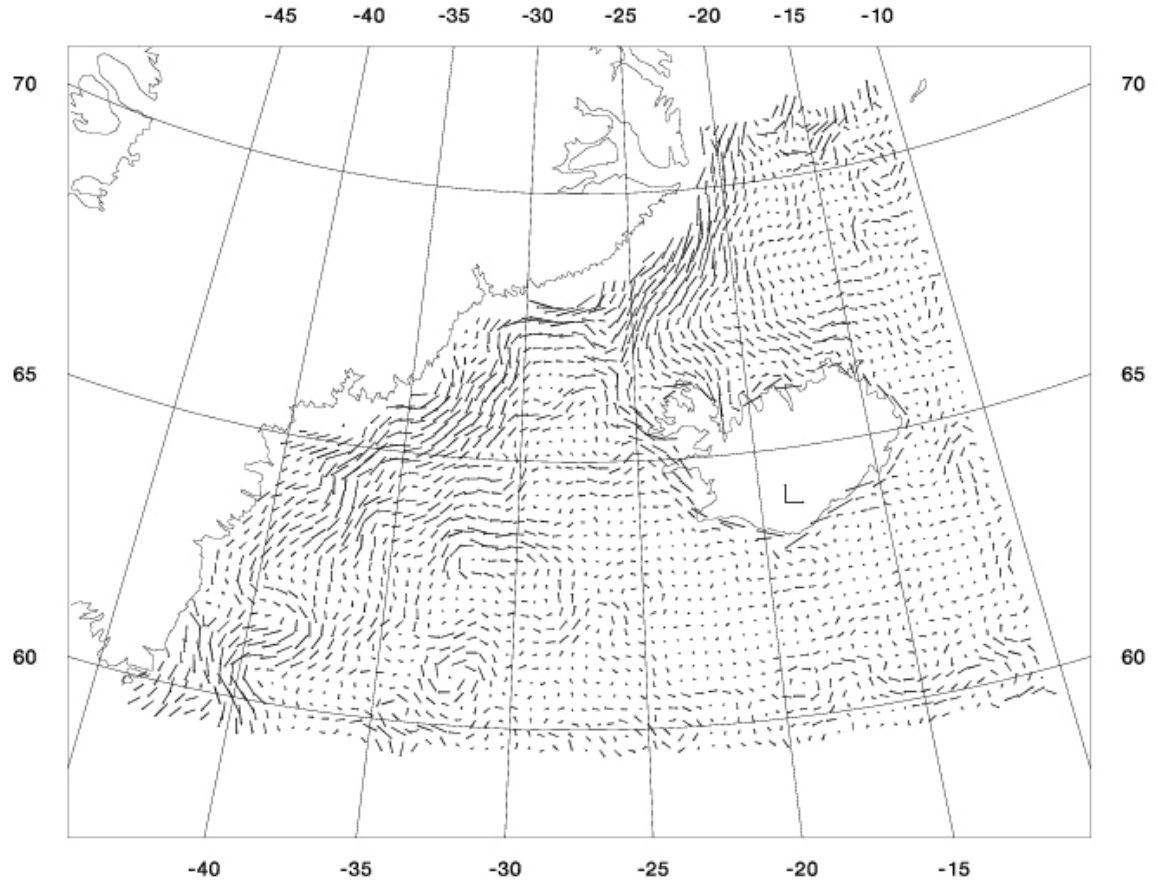

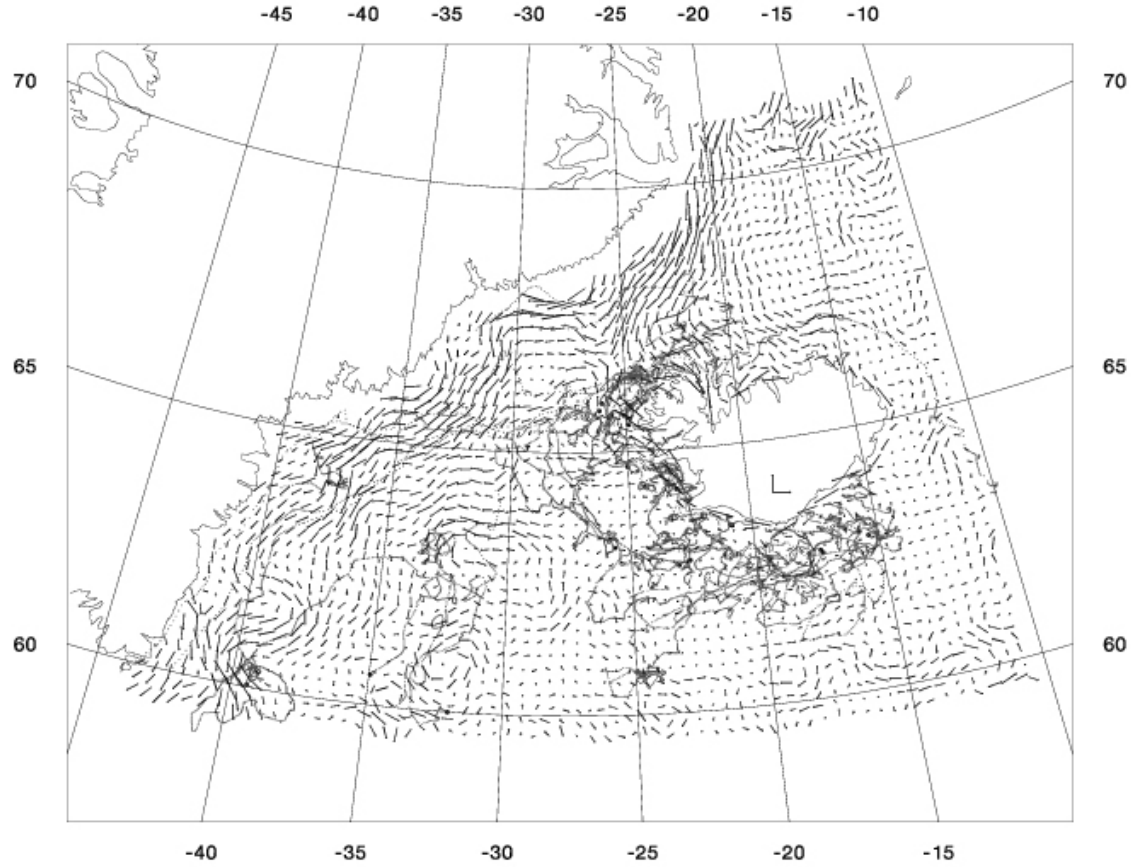

Fig. 21. Distributions of geostrophic current inferred from dynamic topography derived from altimetry in September 1992 (repeat 5), (50 cm/s scale at 64°N; 19°W), and trajectories of near-surface drifters deployed by MRI south and southwest of Iceland in 1995. Thick dots indicate deployment sites.

$$v(\varphi,\lambda) = \frac{\gamma}{f \cdot R \cdot \cos(\varphi)} \frac{d\zeta}{d\lambda} \qquad (4)$$

where $f = (2\omega_e sin\varphi)$ is the Coriolis parameter, γ is the normal gravity and R the radius of the earth. A 0.25 x 0.50 degree grid (latitude (φ), longitude (λ)) consisting of geostrophic velocity vectors were calculated from the spatial slope of the dynamic topography using local collocation, in each central point of each grid cell of the dynamic topography, from the four spatial gradients surrounding this point. The calculated velocities were afterwards subjected to a filter which removed land and erratic points related to the extrapolation used during the processing of the altimeter data. Additionally, all points having velocity greater than 100 cm/s were removed. The results of the calculated geostrophic surface velocities are shown in Figure 20.

Not unexpected, the most prominent feature is the East Greenland Current on its way south along the coast off Greenland, with calculated speeds in the range from 20 cm/s to 80 cm/s. An interesting observation is the westward turn of the current at around (67°N, 25°W), which is also observed in hydrographic data from the same period by a Nordic WOCE cruise (RV Bjarni Sæmundsson, Sept. 1992). During the same cruise, a descending ERS-1 track was followed by high resolution hydrography measurements, 1 nm apart, over a distance of 16 nm.

The Iceland Sea is, as supposed, characterised by a cyclonic circulation super-imposed an eddy field, with speeds in the range 0

cm/s to 30 cm/s, with a remarkable resemblance to surface drifter results reported by Poulain *et al.* (1996). A stronger velocity field is observed in the Irminger Sea with speeds in the range 0 cm/s to 50 cm/s. The overall circulation is cyclonic, however an anticyclonic and cyclonic circulation seems to exist in union in its interior. The weakest current velocities are observed to the south of Iceland in the Iceland Basin. This is surprising according to earlier observations, but not unexpected due to recent published measurements by Otto and van Aken (1996), Krauss (1995) and Valdimarsson and Malmberg (1999). Similarly to their findings, the calculated current field is observed to be erratic and dominated by eddies. Speeds are found to be less than 20 cm/s in most of the area.

What makes this current field derived from altimeter data interesting, and even unique, is the quasi synoptic time scale and the richness at detail which can be observed compared with a relatively poor data set of direct current measurements in the investigated area.

Superimposing the altimeter derived surface velocity field from September 1992 with trajectories of satellite tracked surface drifters 1995 (Valdimarsson, 1998), Figure 21, brings the overall circulation into a completely new perspective: The complex paths taken by the drifters are seen to be remarkably well described by the altimeter derived velocity field.

In the Irminger Sea there is a surprising agreement between the areas where eddies dominate the trajectories and the observed anti- and cyclonic gyres by the altimetry, although three years separate the two data sets. Similar conditions are observed in trajectories of drifters deployed by Krauss (1995), indicating that these features have permanent character. An interesting feature which is observed by the altimetry and both drifter data sets is the "cyclone" located at ca. (60°N, 40°W), which acts as a convergence point.

In the Iceland Basin low mean velocities overlaid by an eddy field are observed by both drifters and the altimetry. In their study Otto and van Aken (1996) report drifter results from the southern part of the Iceland Basin, which show temporal variation in both the mean flow and the eddy statistics. Transient eddies were observed with scalar velocities well above 20 cm/s. An unanswered question not revealed by the drifters of Otto and van Aken (1996) and Krauss (1995) is the origin of the Atlantic Water in the Irminger Sea. Otto and van Aken (1996) suggest that it is most likely a separate northeastward extension of the North Atlantic Current which exists west of the Reykjanes Ridge. However, both the altimeter derived surface velocity field and the MRI drifters indicate that a significant westward transport of Atlantic Water across the Reykjanes Ridge takes place just southwest of Iceland. Hydrographic data support this, as temperatures and salinities observed in the Denmark Strait are too high to be explained only by a northeast ward flow west of the Reykjanes Ridge.

When it comes to the flow immediately north of Iceland the resemblance between the two fields become less pronounced. Less is known about the dynamics of this region, however the

Table 3. Regional altimeter mean current for zonal (u) and meridional (v) components, speed and number of points which enters the calculation of the regional mean current in cm/s for the five sub-areas.

	u	*v*	Speed	n
EGC-N	-14.6	-40.0	42.6	92
EGC-S1	-25.3	-20.9	32.8	118
EGC-S2	-11.4	-22.1	24.9	35
EGC-S3	-25.6	-27.3	37.4	12
SI	-1.9	-1.1	2.2	419

Table 4. Regional drifter mean current for zonal (u) and meridional (v) components and speed in cm/s for the sub-areas.

	u	*v*	Speed
EGC-S1[1]	-10.5	-10.3	14.7
EGC-S1[2]			23.5*
EGC-S1[1]			~60.0*
EGC-S2[1]	-8.7	-25.5	26.9
EGC-S2[2]			65.9*
EGC-S3[1]	-7.1	-10.2	12.4
EGC-S3[2]			73.6*
SI[1]	-0.7	-0.1	0.7
SI[3]	0.8[s]	2.6[s]	2.7[s]
SI[3]	-0.9[w]	-0.5[w]	1.0[w]

[1] Preliminary Icelandic data (Valdimarsson, personal communication, 1997). Total of 61 drifters, deployed in the period 1995-1996.

[2] Krauss (1995). Total of 20 drifters, deployed in the 1988.

[3] Otto and van Aken (1996). Total of 19 drifters, deployed in the period 1990- 1991 and 1993.

* Maximum mean current vector found by the drift of a single drifter within the region.

[s] Summer estimate.

[w] Winter estimate.

shallowness and the presence of the Polar and Arctic Fronts in the area throw doubt on the reliability of the geostrophic relation used during the calculation of geostrophic velocities from altimetry. The path taken by one drifter indicates that some of the difference can probably be explained by the local wind condition. During a northerly storm one drifter was observed to take a westward path for later to join the East Greenland Current. The trajectory and current meter measurements indicate that the mean surface current field in the region can be distorted for longer periods due to such storm events.

Due to the preliminary state of the MRI drifter data set in 1997, it was not possible to make a thorough statistical analysis of the two velocity fields. However, a few estimates of current velocities derived from drifters existed from the region. These velocities are normally given in geographical “bins” of adequate size, following the lines proposed for WOCE. For convenience of comparing, the altimeter derived velocity field was subdivided into areas from which velocity estimates already existed. The mean current vector is estimated in each region by the spatial mean.

For the regional subdivision, five areas were defined: (i) The East Greenland Current north of the Denmark Strait (EGC-N), 68°-70°N, 30°-18°W. This region covers the East Greenland

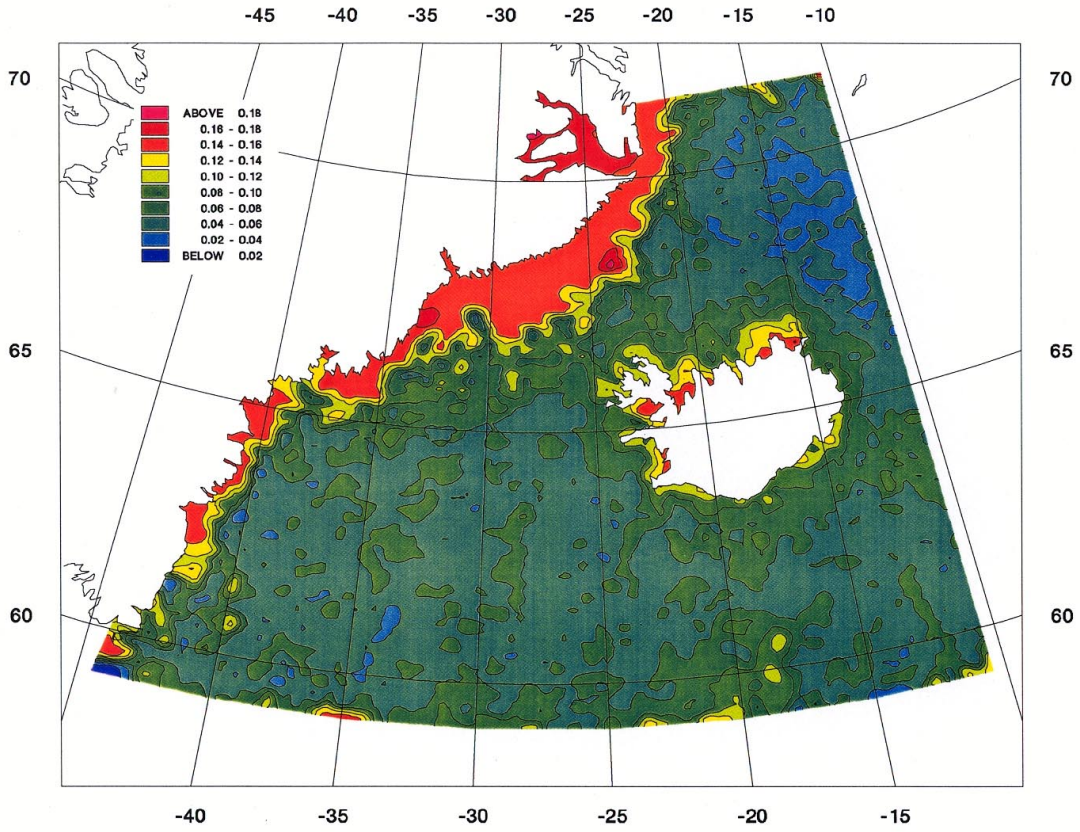

Fig. 22. Mesoscale variability calculated for the period October 1992 - September 1993. Contour interval 0.02 m.

Current just north of the sill in Denmark Strait; (ii) The East Greenland Current south of the Denmark Strait (EGC-S1), 63°-65° N, 42°-33°W. This region is characterized by a wide continental shelf of approximately 220 km, with the cold water of the EGC located on the shelf and joined on the shelf break by warm water of the Irminger Current; (iii) The East Greenland Current south of the Denmark Strait (EGC-S2), 61°-62°N, 43°-38°W. In this region the extension of the continental shelf has decreased to 55 km, the configuration of currents are the same as in (ii); (iv) The East Greenland Current south of the Denmark Strait (EGC-S3), 59°-60° N, 43°-40°W. The continental shelf has in this region decreased additionally to only 30 km, the configuration of currents are the same as in (ii); (v) The region south of Iceland (SI), 60°-63.5°N, 28°-13°W. In this region the circulation and transports was in 1997 still a matter of dispute (Otto and van Aken, 1996).

Since then further research with surface drifters in the area has strengthened the circulation scheme in the Iceland Basin (Valdimarsson, 1998; Valdimarsson and Malmberg, 1999).

The regional altimeter mean values of the current component for the above defined sub-regions are listed in Table 3. The main points of these findings are the strong East Greenland Current and the weak west-southwesterly current in the region south of Iceland. The strong East Greenland Current observed north of the Denmark Strait sill is seen to continue to the south with nearly the same strength after joining the Irminger Current, showing minor variations along its southward path towards Cape Farewell.

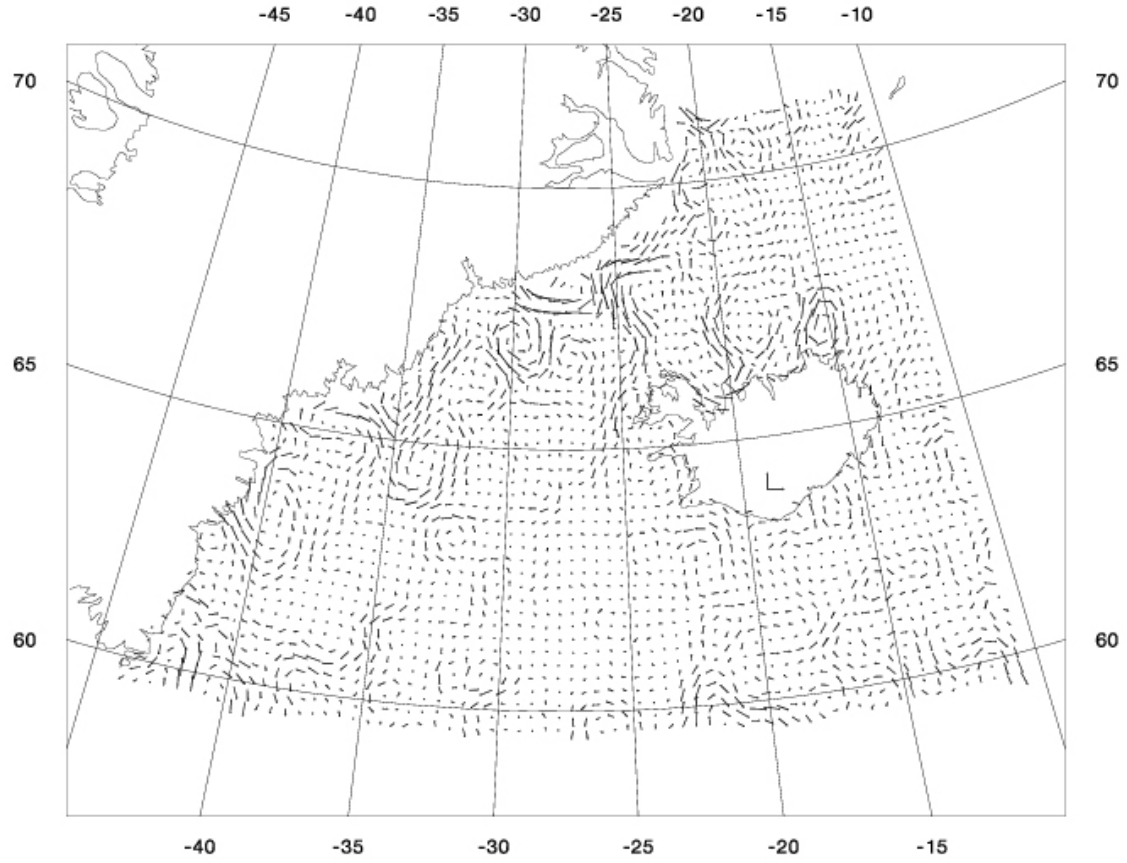

Fig. 23. Velocity variations calculated as the difference between the velocity fields of repeat 4 and 5 (20 cm/s scale at 64°N; 19°W).

The regional drifter mean values of the current derived by different authors for the defined sub-regions are listed in Table 4. Taken into consideration the variability which exists in the region, there is found a remarkable resemblance between the altimeter and drifter derived mean currents in the regions EGC-S2 and SI. For the two other sub-regions in the East Greenland Current south of the Denmark Strait the altimeter derived mean currents are generally higher than those derived by the drifters. However, the altimeter values are well below the maximum values derived by a single drifter passing the region.

In order to get a better understanding of the variability of the region, the mesoscale variability have been calculated using the sea surface height variability. Figure 22 shows the mesoscale variability for a one year period from the 35-days repeat mission (October 1992 to September 1993). The highest variability are associated with the continental shelves, the ridge system between Greenland and Scotland, and the deeper parts of the Iceland Basin west of the Rockall Plateau. Notice, that near to Greenland the number of points which enters the determination of the standard deviation are too few to make a valid estimate of the variability. The findings in the Iceland Basin are in agreement with eddy kinetic energy observations obtained by Heywood *et al.* (1994), and Otto and van Aken (1996). In oceanographic studies, the eddy kinetic energy (EKE) derived from altimetry is more informative than the mesoscale variability derived from sea surface heights. This is because the EKE takes the sea surface slope on eddy scales,

i.e. the vertical motion of adjacent points, into account. However, it has a major weakness associated with the changes in the mean current field and mesoscale current patterns which are under influence of topography. A sudden change in the mean current field (i.e. transport) e.g. of the East Greenland Current will, by the eddy kinetic energy scheme used up to now, be interpreted as a change in the eddy field. The eddy kinetic energy is normally obtained as the variance of eddy velocity, disregarding the phase changes. Hence, topographically steered eddies, which are of more stationary character, will not show up in altimeter derived eddy fields. In order to obtain a more detailed information of the eddy kinetic energy field, future schemes should take into consideration these phase changes. One possible way could be to make use of the velocity variability between the single repeats. Figure 23 shows an example of the velocity variation which can be obtained between two repeats, here given as the difference between repeat 4 and 5. The Figure gives a good impression of the magnitude and location where variations have taken place during a 35 days period. A feature, which is likely to be linked to the variation in the mean field, is observed just west of Iceland in the Denmark Strait, seen as a elongate “current” emanating from the East Greenland Current and continuing southward along the Icelandic shelf. The situation possibly arise as a strengthening of the East Greenland Current with a subsequent weakening of the northward transport of the Irminger Current. The discussion will be left here, and handed over to future study.

From the discussion above it can be concluded that the dynamic topography derived with the use of geoid model GGEOID93B is capable of reproducing many of the observed current features in the region, using the geostrophic assumption. The geoid model GGEOID93B is therefore the best choice at present. However, unsolved problems connected to the north Icelandic shelf and the high velocities observed in the East Greenland Current still exist. There is no doubt that some of the problems observed in the East Greenland Current can be ascribed to inaccuracies in the geoid model and to the lack of valid altimeter points near Greenland, caused by sea ice.

ERS-1 35 days mean dynamic topography evaluated against tide gauge and TOPEX/POSEIDON sea level

The following analysis is intended as a quantitative check on the time-variable ERS-1 35 days mean dynamic topography for further use in the modelling. The question is: Can the 35 days mean dynamic topography time series (represented by 18 repeats) in its present form to a certain degree of accuracy describe the timing and ranging of the sea level variations observed by the TOPEX/POSEIDON (T/P) altimeter and tide gauge sea levels? In this connection it must be remembered that every time step in the ERS-1 derived time series is derived on the basis of data from a 35 days period (i.e. data from one repeat).

For the analysis, a tide gauge and two T/P altimeter cross-over points were used. The tide gauge time series is from Reykjavik Harbour (64.15°N, 21.93°W), a coastal shallow water station with

records covering the period from January 1992 to December 1994. Hourly sea level measurements were prior to the analysis averaged into a daily mean sea level. The tide gauge record is in the following not connected to a benchmark, instead the relative sea levels will be related to the time mean over the observation period which are useful for the intercomparison with altimeter data. Two T/P altimeter cross-over points are considered. The first cross-over point is located on the Icelandic continental shelf (~64.25°N; 24.17°W) near to the tide gauge. The distance between the two location is approximately 100 km and the water depth of the T/P point is in the range of 200 m to 400 m. The other cross-over point is located south of Iceland (~61.98°N; 19.82°W) over deep water (1600-1800 m). T/P geophysical data records from AVISO were selected for the two cross-over points for repeat 1 to 86 covering the period October 1992 to January 1995. Prior to use, the altimeter data were corrected for geophysical effects applying the geophysical corrections supplied with the geophysical data records (GDR-M). The Andersen/Grenoble ocean tide model version AG95.1 were used for the corrections of ocean tides, following the same methodology of ERS-1 initial data processing as described in Chapter on data and methods. The accuracy of a single-pass sea surface height measurement is specified to be 4.7 cm (given as root-sum-square value) (Fu *et al.,* 1995) of which orbit errors constitute 3.5 cm making it unnecessary to correct for orbit errors. With a repeat cycle of 10 days for T/P two observations are obtained in cross-over points every 10 days.

In the following the model input ERS-1 35 days mean dynamic topography data time series are validated. Two model points are used in the validation, both of them selected such that they are less than 20 km from the nearest T/P cross-over point. The first point (18,21 or 64.25°N, 24.02°W) is located at the T/P cross-over point nearest to Reykjavik Harbour. The other point (28,8 or 61.97°N, 20.08°W) is located near to the T/P cross-over point south of Iceland over deep water.

Before comparing ERS-1 sea levels with tide gauge and T/P derived sea levels, the T/P altimetry is compared with in situ sea level data from Reykjavik Harbour. Similar comparisons have been performed in the equatorial Atlantic Ocean (Verstraete and Park, 1995) and in the Indian Ocean (Park and Gamberoni, 1995). Both works found a RMS difference within 2.2 cm between the T/P data and the in situ sea level when filtered for effects with a period of less than 60 days.

Comparison of T/P and Tide gauge sea level time series Low-Passed at 35 days

The comparison differs in three major aspects from the analysis of Verstraete and Park (1995) and Park and Gamberoni (1995). Firstly, they use a spatial average (2° along track) to remove high-frequency fluctuations, whereas this comparison use a single cross-over point without any spatial averaging. Secondly, they use the so-called adjusted sea level (ζ-ζ_a) where the altimetric sea level ζ has been corrected for the inverse barometer effect ζ_a. In the present case the altimetric sea level ζ is used instead. The reason

owes to the fact that the tide gauge is of the classical kind with a float and therefore responds to the atmospheric pressure variations. Thirdly, 35 and 90 days Gaussian low-pass filters were used instead of 30 and 60 days.

Both the T/P and the tide gauge time series are irregular in time and contains high-frequency fluctuations of periods less than 10 days. For T/P because of the mixing of two tracks. In order to get a platform for comparing T/P and tide gauges sea levels with ERS-1 sea levels a smoothed time series, interpolated at regular time intervals using a successive correction scheme with a Gaussian filter were adapted from Park and Gamberoni (1995).
The scheme is described by the formula

$$H(t, p+1) = H(t, p) + \sum_{i=1}^{n} w_i(t)[\zeta_i - H_i(p)] / \sum_{i=1}^{n} w_i(t) \qquad (5)$$

where $H(t,p)$ is the interpolated value at time t from the pth iteration, ζ_i is the observed sea surface height at time t_i, $H_i(p)=H(t_i, p)$ is the estimate of from the pth iteration. The Gaussian filter is given by the weight function

$$w_i(t) = \exp\left[-(t - t_i)^2 / 1.44T^2\right] \qquad (6)$$

where T is the timescale. The number of iterations depend on the convergence criteria which was set to 0.4 cm. The response function of the Gaussian filter has a cutoff period near T and a half-amplitude pass near $2T$.

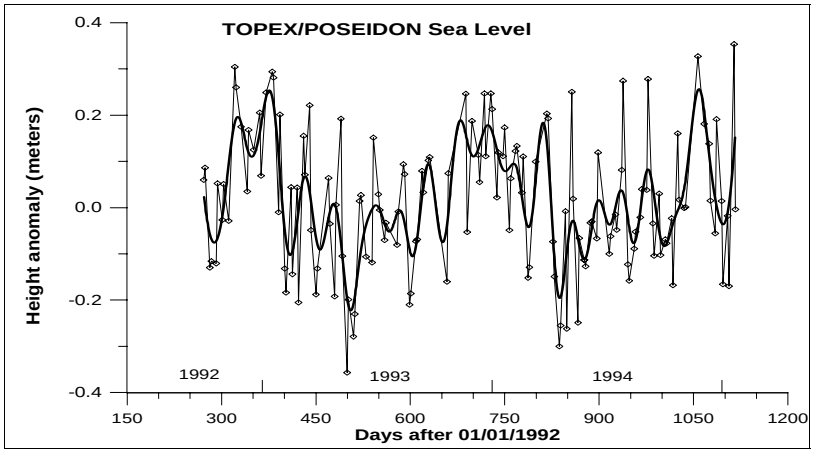

Fig. 24. T/P sea level time series computed in the cross-over point nearest to the Reykjavik harbour tide gauge. The superimposed smooth thick solid curve was computed using a 35-days Gaussian filter.

Figure 24 shows the smoothed altimetric time series at 1-days intervals obtained with T equal to 17.5 days along with the raw time series. High-frequency fluctuations of periods much less than 35-days half-amplitude pass window are seen to have been removed, while signals of longer periods are well preserved without any deformation of phase. A phase-preserving interpolation scheme is of importance in a comparison of two different sets of time series. The most noticeable feature in the smoothed T/P altimetric time series are the oscillations of sea level with periodicity in the interval about 50-70 days superimposed on the dominant low-frequency variation.

Figure 25a shows the comparison of the 35-days low-passed T/P and the tide gauges derived time series at Reykjavík harbour,

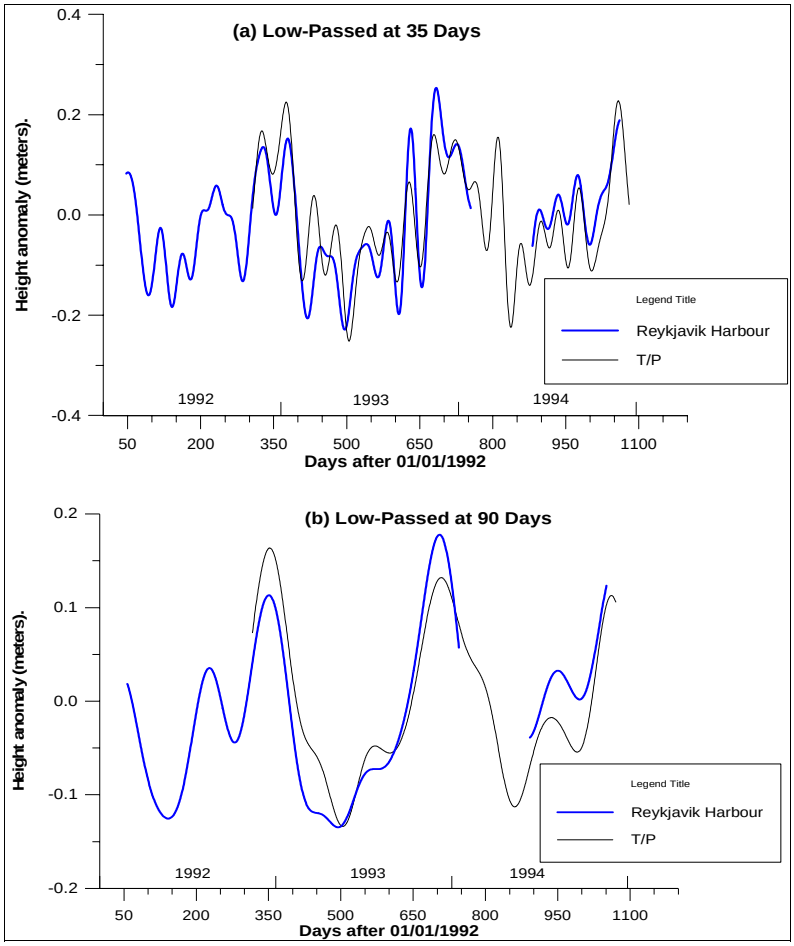

Fig. 25. Comparison of Sea level time series from T/P altimetry in the cross-over point nearest to Reykjavik and tide gauge records at Reykjavik harbour. Data low-pass filtered using a) a 35-days and b) a 90-day Gaussian filter.

with a 25-month period of overlapping from October 1992 to December 1994. Note that each time series has been centred about their respective mean sea level over the 25 months of overlapping and the lack of tide gauge data for a two months period in 1994. The low-frequency and even the high-frequency sea level signals seen in the tide gauge data are remarkably well represented in the altimetric time series, in particular in the range and timing of short period sea level variation. One must remember that the two observation points are separated by a distance of ~100 km, and that they represent respectively a coastal station and a continental shelf point, having very different dynamic conditions. Further note that there is a lack of T/P observations in the period day 620 to 700 probably resulting in a less pronounced maximum in late 1993. The RMS difference between the two time series is 6.2 cm with a correlation coefficient of 0.83. This is an unexpected high RMS value compared with the results found by Verstraete and Park (1995) and Park and Gamberoni (1995). For example Verstraete and Park (1995) found a RMS difference of 2.4 cm with correlation of 0.87 in the equatorial Atlantic, based on a 30-day Gaussian window. The high RMS value found in the present case was suspected to be mainly the result of the tidal aliasing, due to imperfectly removed short-period tides, which is connected to the sampling rate of T/P, and to the use of only a single cross-over point, instead of using a noise reducing spatial average scheme.

Tidal alias periods for T/P can described using the formula given by Parke *et al.* (1987),

$$\tau = \left| 2 \cdot \pi \cdot P / \Delta \phi \right| \tag{7}$$

with

$$\Delta\phi = 2 \cdot \pi \cdot P / T \qquad -\pi < \Delta\phi < \pi \tag{8}$$

where τ is the alias period, P (= 9.9156 days) is the repeat cycle period of T/P, $\Delta\phi$ is the tidal phase change (defined within the range $\pm\pi$) over the period P, and T is the period of a given tidal constituent. In Table 5 the alias periods for the eight most prominent major diurnal and semidiurnal constituents are shown, along with available RMS errors obtained in a comparison with 65 tide gauge readings in the Northwest European shelf region for each of these tides from the AG95.1 model (Andersen *et al.*, 1995).

In order to remove the possible tidal aliasing it was decided to apply a 90-days Gaussian filter on the data sets. Figure 25b shows a comparison with the same 90-days Gaussian window applied to both the T/P and tide gauge sea level times series. The tide gauge record is clearly characterized by a seasonal signal in the three year period, represented by two sea level maxima in August and December and two minima in May-June and October. Although the "secondary" maximum and minimum is less pronounced in 1993. A ten year long time series from the eighties reveals that the seasonal description by two minima and maxima are characters which are usually found at the tide gauge. However the "secondary" minimum and maximum are over most of this period characterized by amplitudes which are similar to the primaries and their timing varies from the above mentioned, indicating that changes have taken place in the seasonal sea level pattern since the eighties. The low-frequency sea level variations in the nineties are observed to be in good agreement with the local low-frequency pressure field, but the steric sea level variations, which are believed to have minimum in March-April and maximum in September, are difficult to distinguish. The much stronger pressure signal overshadows the weak steric signal. The tide gauge shows a 360-day signal with an amplitude of about 14 cm during the 27 months of measurements. This signal is well reproduced by T/P altimetry, although there seems to be a trend and phase change between the two data sets. The phase change (10-20 days) can possibly be explained by the different sampling rate of the two data

Tide	Tidal Period hours	Alias Period days	Model Tide Error cm
O1	25.819342	45.7	0.70
N2	12.658348	49.5	
S2	12.000000	58.7	2.23
M2	12.420601	62.1	3.23
Q1	26.868357	69.4	
K2	11.967235	86.6	
P1	24.065890	88.9	
K1	23.934470	173.2	1.29

Table 5. T/P tidal alias periods for eight major diurnal and semidiurnal constituents, RMS errors in the Northwest European shelf region AG95.1 tides.

sets, whereas the observed trend was suspected to be introduced by local difference in the long period sea level variations between the two points. The RMS difference between the two time series is 4.0 cm with a correlation coefficient of 0.90.

Compared with results of Park and Gamberoni (1995) based on a shorter period (October 1992 to July 1993), RMS difference of 1.9 cm with a correlation coefficient of 0.80 using a 60-days Gaussian filter are found, showing no trace of a trend. Opposite, Verstraete and Park (1995) finds for a little longer period (October 1992 to December 1993) a RMS difference of 2.2 cm and a correlation coefficient of 0.88 using the same 60-days Gaussian filter, which indicates a trend between the two time series.

Performing an analysis similar to the above two described periods using instead a 90-days Gaussian filter, one observes, for the period October 1992 to July 1993, a RMS difference of 2.4 cm and a correlation coefficient of 0.97 and for the period October 1992 to December 1993 a RMS difference of 3.6 cm with a correlation coefficient of 0.94. The results show a pronounced deterioration of the RMS difference and the correlation coefficient with time. The tide gauge was inspected carefully. The authorities in Reykjavik Harbour were contacted and the status of the tide gauge was checked. The tide gauge had been routinely checked on weekly basis and had been found functioning properly most of the period, although a hole in the well was observed at the end of April 1994 resulting in rejection of data records from that day and back to a more thorough check of the tide gauge 2 months before, explaining the lack of data from this period. The overall performance of the tide gauge in the period 1992-1994 is therefore high.

Some of the difference observed between the two time series in late 1993 are likely to be explained by the lack of T/P observations from the period day 620 to 700 resulting in a less pronounced maximum. However the observed difference in 1994 cannot be explained by lack of T/P measurements. A number of theories were considered, in order to explain the observed trends between the two time series, ranging from coastal wave setup, Kelvin waves to long period tides. In July 1996, the solution to the problem was found, with the announcement by the TOPEX group at NASA's Jet Propulsion Laboratory of the discovery of an error in the TOPEX algorithm which corrects for oscillator (clock) drift. The error was observed to give a shorter range estimate with time after mid 1993, with reported drift rates of about 10 mm per year, i.e giving rise to an increasing sea level, which prior to the error discovery was interpreted as a fast global sea level rise of about 6 mm per year by a number of sources. New corrected T/P altimeter data have not been drawn into this analysis, as it is believed that the correction will not change the results of the following comparison significantly. Further the comparison period is limited to 1992 -1993.

The conclusion drawn from the above analysis is similar to others (e.g. Verstraete and Park, 1995): T/P derived altimetric sea level anomalies is of a high quality when used on timescales greater than 35-days with a precise tide model.

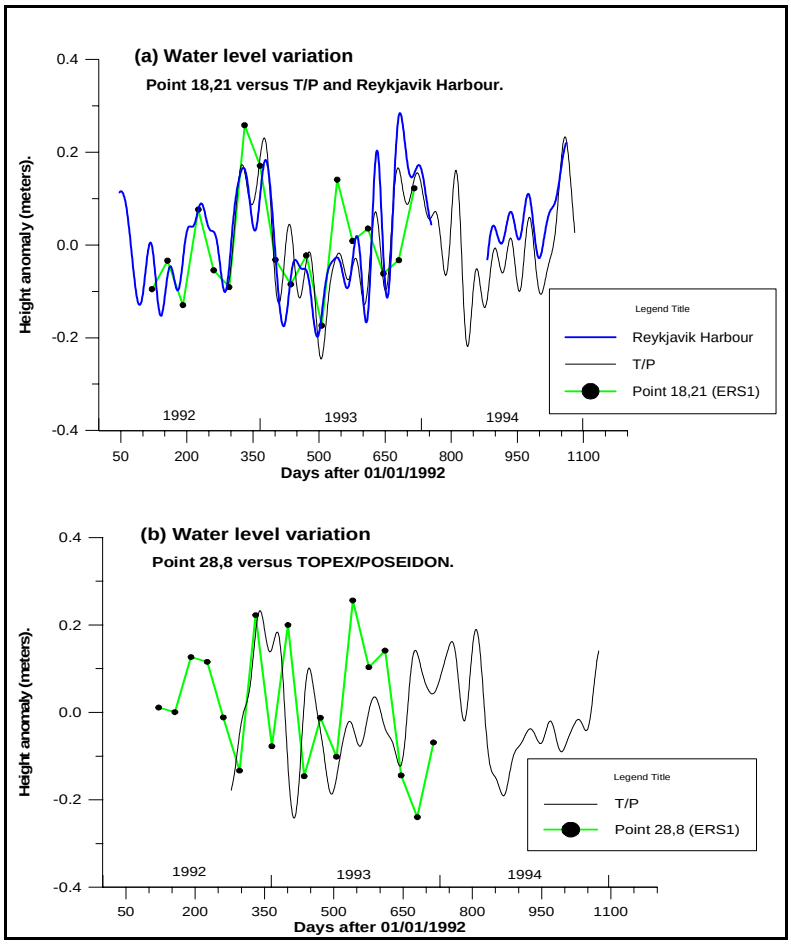

Fig. 26. Comparison of sea level time series derived from ERS-1 altimetry in model point a) 18.21 and b) 28.8, T/P altimetry in a cross-over point nearest to the model point and the tide gauge records for Reykjavik harbour. The two last data sets have been low-pass filtered using a 35-days Gaussian filter.

Comparison of ERS-1 sea level against T/P and Tide gauge sea level time series Low-Passed at 35 days

The above results show that the T/P derived altimetric sea level anomaly is in good agreement with observed tide gauge derived sea level anomalies, within about 6.2 cm RMS on timescale greater than 35 days. T/P sea level data are therefore drawn into the validation of the ERS-1 dynamic topography time series on equal basis with the tide gauge records from Reykjavik Harbour.

It is of interest to validate the ERS-1 altimetric dynamic topography time series sea level variations which are used as model input described later. Two model points being representative for an aerial extent of 400 km^2 are used in the following. Both points are selected so that the distance is less than 20 km from an adjoining T/P cross-over point. Model point (18,21 or 64.25°N, 24.02°W) was selected located at the T/P cross-over point near Reykjavik Harbour. The other model point (28,8 or 61.97°N, 20.08°W) is located near to a T/P cross-over point south of Iceland over deep water. The time mark for the single repeat or time step was set in the middle of each repeat cycle. Thus the ERS-1 time series have a length of 18 time steps or repeats.

A comparison of this type is not straightforward, due to the limited number of ERS-1 time steps and the possibility that the ERS-1 will observe short period transient atmospheric phenomena which are not resolved in the T/P data set. So the comparison below can only be of qualitative character.

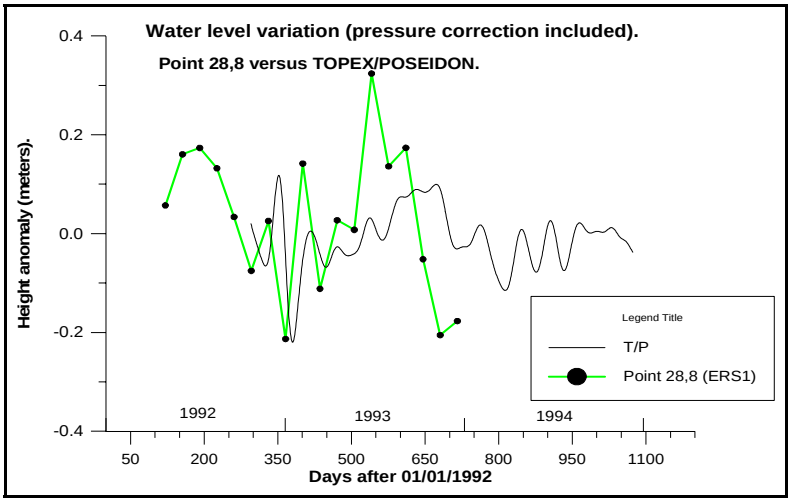

Fig. 27. Pressure corrected sea level time series derived from ERS-1 altimetry in model point 28.8 and T/P altimetry in a nearby cross-over point low-pass filtered using a 35-days Gaussin filter.

Figure 26a,b shows the comparison of the ERS-1 altimetric dynamic height time series for model point (18,21) and (28,8) with the 35 days low-passed T/P and the tide gauges (Reykjavik Harbour) time series. Note that each time series has been centred around their respective mean sea level for the overlapping period and that the overlapping period between T/P first starts at ERS-1 repeat 6. Low-frequency and to a certain degree also the high-frequency variations seen in the tide gauge data (Fig. 26a) are remarkably well represented in the ERS-1 altimetric time series, in particular for the first twelve ERS-1 repeats (i.e. up to day 506). For the first 12 repeats a standard deviation between the two time series of 6.3 cm are found with a correlation coefficient of 0.90, which is comparable to the result found between the tide gauge data and T/P altimetry. For the same period (i.e. repeat 6 - 12) a standard deviation of 7.3 cm and with a correlation coefficient of 0.89 are found between T/P and ERS-1 altimetry.

Figure 26b shows the comparison of the ERS-1 altimeter time series from the model point (28,8) and the 35 days low-passed T/P time series south of Iceland. It here becomes clear that the ERS-1 altimetry have problems describing the sea level variations after repeat 12. The reason is not known whether it is connected to possible combined effects of orbit errors and atmospheric pressure variations. Even for repeat 6 - 12 there are problems, which are likely to be associated with the setting of the ERS-1 time marks which are set in the middle of each repeat cycle. By fitting the time marks and disregarding repeat 8 a relatively low standard deviation and high correlation coefficient can be obtained for repeat 6 - 12. An inspection of the original T/P data set shows a sizeable drop in the sea level in the vicinity of repeat 8, which have disappeared during the filtering process, indicating that an unambiguous comparison between the two data set is not possible.

Figure 27 is included to show the comparison of the ERS-1 altimeter time series from the model point (28,8) and the 35-days low-passed T/P time series south of Iceland, where the inverse barometer effect correction have been used. The atmospheric pressure connected to sea level variations should in this case have been eliminated, under the condition that the atmospheric load is added instantaneously and with 100%. Both the ERS-1 and the T/P time series experience the same variations from repeat 6 to 12,

after which the agreement decreases as in the case above. It is interesting to note that at the end of 1992 a short period oscillation with amplitude of over 10 cm are observed in both data sets. Compared with the seasonal signal observed in the T/P data set this is a suspiciously high amplitude. Atmospheric pressure observations from Reykjavik shows for the same period unusual high fluctuations with range up to 38 mbar over short periods. This coincidence throws doubt on the reliability of the inverse barometer effect correction used, particularly during periods with considerable pressure variations.

From the above findings it was decided only to include ERS-1 altimetric mean dynamic topography from repeat 1 to repeat 12 in the coming modelling, due to an apparent increase in RMS difference between T/P and ERS-1 after repeat 12. In addition it was found advisable not to use pressure corrected altimeter data from the region.

MODELLING IN THE DENMARK STRAIT AREA AND ADJACENT SEAS

The promising results of the dynamic topography derived from satellite altimetry, with respect to deducing the surface circulation in the study area, makes it interesting to see whether the inclusion of these results in a limited area model can increase our knowledge of the circulation and transports in the layers *below* the surface layer in the region. In the following simulations it is attempted to apply altimetry at the open lateral boundaries which make up more than 70% of the total model boundary. Providing conditions at open boundaries has traditionally caused difficulties for numerical models in this region (e.g. Legutke, 1987, 1991; Stevens, 1991; Heburn and Johnson, 1995).

The limited area model used in this work is a fully three-dimensional and non-hydrostatic, primitive equation ocean circulation model, developed at the Danish Hydraulic Institute (DHI), referred to as the SYSTEM 3 or MIKE 3, Rasmussen (1991). The model has been documented in detail by Rasmussen *et al.* (1990) and DHI (1994).

Model Description

The model is based on the primitive equations which are discretized on a Cartesian grid; *x* and *y* are the horizontal coordinates and *z* denotes the vertical direction pointing upwards with origin in the undisturbed sea surface.

The basis equations are the Navier-Stokes equation, the mass conservation equation, the concentration equation for salt, the energy equation, and the equation of state,

$$\frac{D\vec{U}}{Dt} + 2\vec{\Omega}x\vec{U} = -\frac{1}{\rho}\nabla P - \vec{g} + \nabla\cdot\left(\nu_T\nabla\vec{U}\right) + \vec{F}_{ext} + S_{ss} \tag{9}$$

$$\frac{1}{\rho}\frac{D\rho}{Dt} + \nabla\cdot\vec{U} = S_{ss} \tag{10}$$

$$\frac{1}{\rho}\frac{D(\rho S)}{Dt} = \nabla\cdot(\kappa_s\nabla S) + S_{ss} \tag{11}$$

$$\frac{1}{\rho}\frac{D(\rho T)}{Dt} - \frac{\alpha T}{\rho c_p}\frac{DP}{Dt} = \nabla\cdot(\kappa_T \nabla T) + \frac{1}{\rho}Q_H + S_{ss} \qquad (12)$$

$$\rho = f(S, T, P) \qquad (13)$$

where $\bar{U}$ is the velocity vector, P the pressure, ρ the density, $\vec{\Omega}$ the earth's angular velocity, $\vec{g}$ the gravity, ν_T the eddy viscosity, F_{ext} the external forcing, S and T the salinity and temperature, κ_S and κ_T the eddy diffusivity for salt and heat, respectively, α the thermal expansion coefficient, c_p the specific heat capacity, Q_H the heat exchange, S_{SS} denotes the respective source-sink terms and t is the time. The density is calculated as a function of T, S and P, following the guidelines of UNESCO (1981). The atmospheric pressure is included in the model through the pressure term in eq. (9), and applied instantaneously in the z-direction. The S_{SS} terms handles the possible inclusion of precipitation, evaporation and radiative exchange with the surroundings. The dynamic height (or the sea surface elevation) ζ which is of interest in this study is introduced through the kinematic boundary condition mentioned later. The prognostic variables of the model are the three velocity components, pressure (sea level) and the two scalar quantities temperature and salinity. A more thorough treatment of the above equations and their Reynolds decomposition are given by Rasmussen *et al.* (1990) and DHI (1994).

The turbulent closure scheme is the Smagorinsky eddy viscosity formulation. This is the most used scheme for the subgrid scale eddy viscosity and was proposed by Smagorinsky (1963). Here the eddy viscosity in the stratified case, ν_T, is linked to the filter size (the grid spacings) and the mean rate of strain $\overline{S_{ij}}$ i.e. to the deformation of the flow field. In the unstratified case ν_{T0} is given by

$$\nu_{T0} = l^2\left(2\,\overline{S_{ij}}\,\overline{S_{ji}}\right)^{1/2} \qquad (14)$$

where

$$\overline{S_{ij}} = \frac{1}{2}\left(\frac{\partial \overline{U_j}}{\partial x_i} + \frac{\partial \overline{U_i}}{\partial x_j}\right) \qquad (15)$$

where l is a characteristic length scale. In order to take into account the different grid spacing the classical formulation is split into a horizontal and vertical term. Thus, the length scale l is split into two,

$$l = \begin{cases} C_{S,h}\sqrt{(\Delta x)^2 + (\Delta y)^2} \\ C_{S,v}\Delta z \end{cases} \qquad (16)$$

where $c_{S,h}$ and $c_{S,v}$ are constant in space, the value of $c_{S,h}$ is set to 0.176 and $c_{S,v}$ to 0.352 during the experiment.

In the stratified case the eddy viscosity is damped according to the local gradient Richardson number ($Ri = -g(\partial\rho/\partial z)/\rho(\partial U/\partial z)^2$) using a generalization of the classical Munk-Anderson formulation,

$$\frac{\nu_T}{\nu_{T0}} = \frac{1}{(1 + \psi \cdot Ri)^{\alpha}} \tag{17}$$

where ψ and α are dimensionless constants set to respective 10 and -0.5.

The eddy diffusivities for salt and heat (κ_S and κ_T) are assumed linearly related to the eddy viscosity through the Schmidt ($Sc=\kappa_S/\nu_T$) and Prandtl ($Pr=\kappa_T/\nu_T$) numbers, which are both set to 0.05 during the experiment. The kinematic boundary condition used is

$$U_z(z=\varsigma) = \frac{\partial \varsigma}{\partial t} + U_x \frac{\partial \varsigma}{\partial_x} + U_y \frac{\partial \varsigma}{\partial y} \tag{18}$$

where the pressure is linked to the surface elevation ζ from the free surface and down to the first computational node, by the hydrostatic relation

$$P(z) = -\rho g (z - \varsigma). \tag{19}$$

The momentum flux through the sea surface at *z=0* is computed with a quadratic drag law

$$\vec{\tau} = \rho \nu_T \frac{\partial}{\partial z}\vec{U} = \rho_a C_D \left|\vec{W}_{10}\right| \vec{W}_{10} \tag{20}$$

where ρ_a is the air density, $\vec{W}_{10}$ is the 10 m wind speed derived from observed data and C_D the drag coefficient has been set to

$$C_D = \begin{cases} (1.2 + 0.54\vec{W}_{10}) \cdot 10^{-3} \; for \; \left|\vec{W}_{10}\right| \leq 26\, m/s \\ 2.6 \cdot 10^{-3} \; for \; \left|\vec{W}_{10}\right| \geq 26\, m/s \end{cases} \tag{21}$$

The bottom friction is computed with a quadratic drag law assuming a logarithmic velocity profile just above the sea bed

$$\vec{\tau} = \rho \nu_T \frac{\partial}{\partial z}\vec{U} = \rho C_b \left|\vec{U}\right| \vec{U} \quad at \quad z = -H(x,y) \tag{22}$$

where $\vec{U}$ is the velocity and C_b is the drag coefficient expressed as a function of the total water depth, *H*, the distance above the bottom, z_b, the length scale in eq. (16), *l*, the von Kármán's constant, κ, the roughness length, z_0 and the height at which the logarithmic and Smagorinsky closure derived profiles are identical, *z**,

$$C_b = \left(\frac{2\sqrt{2}}{3} \frac{H}{l} \left(\left(1 - \frac{z^*}{H}\right)^{3/2} - \left(1 - \frac{z_b}{H}\right)^{3/2} \right) + \frac{1}{\kappa} \log\left(\frac{z^*}{z_0/30} \right) \right)^{-2} \tag{23}$$

z_0 is set to a constant value of 0.25 m in the model domain. At the open lateral boundaries, which make up more than 70% of the model's lateral boundaries, temperature and salinity are set to values derived from the hydrographic data set 1988-1995 discussed above in the section on data and method. The specified transport across the open boundaries, which must be specified in a limited area model, are obtained from the satellite derived sea surface elevation discussed further in the section on evaluation of the dynamic topography. It is the inclusion of sea surface elevation which makes this study interesting, as most other studies from the

region have used prescribed transports at the open boundaries. Furthermore none of the studies have had open boundaries for more than 70% of the model boundaries.

Thus, the variations of all prognostic variables in time and space have to be prescribed at the open lateral boundaries. However, during outflow conditions, scalar quantities as temperature and salinity are advected out of the model domain as determined by the interior of the model. Through the closed lateral boundaries and through the bottom, there is no flux of heat or mass. Additionally, a free-slip condition is used at closed lateral boundaries.

On a discretized form the partial differential equation can now be solved by a finite difference scheme (FDS) on an Arakawa C staggered grid. Where the velocities u, v and w are defined between the nodes, the scalar quantities such as the pressure, salinity and temperature are defined at the nodes. The solution of the hydrodynamic equations are advanced in time by applying two special techniques and using an Alternating Directions Implicit (ADI) technique in combination with the artificial compressibility method proposed by Chorin (1967). The ADI technique makes use of the fact that inversion of a matrix may be split into three operations according to the three directions. During each operation, only the prognostic variables directly associated with the directions, are considered as prognostic whereas the other direction variables are locked, i.e. only the pressure and the u-velocities are solved during a x-direction operation.

The first of the two special techniques is called the “fractioned-step” technique, which is a time staggering of prognostic variables, Figure 28, described in detail by Leendertse (1967).

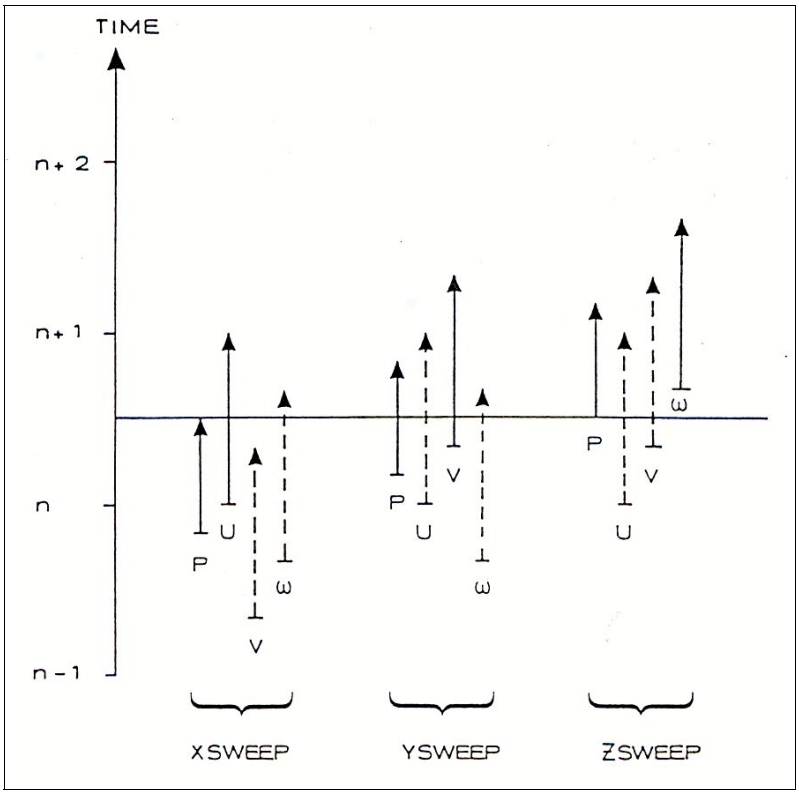

Fig. 28. Time staggering of the prognostic variables. By Rasmussen et al., 1990.

The second special technique is called “side-feeding”, which is a semi-linearization of the non-linear terms in the equations. For details on the side-feeding technique see Abbott (1979). It has been shown that the discretization used is accurate to the third order, so if all terms are accurate to the third order, the finite difference scheme (FDS) is supposed to have a second order accuracy.

In order to ensure stability and correct development of the flow in time, the Courant number

$$C_{rs} = c\,\frac{\Delta t}{\Delta x} \qquad (24)$$

where c is maximum speed in the domain, must be in the

range of 1 to 10. In a compressible fluid, sound waves would be the fastest propagating waves and *c* should be set to the speed of sound in sea water (~1485 m/s). Thus, this physical value implies a correspondingly small time step to ensure stability. The introduction of an artificial compressibility in the continuity equation makes it possible to choose an artificial speed of sound, c_s, which leads to a practically usable time step. By choosing c_s larger than the shallow-water wave speed ($C^2=g^H$) and smaller than the speed of sound in sea water, the fastest propagating waves such as shock and true sound waves are filtered out, leaving the shallow-water wave (or barotropic waves) which carries the information of the barotropic pressure undisturbed. The use of the artificial compressibility together with the two special techniques makes it possible to use a non-iterative ADI-algorithm, which gives rise to a computationally very efficient solution algorithm.

Scalar quantities such as temperature and salinity are modelled using the QUICKEST (Quadratic Upstream Interpolation for Convective Kinematics with Estimated Streaming Terms) scheme proposed by Leonard (1979). Briefly, this method can be described as based on a conservative control-volume formulation, where upstream interpolation is used to determine higher order derivatives. An extended version to three dimensions by Vested *et al.* (1992) is used in combination with the SHARP scheme (Leonard, 1988), where the SHARP scheme is used as a bound exponential interpolation in regions with steep gradients in the scalar field.

Fig. 29 The model domain and topography, contour values in meter.

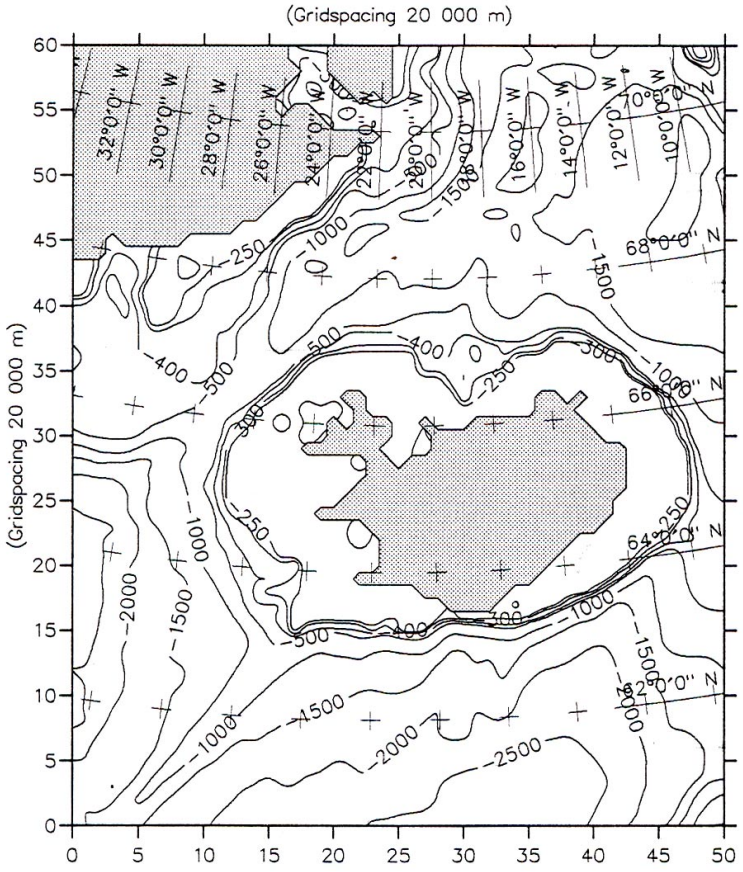

Details of the numerical schemes used to solve these equations have been documented in various papers (e.g. Rasmussen *et al.*, 1990; DHI 1994) and will not be discussed further here.

The model domain and the topography are shown in Figure 29. The latter is derived from the Naval Research Laboratory-Acoustics division, 1980, Map and Chart series, MC-21. The model is set up on a 50×60×20 grid with a resolution of 20 km in the horizontal and 50 m in the vertical. Thus, the equations are solved for 20 horizontal levels in the upper 1000 m of the water column. Variations in the water depth are accounted for by using a bottom boundary fitting approach of the lowest box such that the actual depth is taken into consideration. The model domain is set as a compromise between the spatial extent of the already existing ESOP (European Sub-Polar Ocean

Programme) model from the area and the altimeter data set. Further, the vertical extent is limited to the upper 1000 m, as the main interest in this study is the waters which participate in the circulation above the sill in the Denmark Strait, and hereby reducing the computing requirements.

The resolution is sufficient to resolve mesoscale topographic structures, which are known to be of importance in controlling the circulation of the region (e.g. Legutke, 1991). The model is not eddy resolving, as the baroclinic deformation radius in for example the East Greenland Current is found to be about 8 km (Wadhams and Squire, 1983). This is of minor importance as it is the mesoscale circulation with length scales greater than 20 km which is attempted to be solved here. The model is advanced in time with a time step of 300 s (5 min) which corresponds to a maximum Courant number (eq.(24)) of about 2.6 for surface gravity waves in the model domain.

It was from the start evident that initial fields of the temperature and salinity derived from the Levitus (1982) data set would not be accurate enough in the region. Therefore completely new initial fields of temperature and salinity were produced by use of the hydrographic data set discussed above in the section on data and methods. The two initial fields were obtained by using bilinear spatial interpolation to the model grid points. No subsequent smoothing was applied, as the bilinear interpolation routine acted as a filter. A more detailed analysis routine, taking the complex bottom topography in the region into consideration would have been

Fig. 30. Climatological monthy mean wind fields for September a) Hellermann and Rosenstein (1983) and b) ECMWF fields.

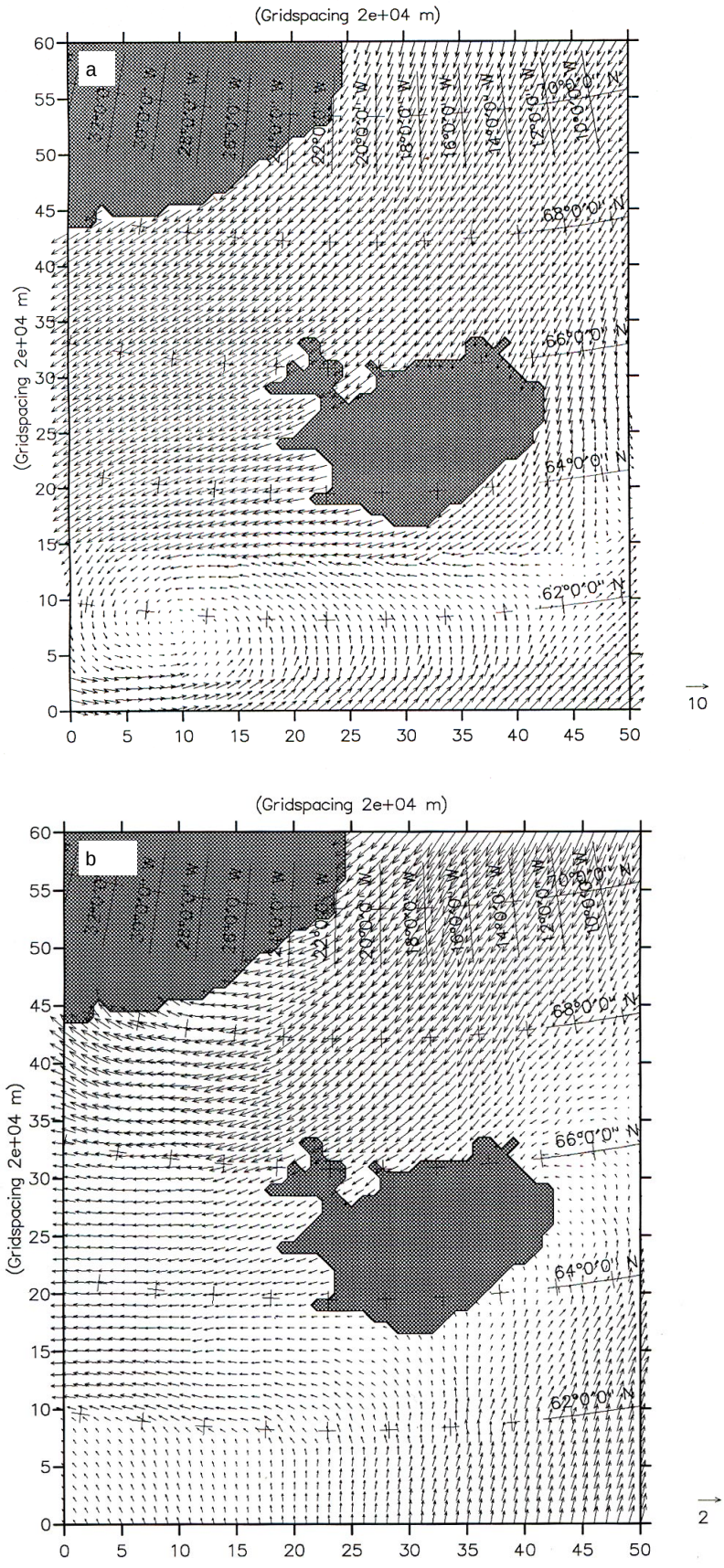

preferred. These new fields used in the following are representative for the seasonal period May to September.

Monthly climatological wind data by Hellermann and Rosenstein (1983) and ECMWF (1988) were used during the simulations. Figure 30 shows an example of the two wind fields. Notice that there is a significant difference between the two wind fields. The Hellermann and Rosenstein field being significantly stronger than the ECMWF field, which is derived from monthly mean pressure fields.

At the open lateral boundaries sea level heights derived from satellite altimetry are used. Temperature and salinity are applied from the two initial fields mentioned above. The satellite derived sea levels are introduced to the model grid points in a similar way as the temperature and salinity fields, i.e. by the use of bilinear interpolation. The above conditions constitute the forcing of the model.

The model is initialized with the new temperature and salinity fields discussed above, and a stagnant velocity field. During the initial spin up, the forcing applied by the sea level at the lateral boundaries are gradually increased over a period of 35 days, in order to prevent the effects resulting from a suddenly applied force. In the present case this is done by a linear interpolation over the period. It was realized very late in this study that the new temperature and salinity fields in themselves constituted a forcing field, and therefore also should have been introduced gradually. As it was not the purpose to evaluate this finding, it is not used in the following model experiments. However, it was very early seen that the model had problems handling the new temperature and salinity fields, so a relaxation scheme was introduced to compensate for these problems. The introduction of the relaxation scheme will be discussed in a later section. The simulations in the following do not include heat exchange with the atmosphere, atmospheric pressure and precipitation/evaporation.

Model results and discussion

From earlier works (e.g. Stevens, 1991; Legutke, 1987, 1991; Aukrust and Oberhuber, 1995) it had become clear that new and more realistic temperature and salinity fields were needed for the region. In the following sections the introduction of the temperature and salinity fields and the modelling results using altimetry at the open boundaries in the limited area model will be discussed and compared with observations from the region. The modelling efforts have, for convenience of understanding, been divided into a number of experiments. In experiment 1 the only driving force is the density field derived from the new temperature and salinity fields discussed in the section on data and methods. The main findings are the circulation and transport in the Denmark Strait which resembles results derived by classical means and the model problems handling the diffusion which leads to mixing in a more than adequate amount. In order to avoid this tendency a relaxation scheme towards the initial temperature and salinity fields was introduced. In experiment 2 two additional forcing terms are applied, dynamic height derived from altimetry at the

open lateral boundaries and wind at the sea surface. The model's response to the applied open lateral boundaries is discussed. It is attempted to solve the numerical problems by introduction of a slightly modified dynamic height field at the open lateral boundaries.

During the model simulations the prognostic variables are saved in two ways, the surface field is saved every three hours (i.e. every 36 time steps), while the total field is saved every 12 hours (i.e. every 144 time steps). In the following there will be referred to snapshot or mean values of the prognostic variables, meaning either a single time step or a four days mean value respectively.

The temperature and salinity fields

The temperature and salinity fields used to initialize numerical circulation models for the region have up to now made use of the Levitus (1982) data set. Because of the space- and time-averaged nature of this data set, it has become very smooth. Strong fronts and topographic signatures in the temperature and salinity fields, and therefore also in the density field, have been weakened to a degree which makes it questionable whether it can be used in connection with open lateral boundary conditions in a limited area model, where inflow points are prescribed by the initial fields. Experiments have shown that ill-posed open lateral boundary conditions with respect to the density field can lead to unrealistic circulation patterns in the interior of a model (e.g Griffiths, 1995). The effect arises as a consequence of the joint effect of baroclinicity and bottom topography known as the "JEBAR" effect identified by Sarkisyan and Ivanov (1971). For a flat-bottomed ocean the effect is non-existent. However, in the case of prominent bottom topography, the baroclinic-topography interaction can give rise to a barotropic current component which is comparable or even larger than the baroclinic counterpart (e.g Mellor *et al.*, 1982; Park and Gambéroni, 1995). It is therefore of great importance that

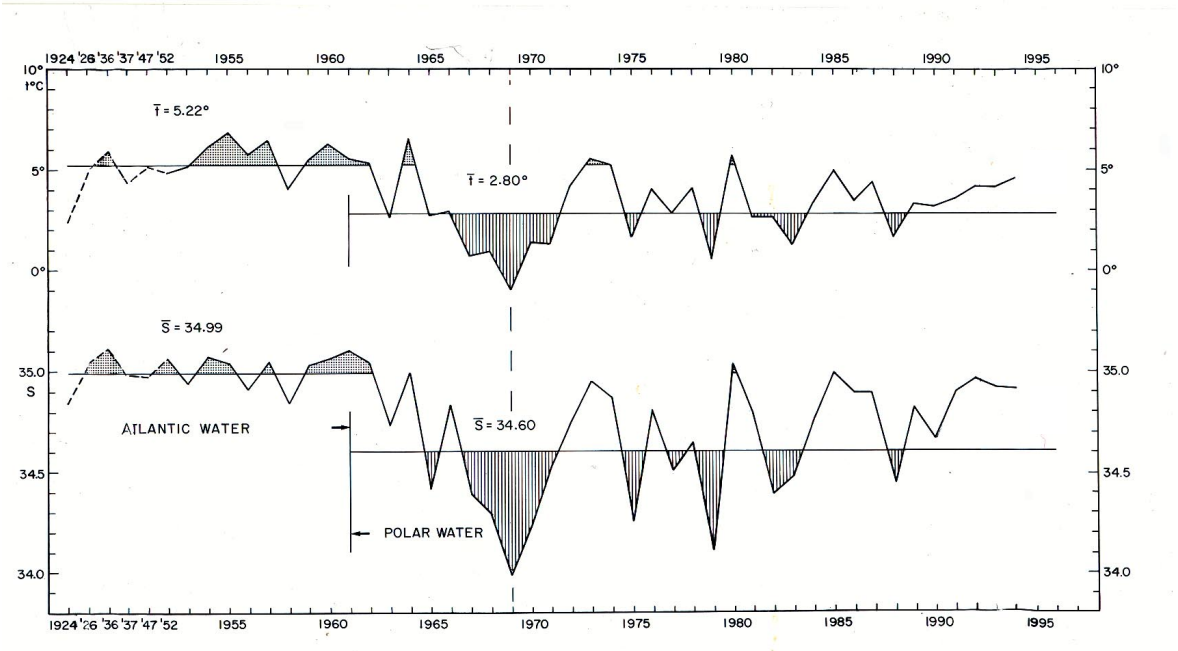

Fig. 31. Temperature and salinity at 50 m depth at a hydrographic station located in North Icelandic waters in May/June 1924, 1926, 1936, 1937, 1947 and 1952-1994 (Malmberg et al., 1996).

the prescribed properties at the open lateral boundaries resemble those observed in the nature.

Another problem connected to the Levitus data set is that it includes data from the period characterized as the "Great Salinity Anomaly" in the late 1960s. During this period the northern North Atlantic and the Nordic Seas undertook a significant change in properties (e.g. Dickson *et al.,* 1988; Blindheim *et al.,* 2000), where changes were observed over most of the region. In the Nordic Seas it was mainly seen as a decrease in temperature and salinity in the upper 1000 m of the water column. The same tendency was also observed over large areas of the North Atlantic. It is therefore not surprising that some of the models from the region report results which are similar to what was observed during the "Great Salinity Anomaly" (e.g. Aukrust and Oberhuber 1995).

Figure 31 shows an example of a time series of temperature and salinity observed in May/June at 50 m depth on the North Icelandic Shelf. It shows that a rather abrupt change in both temperature and salinity occurred during the late 1960s. During a relative short period the shelf waters, which were earlier of Atlantic character with salinities on average of about 35.0 and temperature mostly in excess of 5°C, were suddenly replaced by colder Arctic and Polar waters. This resulted in an average decrease of more than 2°C and 0.4 psu, although conditions have been much more variable during the following years than before 1965. The origin of the changed conditions on the North Icelandic shelf areas in the late 1960s is generally believed to be a new state (mode) caused by increased amount of Polar Water in the East Greenland Current spreading into the East Icelandic Current (EIC) further offshore. Thus, the EIC had changed from an ice-free Arctic current to an Arctic/Polar current, which under unfavourable conditions can preserve drift ice and even support formation of new ice (Malmberg, 1969).

Legutke (1987) questions the Levitus density field, "the problem remains whether the density data used are suitable for diagnostic calculations, where climatological data tends to be smooth by averaging moving fronts". Legutke (1991) shows that a significant adjustment of the temperature-salinity fields to the topography first occurs after a year of spin-up.

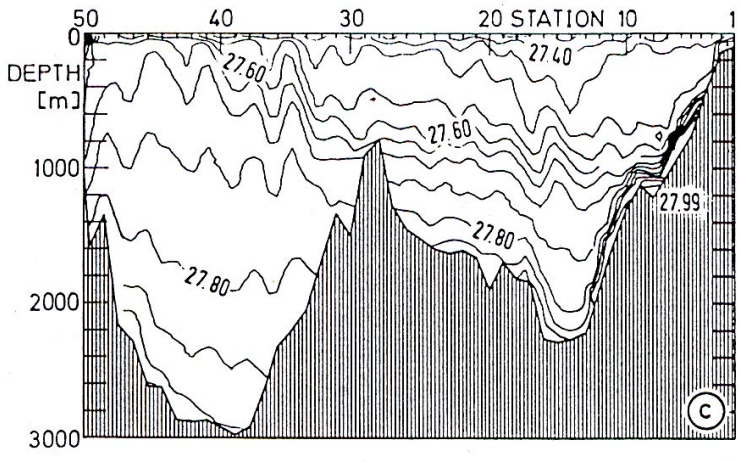

Fig. 32. Potential density along 62° N between Greenland and the Faroes. The contour interval is 0.05 (Krauss, 1995).

With background in the problems described above it was decided to make a new temperature and salinity field data set for the study area. The selection criteria was set by date and quality, i. e. only CTD data after 1987 were used. The data set is described in detail above in the section on data and methods. The main bulk of data were obtained during the months May to September, making it a spring/summer data set. As already mentioned, the data set was spatially interpolated to the model grid by using a bilinear interpolation routine. The problem arose whether further smoothing was desirable. One of the main advantages by smoothing would be removal of a supposed eddy field which could exist in the data set, on the expense of the more stationary field. An inspection of the data set revealed that many of the observed fluctuations in the density field were closely connected to variations in the bottom topography. Figure 32 gives an example of a potential density section in the North Atlantic along the 62°N latitude between Greenland and the Faroe Islands. It clearly appears that the stratification is highly dominated by eddy like features, however many of them seem to be closely related to the bottom topography. From just a few sections in the region it becomes clear that to make a division between transient and permanent (topographic) features is an almost impossible task.

Based on initial test run results using unsmoothed fields, it was decided to use only unsmoothed fields in the rest of the study.

Experiment 1 (pure density runs)

In the two runs described in the following, the model is integrated for 29 days (8064 time steps, where one time step equals 300 s) under the conditions that the only driving force is the density field and at the open lateral boundaries the sea surface elevation are set to a constant equal to zero. The difference between the two density runs discussed below, is that in the first case the temperature and salinity fields are allowed to adjust freely to the model parameterization and in the second case they are relaxed towards the initial fields.

The relaxation scheme used on the temperature and salinity fields is

$$S_{field}=(1-\alpha)S_{model}+\alpha S_{initial} \quad (25)$$

where S_{field} is the new field after the relaxation, S_{model} is the model derived field, $S_{initial}$ is the initial field and α is a weighting coefficient. The relaxation time scale is set to 100 minutes and the weighting coefficient α is set to the constant value of 0.5 all over in the model domain. The relaxation scheme makes it possible to control the temperature and salinity fields, and only allows for minor deviations from the initial fields. In the present case the model derived fields are adjusted to the initial fields every 20 time steps by the relaxation scheme. One major problem using a relaxation scheme of this type is the possibility that the density field is improperly adjusted to the topography from the start. This can give rise to unrealistically strong boundary currents near steep topographic features. Thus, there is always the possibility that a JEBAR effect can cause spurious topographic currents.

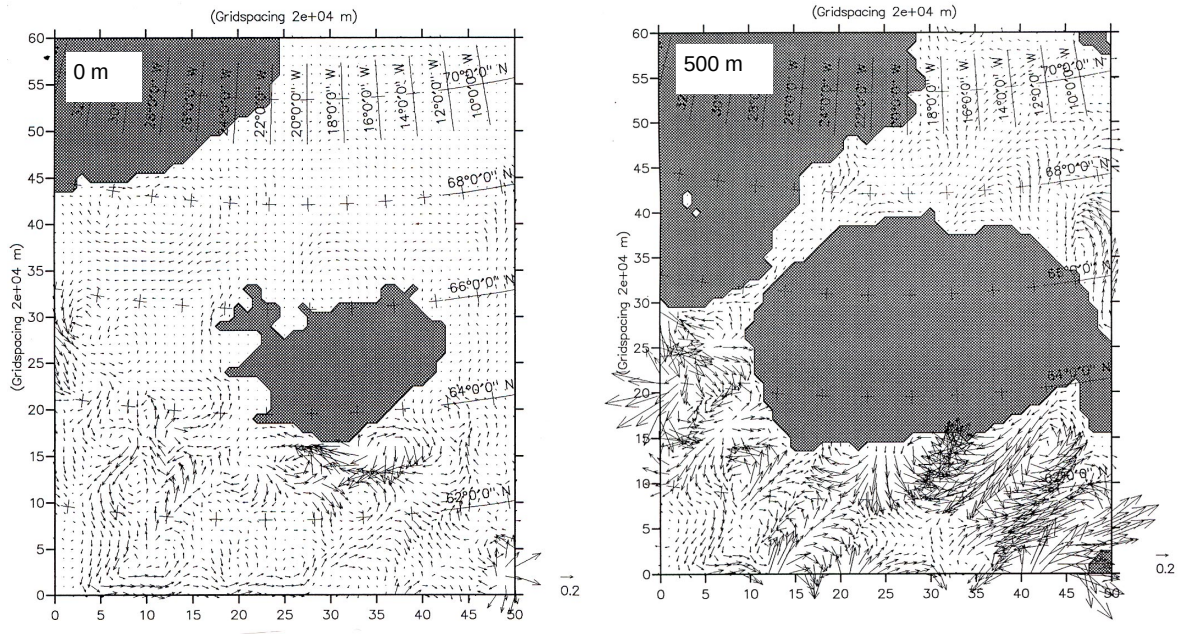

Fig. 33. Horizontal velocity field in the surface layer and at 500 m after 27 days for the density field allowed to adjust freely according to the forcing and parameterization of the model (20 cm/s scale at the lower right).

As mentioned above the sea surface elevation is in the following prescribed to zero along the open boundaries, while the vertical shear is left free to adjust. The distribution of inflow and outflow along the sections is thus not given a priori, but is determined by the dynamics of the model. The temperature and salinity are prescribed at inflow points. Under outflow conditions, however, scalar quantities are advected out of the model as determined by the interior.

Figure 33 displays a snapshot of the velocity fields in the surface layer (layer 20) and at 500 m depth (layer 10) after 27 days for the density field which is allowed to adjust freely according to the forcing and parameterization of the model.

Not unexpected, the most prominent feature is the high level of wave energy in the velocity fields, with the highest levels observed south of the ridge between Greenland and Scotland. The open boundaries which are set to zero do not allow the barotropic flow (associated with the sea surface elevation) to leave or enter the domain, instead it is being distorted and reflected off the boundaries. The wave energy is at depth additionally increased by the density effects. Connected to these oscillations an intense mixing of the temperature and salinity field is observed, making these fields almost unrecognisable compared with the initial fields already after 27 days.

The pronounced difference in wave energy which is observed in the regions north and south of the ridge, suggests that the dynamics of the two regions are of completely different character. With the circulation in the Iceland Sea to the north of the ridge being more dependant on the barotropic component of the flow, i.e. on the sea surface elevation. Whereas the circulation in the Iceland Basin south of the ridge is more dependant on the baroclinic component of the flow, i.e. on the density fields. These findings are in agreement with direct current meter observations from the regions, which show strong baroclinic character in the Iceland Basin (van Aken, 1993) and a more barotropic character in the East Greenland

Current to the north (Fahrbach *et al.*, 1995).

Figure 34 illustrates the point, by showing two vertical sections of the model initial density field, a west-east section along model point *x*,10 and a south-north section along model point 30,*y*, respectively. Here the steepest slopes of the isopycnals are observed to the south of the ridge, indicating that the baroclinic flow component is of greater importance in the Iceland Basin than in the Iceland Sea.

The above results indicate that when it comes to the integration of open lateral boundaries using sea surface elevations in a limited area model for the region, the model is less sensitive to the choice of prescribed sea level at the northern boundary than at the southern boundary. At the southern boundary it is of vital importance to describe the sea level correctly from the start in order to avoid the initial oscillations. Similar problems connected to the choice of southern boundary conditions in the region have been reported by Stevens (1991) and Griffiths (1995).

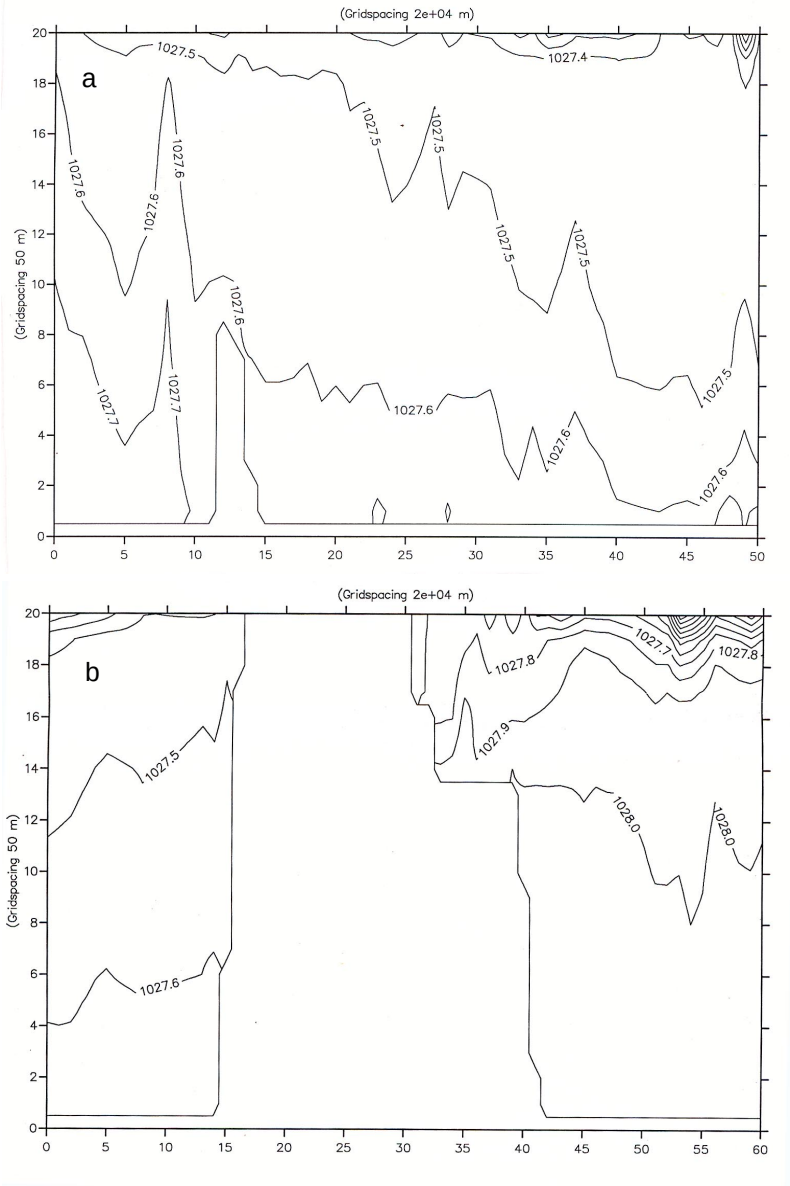

Fig. 34. Distiribution of density on a vertical plane extending a) west-east along model point x, 10 and b) south-north at model point 30,y. The contour interval is 0.1 σ_t units.

Stevens (1991) observes, using Levitus data, that a treatment of the southern boundary (in his case 58°N) using a simple choice of a prescribed barotropic stream function is not possible. Stevens found that the boundary data are not consistent with the topography and the density field which forces the stream function. Opposite at the northern boundary (~83°N) where he observes that the stream function is able to adjust within a single grid point from the approximate boundary data to a value consistent with the equations of motion.

Griffiths (1995) notes the importance of the right choice of location of the open boundaries, in order to get the mass transports correct. For a limited area model of the Iceland-Faroe Front she used unforced open boundaries to the north (67°N) and south (59 or 60°N), and observed two different circulation patterns in her model depending on which of her southern boundaries she choose. The discrepancy between the two she explains by the JEBAR effect where the presence of a baroclinic ocean in conjunction with topography can drive a barotropic current.

At a late stage of the work with MIKE 3 it was realised that a way to reduce the oscillations was to apply a baroclinically derived sea surface height at the boundaries almost instantaneously during the initial spin up, to respond to the sea surface height derived in the interior of the model, see next section.

In order to reduce the high level of oscillations and subsequent mixing which are likely to occur during the initial spin-up, two schemes were considered. The first scheme is to raise the eddy viscosity coefficients during the initial spin-up to dampen possible initial oscillations and the second would be the use a relaxation scheme as described in the start of this section. The results above indicate that an additional increase of the viscosity coefficients would just lead to an increase mixing, so that scheme was rejected. It has lately been shown that the model used has problems with grid diffusion, which is experienced to produce mixing in a more than adequate amount (Andersen, 1996). It was therefore decided to test the relaxation scheme for its eventual use in the following experiments. An advantage is that the density field is kept approximately fixed to the initial field, avoiding the problem which is connected to the parameterization of the horizontal and vertical diffusive coefficients of momentum, temperature and salinity. As Stevens (1991) notes that the vertical mixing in the ocean is still poorly understood and poorly treated in general circulation models. A further discussion of the problems concerning a better choice of parameterization of the horizontal and vertical diffusive coefficients of momentum and tracer (heat and salt) will not be given here. As indicated by model results from the Atlantic and the Nordic Seas it takes lots of effort just to parameterize the model and choose the right boundary conditions (e.g. Stevens, 1991; Legutke 1991; Aukrust and Oberhuber, 1995; Böning *et al.*, 1996). It then takes many model years before the fields (temperature, salinity and therefore density) significantly adjust to the applied forcing and topography.

Fig. 35. Horizontal velocity field in the surface layer and at 500 m after 27 days for the density field making use of the relaxation scheme. (20 cm/s scale at the lower right).

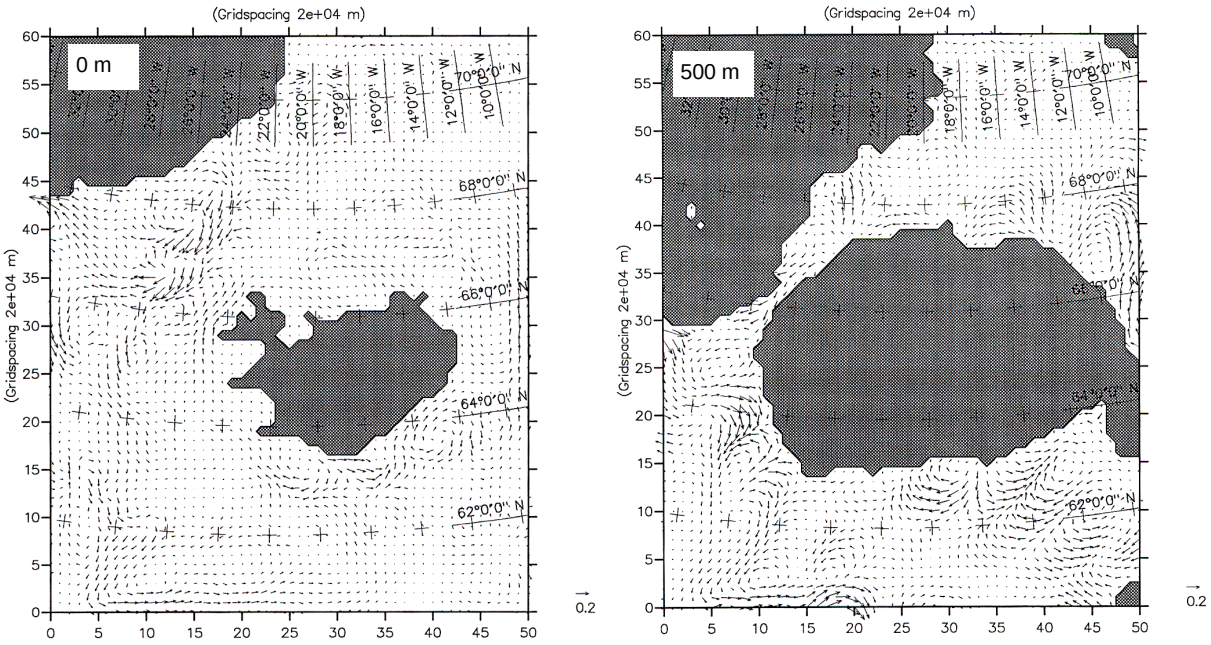

Figure 35 displays a snapshot of the velocity fields in the surface layer (layer 20) and 500 m (layer 10) after 27 days for the density field which makes use of the relaxation scheme.

Compared with Figure 33 the oscillations is dampen to a level which is acceptable with respect to the applied open lateral boundaries. In the interior of the model the East Greenland Current has become apparent.

Thus, the relaxation scheme used in connection with a "realistic" density field makes it possible to shortcut the time consuming spin-up which is required when using the Levitus data set. However it should be stressed here, that the used temperature and salinity fields are not perfect.

Based on initial test runs it has become apparent that a four day mean value of the velocity field discussed above is able to remove

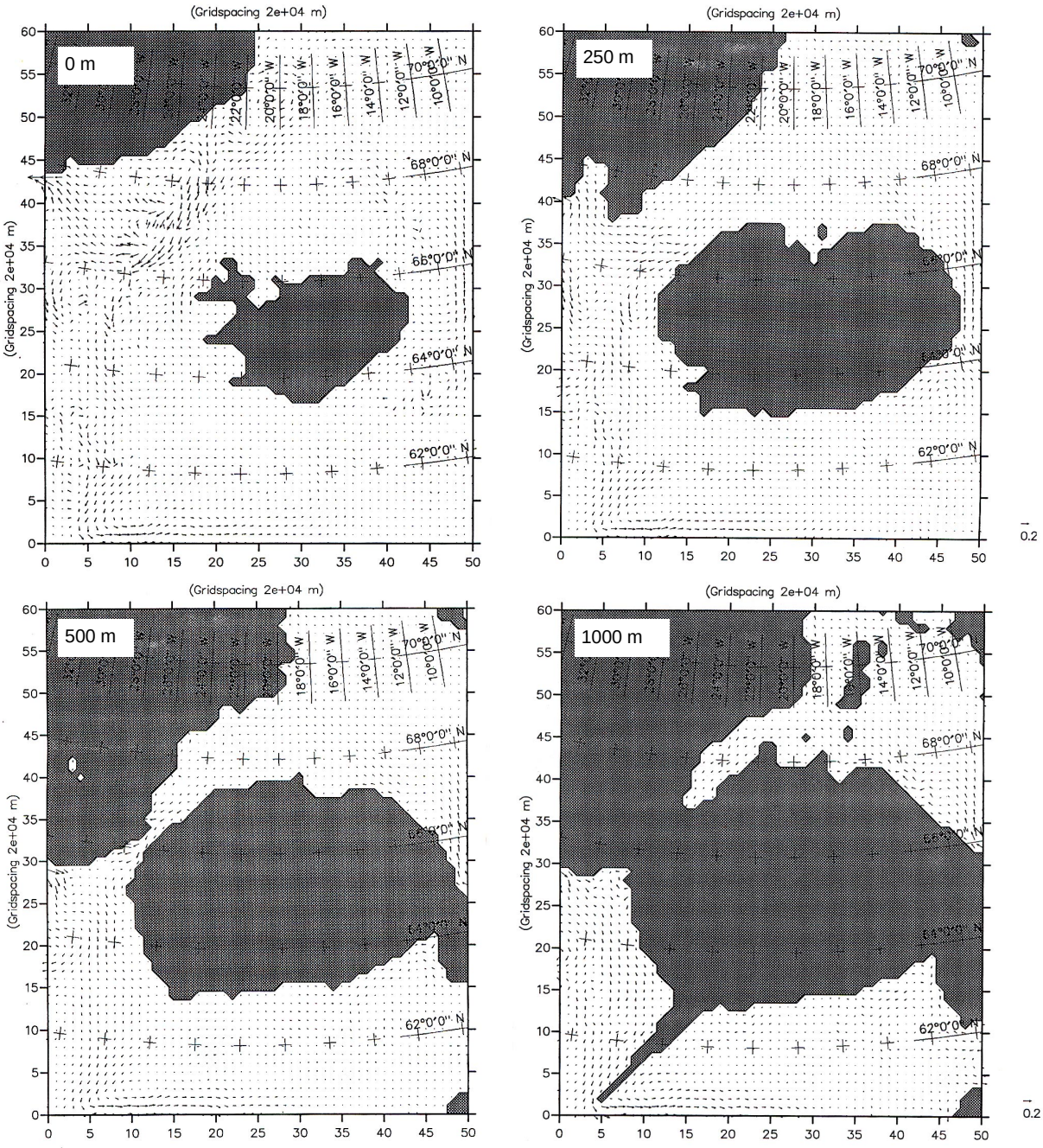

Fig. 36. The mean velocity field in the surface layer, at 250, 500 m and 1000 m after 27 days for the experiment using the relaxation scheme (20 cm/s scale at the lower right).

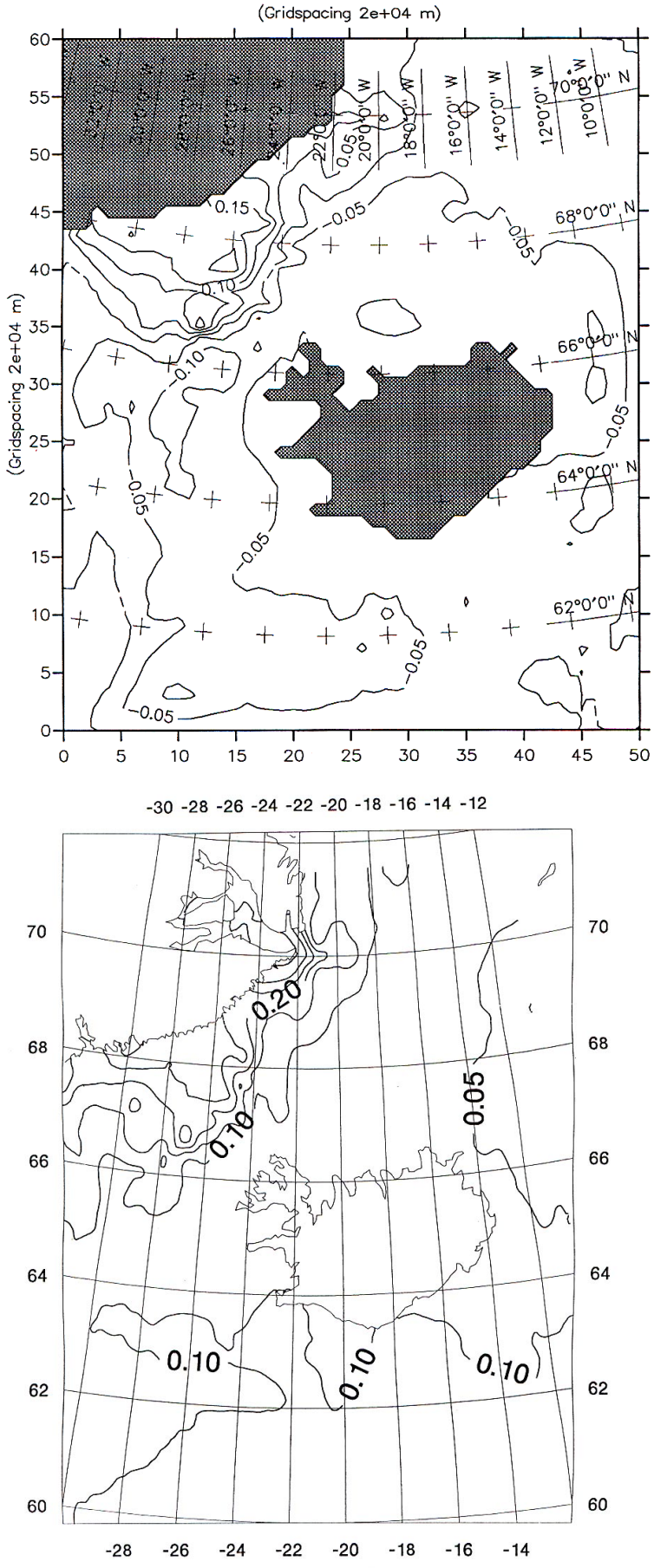

the high frequency oscillations observed in the velocity field, and what remains are the more robust features in the velocity field. Figure 36 shows the mean velocity field in the surface layer (layer 20), 250 m (layer 15), 500 m (layer 10) and 1000 m (layer 1) after 27 days, for the experiment using the relaxation scheme.

As expected the best model feature is the East Greenland Current and the circulation in the Denmark Strait. The circulation is very similar to the one obtained with the use of dynamical calculations assuming geostrophy. As pointed out by Malmberg *et al.* (1995) there is an accordance between the geostrophically calculated velocities derived from the density field in the upper 200 m and the velocities measured by current meters in the cold and low saline waters in the Denmark Strait. The Irminger Current is observed as a northward flow of Atlantic water on the west Icelandic shelf with velocities of the order of 10 cm/s. The highest velocities are observed in the East Greenland Current near the Icelandic continental slope with velocities of the order of 20-30 cm/s at the surface and on the East Greenland Shelf an anticyclonic gyre is observed over the Øst Bank (~67°30'N, 30°W), in agreement with observations (Krauss, 1958; and unpublished Nordic WOCE 1992 data). More unexpected are the low velocities observed in the Iceland Basin, compared

Fig. 37 The mean dynamic topography derived by a) the model at day 27 and b) the dynamic height anomaly relative to 150 dbar derived from the hydrographic data set 1988-1995. Units are in meter.

with results by Griffiths (1995) who for a similar experiment found velocities in the range 10 to 20 cm/s.

The mean transport through a section in the Denmark Strait has been calculated (between model points (10,47) and (20,30)) giving values of 1.53 Sv to the northeast divided between the two currents on the two shelves, and 5.83 Sv to the southwest. This is in agreement with what is generally accepted as the transport through the Denmark Strait. Unfortunately, it has not been possible to differentiate between the transport estimate of different water masses.

Figure 37 shows a comparison of the mean dynamic topography derived by the model at day 27 and the dynamic height anomaly relative to 150 dbar derived from the hydrographic data set. A remarkable resemblance is observed between the two fields, indicating that the best way to handle the temperature and salinity fields at present is through the use of the relaxation scheme.

A feature seen in Figure 36 which is not fully understood, is the "current" which emanates from the EGC. It is seen as a southward flow along the Icelandic continental slope which continues south along the Reykjanes Ridge until it turns east at the southern boundary. This "current" is believed to be generated by the ill-posed boundary conditions and it appears to be a very robust feature which can be observed in the coming model runs. However model results in the framework of the World Ocean Circulation Experiment Community Modelling Effort shows evidence of a similar circulation pattern (Böning *et al.,* 1996; Redler and Böning, personal comm., 1996).

The discussion above can be summarized as follows: The best way to handle the uncertainties which are connected to diffusion is by the introduction of a relaxation scheme for the temperature and salinity fields. Away from the boundaries the model is able, with the use of a realistic density field, to model transports in the Denmark Strait which is in agreement with generally accepted values derived by other means. In the following experiments it is therefore decided to make use of the relaxation scheme.

Experiment 2 (altimeter data applied at the open boundaries)

In the following experiments the dynamic sea surface heights derived from satellite altimetry will be introduced at the open lateral boundaries of the model. Since the applied temperature and salinity fields consist mainly of data from the spring-summer period, it was decided to make use of satellite data from the same seasonal period only. In the following, repeat 4 from the ERS-1 35 days repeat cycle, which is representative for August 1992 will be used. Notice that, as mentioned above in the section on evaluation of the dynamic topography, the dynamic heights used are not corrected for inverse barometer effects. In addition to the dynamic heights applied at the open lateral boundaries, climatological monthly mean wind data from the European Centre for Medium Range Weather Forecasts (ECMWF, 1988) was applied as a dynamical boundary condition at the sea surface.

During preliminary experiments a number of different types of initial spin-up procedures were tested, all leading to nearly the

same results. The spin-up used in the following starts with the initial sea surface height field set to zero all over in the model domain which also includes the open lateral boundaries. The open boundaries are then over a period of 35 days allowed to adjust linearly to the prescribed open boundary values determined by the altimetry. The wind stress is applied instantaneously.

Experiments with prolonged periods of wind action (up to 6 month) after the initial spin-up revealed no major difference in the velocity field compared to 35 days initial spin-up trails. An experiment with the much stronger Hellermann and Rosenstein (1983) wind field compared to the ECMWF field gave similar results. A similar result is obtained by Griffiths (1995) for a limited area model of the Iceland-Faroe front. A possible explanation is that the applied sea surface elevation at the open boundaries already contains the mean wind signal, which makes the results less sensitive to the applied wind stress field. Another possible explanation is that the areal extent of the model is so limited that a realistic wind action is not possible.

During the initial work with the altimeter data set, a number of test runs were performed where the only driving force, except for the density field, was the satellite altimetry applied at the sea surface as inverse barometer effects through the atmospheric pressure term in the model. Applying this term as a stationary field will not add any force to the water column, as the atmospheric pressure and the adjusted sea level will cancel each other. However, when it comes to the time varying part of the pressure field induced by the altimetry over a 35 days period, which is observed to have variation of the order of ±10 mbar (or ~±10 cm when speaking of sea surface heights) the situation completely changes. Now, a force is applied on every water parcel through the time varying pressure terms in the governing equations. The results of the simulations, not shown here, are very similar to the density experiment described above. However, weak evidences of fluctuations were found in the more robust features of the velocity field in the Denmark Strait. During a simulation a strengthening of the Irminger Current along the west coast of Iceland was observed in connection with an assumed inflow scenario to North Icelandic waters. The test series was not followed up. Though it would have been a good opportunity to test the response of the model to variations in the applied pressure field and at the same time estimate their importance. Is it therefore possible, that the observed variations in sea level discussed above in the section of evaluation of the dynamic topography, are responsible for strengthening or weakening of existing currents, or even causes the on set of currents, especially with respect to the dynamics and the variations of the North Icelandic Irminger Current, which is observed to be intermittent in nature. The use of atmospheric pressure and its time variations is a field overlooked by modellers. It have not been possible to find any model studies from the region which reports on the effect of using atmospheric pressure variations when studying the circulation in the Nordic Seas. The question must here rest for later investigation.

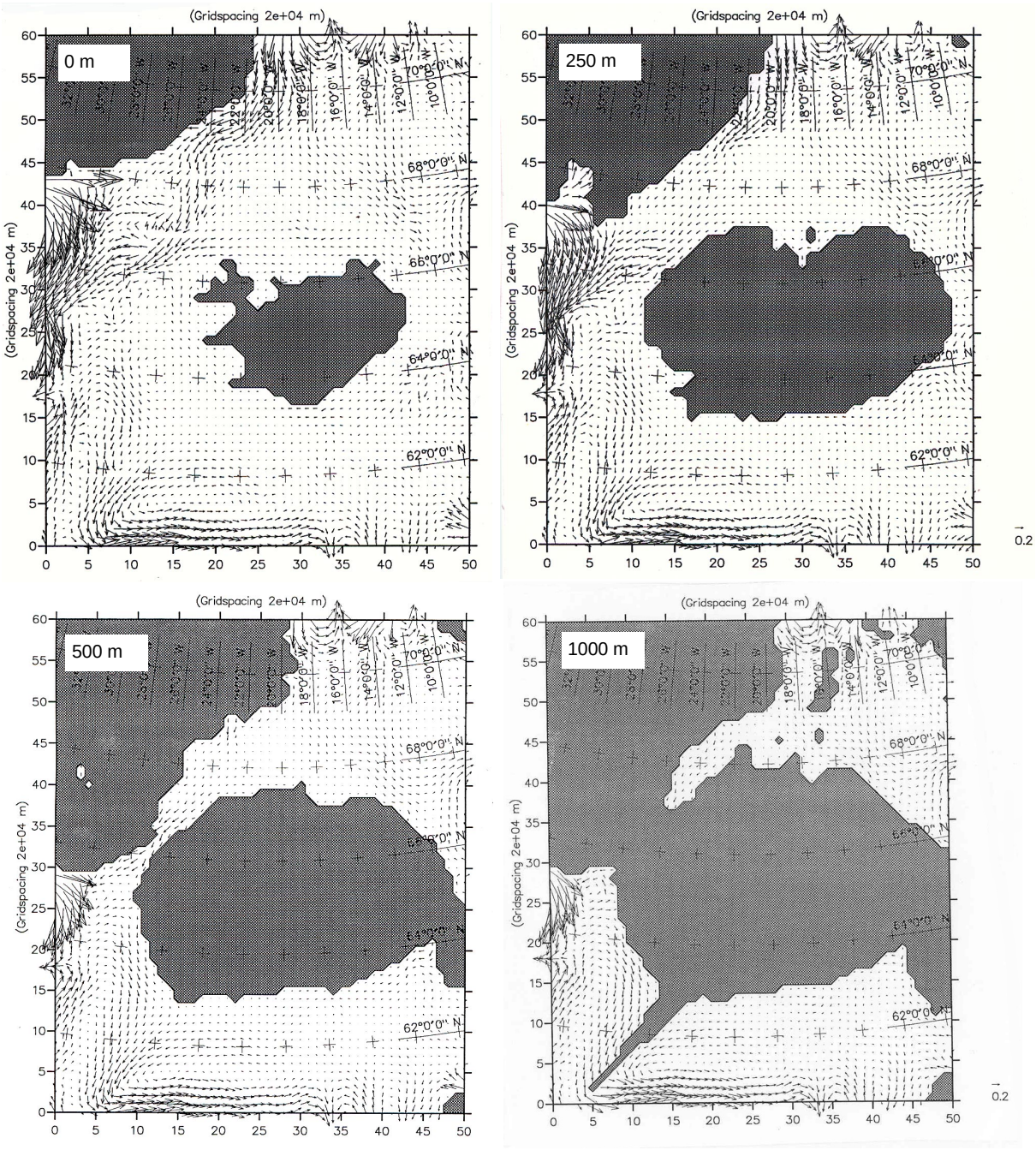

Fig. 38. The mean velocity field in the surface layer, at 250 m, 500 m and 1000 m for repeat 4, where the original altimetry data set is applied at the open boundaries (20 cm/s scale at the lower level right).

In the following discussion and description of the results repeat number will be referred to instead of time. For example repeat 4 refers to the time where the boundary condition for repeat 4 is working optimally.

Figure 38 shows the mean velocity field in the sea surface layer, 250 m, 500 m and 1000 m depth for repeat 4 being representative for August 1992, where the original altimetry data set is applied at the open boundaries.

Besides the obvious problems near the western and southern boundaries, which are discussed later, an interesting circulation field has developed in the rest of the model domain, especially in the region north of Iceland, i.e. in the Iceland Sea. The progress of the East Greenland Current (EGC) from the north is seen as a concentrated current following the bottom topography along the

coast of East Greenland southward towards the Denmark Strait. The highest velocities are generally observed over the steeper parts of the continental slope, in agreement with observations. A few grid points from the northern boundary the surface velocity of the East Greenland Current is observed to be in the range 20 cm/s to 40 cm/s, which is in agreement with observations. Approaching the Denmark Strait the main bulk of the EGC is forced by the bottom topography into a more southerly direction leaving the coast of East Greenland, bringing the current nearer to the continental slope of Iceland. Here the bottom topography (continental slope) of Iceland participates in the steering of the current. This influence holds until the sill of the Denmark Strait, where it again turns back to the East Greenland shelf areas. The model results show that the highest velocities in the Denmark Strait are found over the deeper parts of the Strait and over the Icelandic continental slope, which is in agreement with conventional observations. The observed vertical variations of the velocity field associated with the East Greenland Current are observed to resemble the few current meter measurements from the area. The current is observed to undergo a transformation from more barotropic in the northern part (around 70°N) to more baroclinic in the southern part (around 68°N) (Malmberg *et al.*, 1995).

It is interesting to note that, compared with the pure density run results (Figure 36), no major changes in the circulation pattern have taken place in the surface layer in the Denmark Strait. On the other hand, a noticeable change is seen in the deep part of the water column, as a strengthening of the current towards the southwest along the Icelandic continental slope. These findings suggest, that the surface layer in the Denmark Strait is mainly driven by the local density field, whereas the intermediate and deep layers seem to be driven by the dynamics of the surrounding regions. The finding throws doubt on the reliability of using geostrophic estimates of the transport through the deep parts of the Denmark Strait.

The mean transports through the section in the Denmark Strait have been calculated giving values of 0.1 Sv to the northeast and 12.0 Sv to the southwest, i.e. a doubling of the transport to the southwest is experienced compared to the pure density run discussed above. As for the density experiment it has not been possible to differentiate between the transport of the different water masses. A total transport of 12.0 Sv to the southwest in the Denmark Strait is perhaps at the upper limit, however compared with the purely density derived transport of 5.83 Sv the addition of the barotropic component of the flow would more likely give a transport in the range of 9 to 10 Sv.

As already mentioned in the section on general circulation, the present knowledge of some details about the circulation in the Iceland Sea is still limited. For example the origin of the East Icelandic Current has been described only in general terms (e.g. Stefánsson, 1962; Malmberg and Blindheim, 1994), as being formed from a branch of the EGC to the north of Iceland which joins the cyclonic circulation in the Iceland Sea and eventually

mixes with the North Icelandic Irminger Current. The model results shown in Figure 38 confirm these ideas, and propose a more complete picture of the system, where the main key in the description seems to be the presence of the Kolbeinsey Ridge (i.e. topography). The model results show that the EGC is not only steered by the topography of the East Greenland continental slope, but also by the western slope of the Kolbeinsey Ridge, which divides the EGC from the cyclonic circulation observed in the Iceland Sea. The part of the EGC which is influenced by the topography of the Kolbeinsey Ridge, follows it to the south to the Spar Fracture Zone at ~69°N. There the current turns southeast and joins the cyclonic circulation of the Iceland Sea, leaving a relative large and dynamically interesting area in between it and the EGC. Along the northeast Icelandic continental slope the current becomes known as the East Icelandic Current. The model results indicate that the current has a strong barotropic character in the upper 1000 m of the water column.

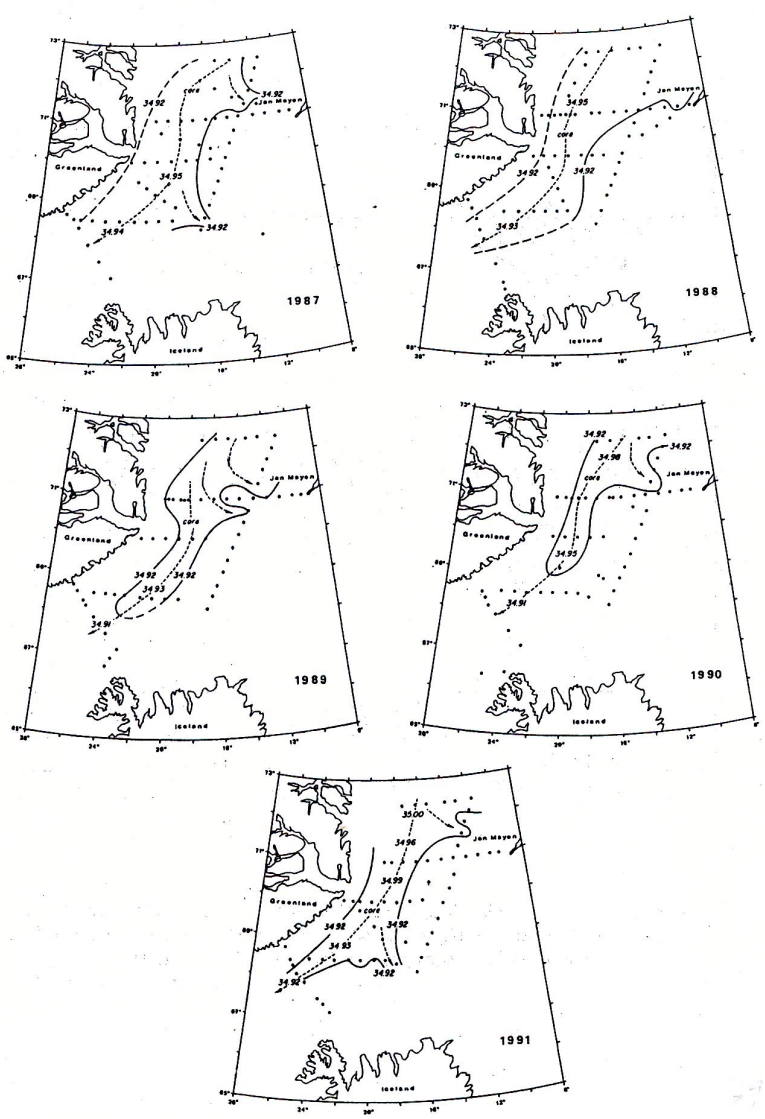

Fig. 39. The location of stations in the Icelandic-Danish Greenland Sea Project (GSP) 1987-1991 in the western Iceland Sea in September and the horizontal distribution af salinity maximum in the 0-500 m layer expressed by the 34.92 isohaline and the core values (Malmberg et al, 1996).

It is difficult to verify the branching of the EGC. However, one observes that the circulation described above is not only limited to the surface layer but can be traced down to a depth of at least 1000 m. A good tracer for water movements in the region is the lower Arctic Intermediate Water (lAIW), which is known to originate from the West Spitzbergen Current and is characterized by a salinity maximum in the upper parts of the water column. Figure 39 (Malmberg *et al.,* 1996) shows the distribution of the salinity maximum in the 0-500 m layer expressed by the 34.92 isohaline and core values.

Two of the years, 1987 and 1991, indicate a branching of the lAIW located in the EGC. On the other hand, years where no branching of the lAIW is observed, do not necessarily mean that the current is absent, it more likely indicates that the lAIW is not located over the western slope of the Kolbeinsey Ridge. An additional weak support to the proposed topographical steering by the Kolbeinsey Ridge and subsequent branching of the EGC is that a correlation seems to exist between the hydrographic conditions along the 71°N section and a section northeast of Iceland which

covers the East Icelandic Current. In years where the lateral extension of the EGC in the surface layer is observed to be wide at the 71°N section, polar conditions are observed in the EIC at the "same time". The opposite situation is when the EGC, and therefore Polar Water, is observed near to the East Greenland Coast, arctic conditions are observed in the EIC. With an observed mean speed of ~10 cm/s the response of changing condition at the 71°N section will be observed approximately 2 to 3 months later at the section in the EIC, under the assumption that no major change in forcing and mixing takes place in the region.

Similarly to the East Icelandic Current, the model result of the cyclonic gyre in the Iceland Sea is observed to have a strong barotropic character. Near-surface drifter results published by Poulain *et al.* (1996) show the presence of the cyclonic gyre in the Iceland Sea (Stefánsson, 1962) limited to the west by the Kolbeinsey Ridge. A remarkable resemblance between the model and drifter solutions is observed. The southern part of the gyre is seen to leave the model area between 67 and 68°N, in agreement with drifter observations reported by Poulain *et al.* (1996). The reason why the cyclonic gyre is not seen fully developed to the east, is that the return flow to the north is situated to the east outside the model domain.

A circulation pattern very similar to that observed in the model for the Iceland Sea as above has earlier been observed by Legutke (1991). Using Levitus fields and a too high viscosity coefficient Legutke observed a similar current field which was smooth and without details. Legutke notes, that care has to been taken with an appropriate resolution of mesoscale topographic features, since observations and model results suggest a strong controlling influence of the topography not only on the current but also on the density field, and in particular the influence of submarine ridges are important. With respect to temporal variability she concluded that the treatment of open lateral boundaries constitutes a problem for the application of the model results to observations. The boundary conditions (in her case set to constant transports) can introduce artificial variations in the interior of the model, meaning that the variations in the observed fields in the Nordic Seas depend highly on what happens outside the model domain.

The triangle area bound by the two topographically steered branches of the EGC and the north coast of Iceland represents with respect to hydrography, dynamics and forcing, is a very interesting area. Here occasionally inflow of warm Atlantic Water to the North Icelandic shelf areas is observed to take place through the eastern part of the Denmark Strait. The inflow of Atlantic Water is observed to have great importance for the ecology and marine life in the area (e.g. Jakobsson, 1992; Malmberg and Blindheim, 1994). What makes it an interesting area from an oceanographic point of view is that the hydrographic conditions of the North Icelandic shelf areas can change/shift between three different regimes. A distinction is made between, Atlantic, Polar and Arctic conditions. Several authors have discussed the cause of the observed variability in the Iceland Sea (e.g. Aagaard, 1970; Malmberg and Kristmannsson, 1992; Jónsson, 1992, 1994; Malmberg and

Jónsson, 1997). Attempts have been made to correlate it with the wind stress curl in the Iceland Sea and adjacent areas, indicating that the wind stress curl is a factor controlling the hydrographic variability. The model results give no answer to this problem, as the model is not able to reproduce the observed eastward flow along the North Icelandic shelf, known as the North Icelandic Irminger Current when associated with Atlantic Water. Direct current measurements from the outer parts of the northwest Icelandic shelf at water depths of 250 m, show variable high speed currents with main direction oscillating around an easterly direction. At the same time the temperature is observed to fluctuate between nearly pure Atlantic Water and a mixture of Atlantic and Polar/Arctic waters. Due to its directional steadiness, it is therefore suggested that the current is driven by an interaction between the local topography and the East Greenland Current, which mixes with Atlantic water that is always present in the area. However, during inflow of Atlantic water the current is in addition density driven. Unfortunately, the bottom topography used by the model is too coarse to resolve the finer structure of the shelf which can be of possible importance for the circulation. Future studies must be carried out with a much more detailed bottom topography of the shelf area in order to get a more detailed picture of the circulation on the shelf areas of the model. Furthermore, the influence of the boundary observed at the model's western and southern boundaries discussed below cannot be ruled out as the cause of the none observed eastward transport on the North Icelandic shelf.

The discussion above reveals that the model circulation within the Iceland Sea and the Denmark Strait is in remarkable agreement with observations, however one exception is the area located just north of Iceland between the East Greenland Current and the East Icelandic Current. As will become evident below, some of the disagreements can be explained by the artificial current system which is set up south of the ridge between Greenland and Scotland.

In the region south of the Denmark Strait and Iceland obvious numerical problems are observed at the western and southern boundaries. Lots of effort has been devoted to solving these problems. The most obvious reason would be to throw doubt on the used dynamic heights derived from altimetry, which is known to be questionable near Greenland. In an attempt to solve the open boundary problems a new set of open boundary conditions was constructed from the altimetry. The new western boundary was obtained by lowering all heights by 20 cm. Thereafter the western boundary from model point (0,17) to the coast of Greenland (0,43) was tilted until the height of the point nearest Greenland approximately matched the height nearest Greenland at the northern boundary. In order to avoid possible extrapolation errors obtained during the processing of the altimeter data new boundary data for the northern, eastern and southern boundary were obtained from inside the model domain. For the northern and eastern boundaries the altimeter data was taken 5 grid points inside the model domain, while for the southern boundary it was taken 8 grid inside the model domain. The eastern and southern boundary was then additionally lowered by 10 cm.

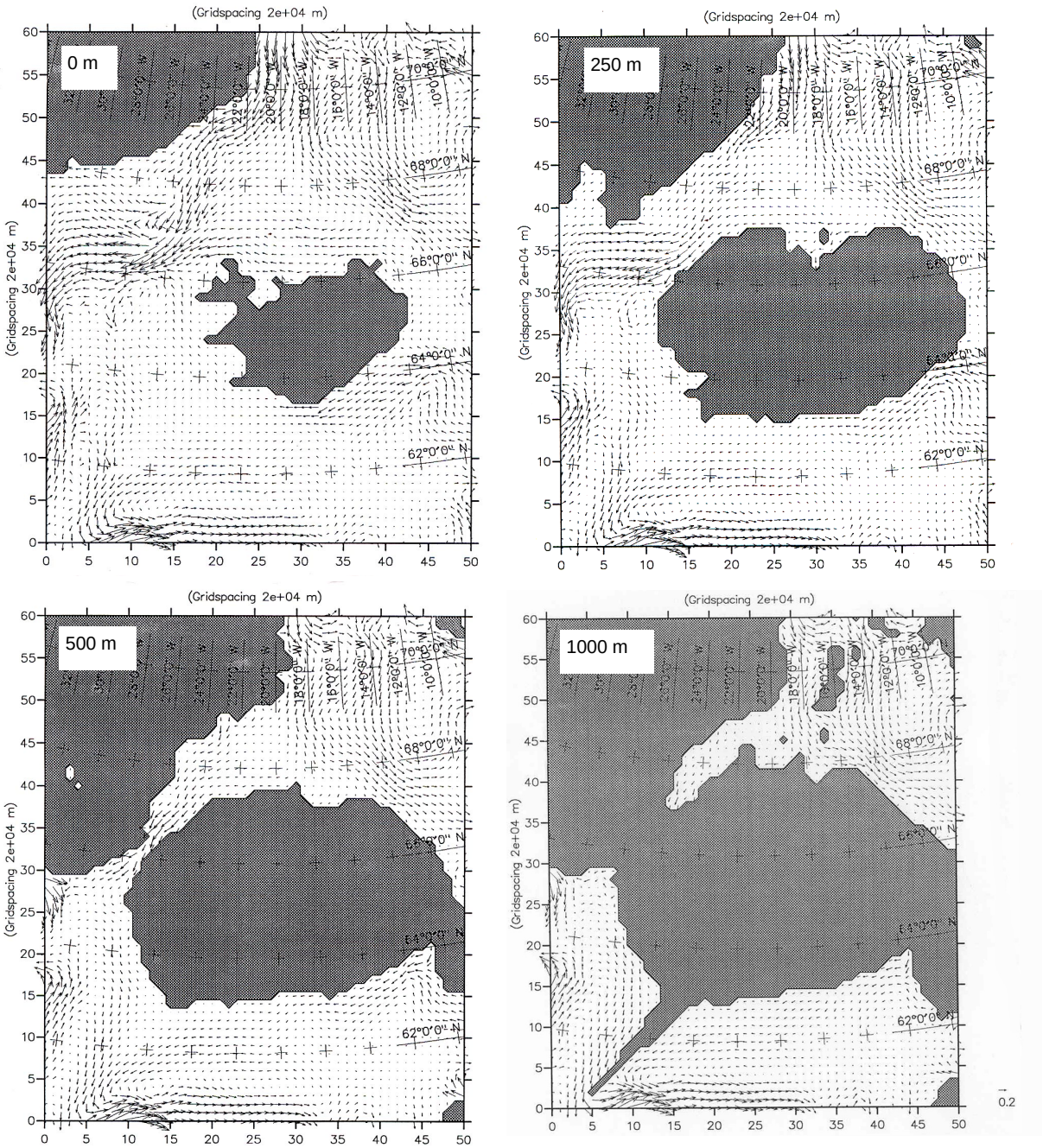

Fig. 40. The mean velocity field in the sea surface layers at 250 m, 500 m and 1000 m for repeat 4, where the modified altimetry data set is applied at the open boundaries. (20 cm/s scale at the lower right).

Figure 40 shows the mean velocity field in the sea surface layer, 250 m, 500 m and 1000 m depth for repeat 4, where the modified altimetry boundary data set has been applied at the open boundaries.

Compared with the results of the original open boundary data set (Figure 38) an overall increase is observed in the velocity field to the north of Iceland, with no general change in the circulation pattern. The increase is explained by a net increase in the southward transport through the northern boundary from 16.2 to 32.7 Sv. The transport through the Denmark Strait is at the same time seen to increase from 12.0 Sv to 19.0 Sv. The numerical problems associated with the downstream gradient of the dynamic height of the EGC, observed at the western boundary near

Greenland are reduced, however on the expense of a strengthening of the westward flow in the surface layer just north of Iceland, a current never observed by direct means. To the south of the Greenland-Scotland Ridge no major changes in circulation and velocities are observed, except for the current southeast of Iceland which is observed to be strengthened. It becomes speculative when the two velocity fields derived from altimetry are compared with the pure density run in Figure 36. One observes that the circulation in all three cases is the same in the region south of the ridge, where the only changes observed are in the magnitude of the velocities between the cases.

As mentioned earlier, it was late in the study realized that the physical integration of the open boundary conditions and the initial spin-up procedure used was wrong. Generally, limited area models need specification of either transport across open boundaries or the sea surface elevation at the open boundaries. It is then normal to apply the forcing at the open boundaries gradually in order to avoid shock waves and initial oscillations, i.e. starting from rest (with no transport or sea level gradients, through or on the open boundaries, respectively). The procedure is likely a left over from the times when models were of hydraulic character and the density was set to a constant, i.e. the initial density field is unforced. However, with the inclusion of a non-constant initial density field the situation changes completely. The procedure is now used in connection with a dynamic density field in the interior of the model where the open boundaries are allowed to adjust only gradually over a certain time period. Thus, a dynamical inconsistency is obtained between the interior of the model and the applied open boundaries. During the first time steps the interior of the model starts to adjust to the density field by setting up a velocity field and a sea surface topography. At the same time the open boundaries are still dynamically inactive not responding to the dynamics of the interior. The model response to the situation as observed in Figure 33, where the open boundary used acts as a reflector. In regions where the circulation is mainly driven by baroclinity (i.e. density) strong oscillations develops, whereas regions which depend less on baroclinity show weaker signs of oscillations. In order to damp the initial oscillations, it is common to raise the eddy viscosity coefficients during the initial spin-up or more infrequently by the use of a relaxation scheme as described above. The initial oscillations are perhaps reduced, however a more serious problem is the mean circulation, which is still influenced during the first time steps by the dynamically inactive open boundaries. The consequence is that during the first few time steps, an artificial circulation develops, dictated by the open boundaries at this stage. In regions where the circulation is determined by baroclinity this can have a fatal influence on the further development of the model, i.e. when the open boundaries reach their optimal strength the current field is distorted to a degree where the boundary conditions have no major influence on the circulation which have developed in the interior of the model.

The model results indicate that a corresponding progress to the status described above have taken place in the region south of the

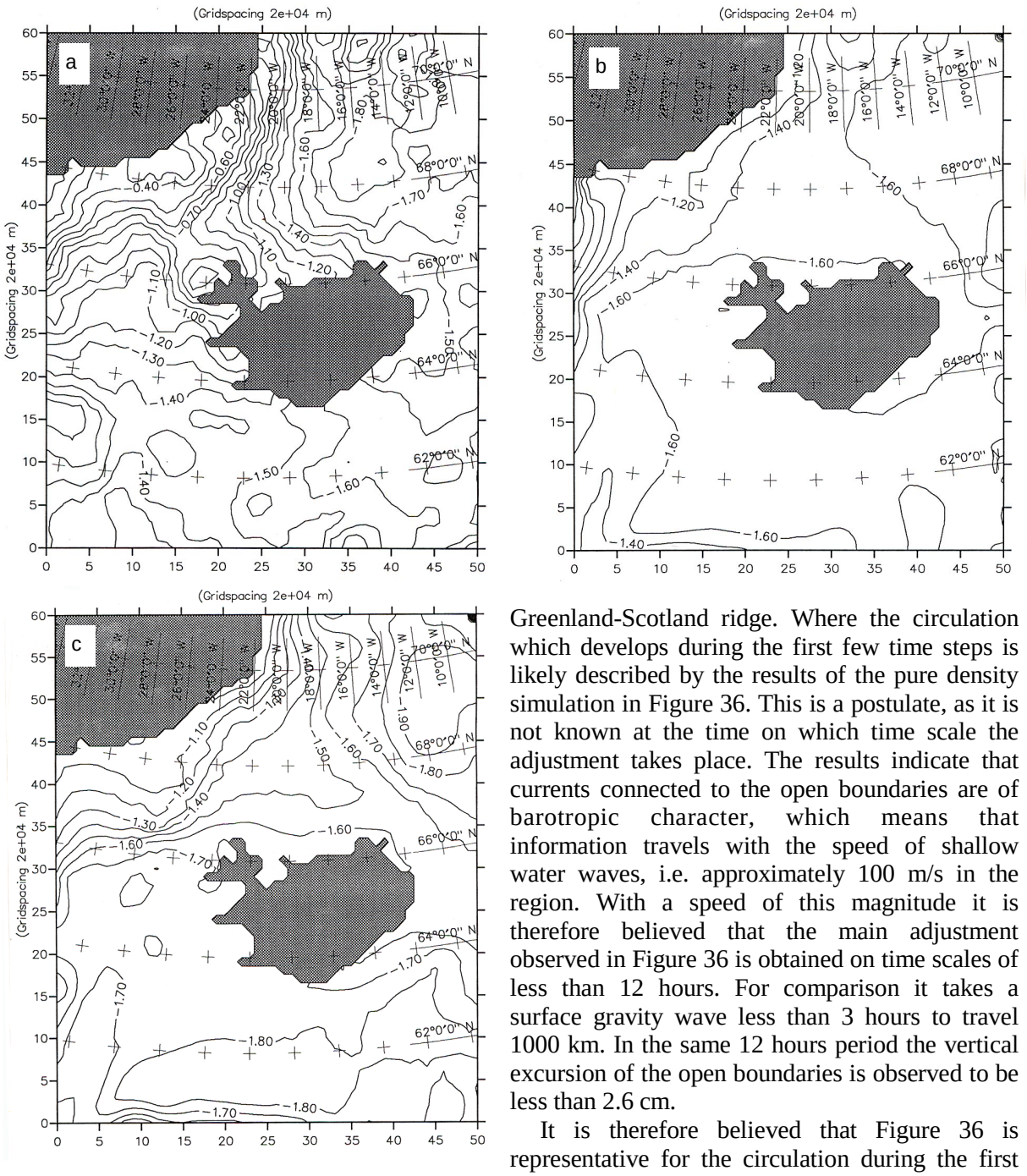

Fig. 41. The mean dynamic topography derived by a) altemtry, b) the model run with original boundaries and c) the model run with modified boundaries. Units are in meter.

Greenland-Scotland ridge. Where the circulation which develops during the first few time steps is likely described by the results of the pure density simulation in Figure 36. This is a postulate, as it is not known at the time on which time scale the adjustment takes place. The results indicate that currents connected to the open boundaries are of barotropic character, which means that information travels with the speed of shallow water waves, i.e. approximately 100 m/s in the region. With a speed of this magnitude it is therefore believed that the main adjustment observed in Figure 36 is obtained on time scales of less than 12 hours. For comparison it takes a surface gravity wave less than 3 hours to travel 1000 km. In the same 12 hours period the vertical excursion of the open boundaries is observed to be less than 2.6 cm.

It is therefore believed that Figure 36 is representative for the circulation during the first time steps. Along the western and southern boundaries artificial currents are observed to develop, seen as a southward and eastward flow, respectively. During the gradual increase of the force applied at the open boundaries a gradual amplification of these currents is observed ending up with the result shown in Figures 38 and 40.

Figure 41 shows the dynamic topography derived from altimetry for repeat 4 and the two model runs described above. Notice that Figure 41b is given with a contour interval of 0.2 m, in contrast to the two others which are given with a contour interval of 0.1 m. The altimetry derived solution shows no resemblance with the two model solution of the region south of the ridge, and the altimeter derived current system discussed above in the section of evaluation of the dynamic topography derived from satellite

altimetry is not reproduced by the model. Instead a remarkable resemblance are observed between the two model solutions and the pure density model solution in Figure 37, indicating evidence of improper handling of the open boundaries during the initial spin-up procedure. The influence is not only limited to the region south of the ridge but as it can be seen in Figure 41b, c it can be followed into the area north of Iceland.

Due to the improper handling of the open boundaries during the initial spin-up of the model, it is not possible to state anything conclusive about the circulation south of the Greenland-Scotland Ridge and in the area just north of Iceland. However the model results for the EGC and in the Iceland Sea discussed previously still remain valid as a much better resemblance is observed between the two model solutions and observations made by other means.

In order to avoid the set up of an artificial current system in a baroclinic region during the initial spin-up of the model, a new initial spin-up scheme is proposed. The scheme takes its origin in the pure density run using the relaxation scheme discussed previously. From a spin-up of this type one can obtain an idea of the dynamic height developed by the model. By using the information of the height field obtained in the interior of the model it is possible, by means of dynamical calculation at the boundaries, to produce at set of open boundary conditions which approximately match the dynamic set by the initial density field. The model is now spun-up again but the new boundary conditions are applied almost instantaneously. If the result of the simulation is giving a satisfactory results the boundary condition will be used in the case where the barotropic field is applied, else the scheme have to be applied again until a better agreement between the interior of model and the open boundaries is found. With a set of density boundary conditions the model are now ready for the inclusion of the barotropic component derived from altimetry. During the initial spin-up the open boundary conditions are almost instantaneously set to density derived open boundaries and then afterwards allowed to adjust gradually to the values determined by the altimetry.

From the discussion above it becomes clear that many unresolved modelling issues that are a consequence of both poorly known parameterization and initialization of the model still remain. In particular, the integration of open lateral boundary conditions which makes use of sea surface elevations needs further investigation.

Beside the obvious initialization problems the results indicate that the use of altimetry in connection with numerical ocean modelling has a great potential.

SUMMARY AND CONCLUSIONS

It is thought-provoking that in a historically well studied region as the Nordic Seas and the northern North Atlantic it is still possible to question even fundamental issues as circulation and transports. Although well monitored in a global sense many areas still need further investigation, especially the intermediate waters of the Nordic Seas which are known to contribute with an essential

part to North Atlantic Deep Water. However, the understanding is hampered by the variability observed in the region. Recent discussions in the literature have been focussed on variations on decadal time scales, even though historical data indicate longer time scales (e.g. Jónsson, 1990). These variations may explain the different circulation schemes which have emerged during the years.

The circulation derived by the use of ERS-1 satellite altimetry in the Denmark Strait and adjacent Seas has been investigated. All available 1/s mean altimetric measurements in the area 59°-71.5°N, 10°-45°W from the entire ERS-1 35 days-repeat mission C, i.e. 18 repeat cycles were used. The best geoid model out of four available for the study area was found using oceanographic arguments, as formal error estimates seldom exist for such models. The best choice was found to be the local geoid model GGEOID93B (Forsberg and Sideris, 1993). Currents computed using the geostrophic assumption and ERS-1 derived 35 days mean dynamic topography relative to GGEOID93B were compared to two different types of in situ data: hydrography and near surface drifter tracks.

When comparing altimetry derived currents with recent near-surface drifter tracks, good agreement is observed. When comparing altimetry derived currents with hydrography, the agreement is striking in the Denmark Strait above the East Greenland continental shelf. However major differences are found in the Iceland Basin, where the dynamic topography derived from hydrography in the traditional way is observed not to resolve the barotropic component of the currents. It can be concluded that the dynamic topography derived with the use of geoid model GGEOID93B is capable of reproducing many of the observed current features in the region, using the geostrophic assumption. The same is not true for the other geoids tested (OSU91A, GGEOID94A and GGEOID96A) so GGEOID93B is therefore the best choice at present. The altimetry even shows evidence of a cyclonic circulation in the Iceland Basin just south of Iceland which is supported by observations described in the section on general circulation, and lately also indicated in a schematic circulation pattern of the northern North Atlantic (Otto and van Aken, 1996). However, unsolved problems connected to the north Icelandic shelf and the high velocities observed in the East Greenland Current still exist. There is no doubt that some of the problems observed in the East Greenland Current can be ascribed to inaccuracies in the geoid model and lack of valid altimeter points near Greenland, due to sea ice.

Measurements from a tide gauge at Reykjavik and altimetry from the TOPEX/POSEIDON (T/P) satellite indicate that the ERS-1 35 days mean dynamic topography is capable of describing sea level anomalies (variations) on timescales of 35 days up to repeat 12. After repeat 12 a significant increase in the standard deviation between ERS-1 and T/P is observed. For the first 12 repeats a standard deviation between the tide gauge and ERS-1 time series of 6.3 cm is found with a correlation coefficient of 0.90, which is comparable with the result found between the tide gauge data and

T/P altimetry. The analysis of ERS-1 and TOPEX/POSEIDON sea level time series show that the inverse barometer effect correction commonly used is unreliable, particularly during periods with considerable atmospheric pressure variations.

The promising results of the dynamic topography derived from satellite altimetry, i.e. being able to deduce the surface circulation in the study area, makes it interesting to see if the inclusion of these results in a limited area model can increase the knowledge of the circulation and transports in the layers below the surface layer in the region. A limited area model has been set up for the Denmark Strait and adjacent Seas. Experiments were conducted integrating dynamic heights derived from altimetry at the open lateral boundaries, which makes up more than 70% of the total model boundary. During the numerical experiments realistic temperature and salinity fields were used. The experiments show reasonable agreement with observations in the East Greenland Current and Iceland Sea. They indicate that the Denmark Strait Overflow is influenced by far-field barotropic currents. However, the results shows huge problems near the western and southern boundary which highly influence on the circulation in the Irminger Sea and Iceland Basin. Earlier works show similar difficulties associated with integrating open lateral boundaries into numerical models for this particular region (e.g. Stevens, 1991; Heburn and Johnson, 1995). The results show that many unsolved modelling issues still remain and are a consequence of both poorly known parameters and the initialization of the model. In particular the integration of open lateral boundary conditions which makes use of sea surface elevations combined with a realistic density needs further investigation.

ACKNOWLEDGEMENTS

The author would like to express sincere gratitude to his supervisor Professor Carl Christian Tscherning for his advice, encouragement and friendship during this work. Especial thanks to him for introducing the author to the field of satellite geodesy. It is also a pleasure to thank Dr. Svend-Aage Malmberg for his early reading of the original manuscript, but particular the friendly moments where he, during fruitful discussions, shared his vast knowledge of the Nordic Seas and the northern North Atlantic. Grateful thanks also to Erland Rasmussen, Danish Hydraulic Institute, for the help and numerous conversations that were valuable during the modelling work.

A special thanks goes to Heðinn Valdimarsson for the endless discussions on the subject oceanography around Iceland and for his suffering through the drafts of this thesis, always reminding, when needed, that oceanography is “oceanography”. Also, thanks to Ole Baltazar Andersen and Rene Forsberg for valuable conversations and for providing essential data and programs for this work, as well as to Irene A. Mogensen and Thomas Knudsen who made their contribution reading the draft of this thesis.

The Danish Hydraulic Institute is acknowledged for providing a friendly work environment during the modelling phase.

Professor Wolfgang Krauss kindly gave access to data used in this work. Nordic WOCE, ESA, Hafrannsóknastofnunin (Marine

Research Institute, Reykjavík), WOCE, ICES, AVISO, National Survey and Cadastre - Denmark, Institute for Marine Research (Bergen), the Harbour Authorities in Reykjavik, the Icelandic Meteorological Institute and the Science Institute in Reykjavík are acknowledged for providing data, making this work possible.

Financial support was received from the Nordic WOCE with a grant from the Nordic Council Environmental Research Programme and the Commission for Scientific Research in Greenland. Also a MANICORAL grant is appreciated.

And finally to my family and nephew David P. Mortensen, love and appreciation beyond words.

REFERENCES

Aagaard, K. 1970. Wind-driven transports in the Greenland and Norwegian Seas. *Deep-Sea Res.*, 17: 281-291.

Abbott, M.B. 1979. Computational hydraulic. Elements of the theory of free surface flows. *Pitman Publ. Ltd.*, London.

Andersen, O.B. 1995. New ocean tide models for loading computations. *Bull. Int. Mare Terr.*, 102: 9256-9264.

Andersen, O.B., P.L. Woodworth and R.A. Flather 1995. Intercomparison of recent ocean tide models. *J. Geophys. Res., Oceans*, 100(C12): 25261-25282.

Andersen, S. 1996. The hydrography of the Sea of Marmara. *M.Sc. Thesis, University of Copenhagen*.

Aukrust, T. and J.M. Oberhuber 1995. Modeling of the Greenland, Iceland, and Norwegian Seas with a coupled sea ice - mixed layer - isopycnal ocean model. *J. Geophys. Res., Oceans*, 100(C3): 4771-4789.

Belkin, I.M., S. Levitus, J. Antonov and S.A. Malmberg 1998. "Great salinity Anomalies" in the North Atlantic. *Progress Oceanography* 41: 1-68.

Blindheim, J. 1990. Arctic Intermediate Water in the Norwegian Sea. *Deep-Sea Res.*, 37A: 1475-1489.

Blindheim, J., V. Borovkov, B. Hansen, S.A. Malmberg, W.R. Turrell and S. Østerhus. 2000. Recent upper layer cooling and freshening in the Norwegian Sea in relation to atmospheric forcing. *Deep Sea Res.*, I, 47, 655-680.

Böning, C.W., F.O. Bryan, W.R. Holland and R. Döscher 1996. Deep-water formation and meridional overturning in a high-resolution model of the North Atlantic. *J. Phys. Oceanogr.*, 26: 1142-1164.

Callahan, P. 1993. TOPEX/POSEIDON. Project GDR User Handbook. *JPL Rep. D-8944, rev-A. Distrib Active Arch. Cent.*, Jet Propul. Lab., Pasadena, Calif.

Cartwright, D.E., and R.D. Ray. 1990. Oceanic tides from Geosat Altimetry. *J. Geophys. Res.*, 95: 3069-3090.

Cartwright, D.E. and R.D. Ray. 1991. Energetic of global ocean tides from Geosat altimetry. *J. Geophys. Res.*, 96: 16897-16912.

CERSAT 1994. Altimeter products user manual. *Rep. C1-EX-MUT-A21-01-CN, issue 2, revision 6*, IFREMER, Plouzane, France.

CERSAT 1995. Altimeter and microwave radiometer. *ERS products user manual, Ref. C2-MUT-A-01-IF, version 1.2*, IFREMER, Plouzane, France.

Cheney, R.E., J.G. Marsh and B.D. Beckley. 1983. Global mesoscale variability from collinear tracks of Seasat altimeter data. *J. Geophys. Res.*, 88: 4343-4354.

Chorin, A.J. 1967. A numerical method for solving incompressible viscous flow problems. *J. Comp. Physics*, 2: 12-26.

DHI 1994. Mike 3 release 1.0 user guide and reference manual. *Danish Hydraulic Institute*.

Dickson, R.R., J. Meincke, S.A. Malmberg, and A.J. Lee. 1988. The "Great Salinity Anomaly" in the northern North Atlantic 1968-1982. *Prog. Oceanog.*, 20: 103-151.

Dickson, R.R., J. Lazier, J. Meincke, and P. Rhines. 1996. Long-term coordinated changes in the convective activity of the North Atlantic. *NATO ASI Series*, I 44: 211-261.

Dietrich, G. 1957a. Schichtung und Zirkulation der Irminger-See im Juni 1955. *Ber. Dtsch. Wiss. Komm. Meeresforsch.*, 14: 255-312.

Dietrich, G. 1957b. Allgemeine Meereskunde, Eine Einführung in die Ozeanographie. *Gebrüder Borntrager, Berlin*, 492 pp.

Dietrich, G. 1963. General Oceanography, an Introduction. *Interscience Publishers*, 588 pp.

Dietrich, G., K. Kalle, W. Krauss, and G. Sieder. 1975. Allgemeine Meereskunde, Eine Einführung in die Ozeanographie. *Gebrüder Borntrager*, Berlin, 593 pp.

Ellett, D.J., and J. Blindheim. 1992. Climate and hydrographic variability in the ICES area during the 1980s. *ICES Marine Science Symposium*, 195: 11-31.

ESA. 1992. ESA ERS-1 product specification. *ESA SP-1149.*

ESA 1996. Gravity field and steady-state ocean circulation mission, The nine candidate earth explorer missions. *ESA SP-1196* (1), 77 pp..

ESRIN. 1992. ERS-1 User Handbook. *ESA Earthnet Program Office, ESRIN, C. P. 64*, Frascati, Italy.

European Centre for Medium Range Weather Forecasts (ECMWF). 1988. ECMWF Forecast Model, Physical parameterization. *Res. Manual 3, 2nd ed.*, Reading, England.

Eymard, L., L. Tabary and A. Le Cornec. 1994. The microwave radiometer on board ERS-1: Part 2- validation of the geophysical products. *IEEE Trans. Geosc. Remote Sensing*, 34(2): 291-303.

Fahrbach, E., C. Heinze, G. Rohardt and R.A. Woodgate 1995. Moored current meter measurements in the East Greenland Current. *"Nordic Seas" Symp., Hamburg 1995, Ext. Abstr.*, 57-60.

Forsberg, R. and M.G. Sideris. 1993. Geoid computations by the multi-band spherical FFT approach. *Manuscripta Geodaetica*, 18: 82-90.

Fu, L-L., E.J. Christensen, C.A. Yamarone Jr., M. Lefebvre, Y. Ménard, M. Dorrer and P. Escudier. 1994. TOPEX/POSEIDON mission overview. *J. Geophys. Res., Oceans*, 99(C12): 24369-24381.

Fu, L.-L. and R.E. Cheney. 1995. Application of satellite altimetry to ocean circulation studies: 1987-1994. *Rev. Geophys.*, 33(Suppl.) 213-223.

Griffiths, C. 1995. A fine resolution numerical model of the Iceland-Faræ front with open boundary conditions, *J. Geophys. Res., Oceans*, 100(C8): 15915-15931.

Hansen, B. 1985. The circulation of the northern part of the Northeast Atlantic. *Rit Fiskideildar*, 9: 110-126.

Heburn, G.W. and C.D. Johnson. 1995. Simulation of the mesoscale circulation of the Greenland-Iceland-Norwegian Seas. *J. Geophys. Res., Oceans*, 100 (C3): 4921-4941.

Helland-Hansen, B. and F. Nansen. 1909. The Norwegian Sea. Its physical oceanography based upon the Norwegian researches 1900-1904. *Report on Norwegian Fishery and Marine Investigations*, Vol. II, Part I, No. 2, 390 pp.

Hellermann, S. and M. Rosenstein. 1983. Normal monthly wind stress over the world ocean with error estimates. *J. Phys. Oceanogr*. 13: 1093-1104.

Hermann, F. and H. Thomsen. 1946. Drift bottle experiments in the northern North Atlantic. *Medd. Komm. Danm. Fisk. Havunders., serie Hydrografi*, Bind III, nr. 4, 87 pp.

Heywood, K.J., E.L. McDonagh and M.A. White. 1994. Eddy kinetic energy of the North Atlantic subpolar gyre from satellite altimetry. *J. Geophys. Res., Oceans*, 99(C11): 22525-22539.

Hopkins, T.S. 1988. The GIN Sea: Review of physical oceanography and literature from 1972. *Saclant Undersea Research Centre Rep*. No.SR-124, 190 pp.

Ivers, W.D. 1975. The Deep Circulation in the Northern North Atlantic with a special reference to the Labrador Sea. *Ph. D. University of California, San Diego*, 179 pp.

Jakobsson, J. 1992. Recent variability in the fisheries of the North Atlantic. *ICES Mar. Sc. Symp.*, 195: 291-315.

Jónsson, J. 1990. Hafrannsóknir við Ísland, II., Eftir 1937 *Bókaútgáfa Menningarsjóðs*, Reykjavík, 447 pp.

Jónsson, S. 1992. Sources of fresh water in the Iceland Sea and the mechanisms governing its interannual variability. *ICES Mar. Sci. Symp.*, 195, 62-67.

Jónsson, S. 1994. Cyclonic gyres in the North Atlantic. *ICES Mar. Sci. Symp.*, 198: 287-291.

Knudsen, P. 1993. Altimetry for Geodesy and Oceanography. In: J. Kakkuri (ed.): Geodesy and Geophysics. Lecture notes for NGK autumn school 1992. *Finnish Geodetic Inst.*, Helsinki, Finland, pp. 87-129.

Knudsen, P., O.B. Andersen and C.C. Tscherning. 1992a. A preliminary ERS-1 altimeter data analysis in the northern North Atlantic Ocean. *EGS XVII General Assembly, G5*, Edinburgh, April 6-10.

Knudsen, P., O.B. Andersen and C.C. Tscherning 1992b. Altimetric gravity anomalies in the Norwegian-Greenland Sea - Preliminary results from the ERS-1 35 days repeat mission. *Geophys. Res. Lett.*, 19(17): 1795-1798.

Knudsen, P., O.B. Andersen and T. Knudsen. 1996. ATSR sea surface temperature data in a global analysis with Topex/Poseidon altimetry. *Geophys. Res. Lett.*, 23(8): 821-824.

Krauss, W. 1958. Die hydrographischen Untersuchungen mit “Anton Dohrn” auf dem ost- und westgrönländischen Shelf im September-Oktober 1955. *Ber. Dtsch. Komm. Meeresforsch.*, XV(2): 77-104.

Krauss, W. 1995. Currents and mixing in the Irminger Sea and in the Iceland Basin. *J. Geophys. Res., Oceans*, 100(C6), 10851-10871.

Le Traon, P.Y., M.C. Rouquet, and C. Boissier. 1990. Spacial Scales of Mesoscale Variability in the North Atlantic as Deduced from Geosat Data. *J. Geophys. Res.*, 95: 20267-20286.

Leendertse, J.J. 1967. Aspects of a computational model for long water wave propagation. *Rand Mem., RH-5299-Pr*, Santa Monica, California.

Legutke, S. 1987. The influence of boundary conditions in the Greenland-Norwegian Sea. A numerical investigation. In: J.C.J. Nihoul and B.M. Jamart (Eds.): Three-dimensional Models of Marine and Estuarine Dynamics. *Elsevier Science Publishers*, 269-284.

Legutke, S. 1991. A numerical investigation of the circulation in the Greenland and Norwegian Seas. *J. Phys. Oceanogr.*, 21: 118-148.

Leonard, B.P. 1979. A stable and accurate convective modelling procedure based on Quadratic Upstream Interpolation. *Computational methods on applied mechanics and engineering*, 19: 59-98, 1979.

Leonard, B.P. 1988. Simple high-accuracy resolution program for convective modelling of dis-continuities. *International Journal for Numerical Methods in Fluids*, 8: 1291-1318.

Levitus, S. 1982. Climatological atlas of the world ocean. *NOAA Prof. Pap. 13*, 173 pp.

Malmberg, S.A. 1969. Hydrographic changes in the waters between Iceland and Jan Mayen in the last decade. *Jökull*, 19: 30-43.

Malmberg, S.A. and S.S. Kristmannsson. 1992. Hydrographic conditions in Icelandic water, 1980-1989. *ICES Mar. Sci. Symp.*, 195: 76-92.

Malmberg, S.A., and J. Blindheim. 1994. Climate, cod and capelin in northern waters. *ICES Mar. Sci. Symp.*, 198: 297-310.

Malmberg, S.A., J. Mortensen, H. Valdimarsson, E. Buch, J. Briem and S.S. Kristmannsson 1995. Water masses circulation in the Western Iceland Sea. *Nordic Seas. Symp., Hamburg 1995, Ext. Abstr.*, 127-134.

Malmberg, S.A., H. Valdimarsson and J. Mortensen. 1996. Long-time series in Icelandic waters in relation to physical variability in the northern North Atlantic. *NAFO, Sci. Coun. Studies*, 24: 69-80.

Malmberg, S.A. and S. Jónsson. 1997. Timing of deep convection in the Greenland and Iceland Seas. *ICES J. Mar. Sci.*, 54: 300-309.

Mellor, G.L., C.R. Mechoso and E. Keto. 1982. A diagnostic calculation of the general circulation of the Atlantic Ocean. *Deep-Sea Res.*, 29A: 1171-1192.

Menemenlis, D., T. Webb, C. Wunsch, U. Send and C. Hill. 1997. Basin-scale ocean circulation from combined altimetric, tomographic and model data. *Nature*, 385: 681-621.

Meyer, H. H. F. 1923. Die Oberflächeströmungen des Atlantischen Ozeans in Februar. *Veröff. Inst. f. Meereskunde. N.F. Reihe A*, Heft 11.

Minster, J-F., C. Boissier, M-C. Gennero, S. Houry and P. Vincent. 1992. Space and time variability of the Gulf Stream using ERS-1 ALT-OPR02 data. Proceedings first ERS 1 Principal Investigator meeting, *European Space Agency Spec. Publ. ESA SP 359*, 419-424.

Mortensen, J. 1997. Satellite Altimetri and Circulation in the Denmark Strait area and adjacent Seas. *Ph. D. University of Copenhagen*, pp. 169.

Mortensen, J., E. Buch, S.S. Kristmannsson and S.A. Malmberg. 1991. Geostrophic velocities and volume transport calculations in the Western Icelandic Sea, 1987-1990. *GSP Int. Rep.*, 49, Royal Danish Adm. of Nav. and Hydrogr. and Mar. Res. Inst. Rvík, 26 pp.

Nansen, F. 1912. Das Bodenwasser und die Abkühlung des Meeres. *Internationale Revue der Gesamten Hydrobiologie und Hydrographie*, 5(1): 1-42.

Otto, L., and H.M. van Aken. 1996. Surface circulation in the northeast Atlantic as observed with drifters. *Deep-Sea Res.* I, 43: 467-499.

Park, Y.-H. and L. Gambéroni. 1995. Large-scale circulation and its variability in the south Indian Ocean from Topex/Poseidon altimetry. *J. Geophys. Res., Oceans*, 100(C12): 24911-24929.

Parke, M.E., R.H. Stewart, D.L. Farless and D.E. Cartwright. 1987. On the choice of orbits for an altimetric satillite to study ocean circulation and tides. *J. Geophys. Res.*, 92: 11693-11707.

Poulain, P.M., A.W. Varnas and P.P. Niiler. 1996. Near surface circulation of the Nordic Seas as Measured by Lagrangian drifters. *J. Geophys. Res., Oceans*, 101(C8): 18237-18258.

Rapp, R.H. 1994. The use of potential coefficient models in computing geoid undulations, in lecture notes for International School for the determination and use of the geoid. DIIAR-Politecnico di Milano. International Geoid Service, pp. 71-99.

Rapp, R.H., Y.M. Wang and N.K. Pavlis. 1991. The Ohio state 1991 geopotential and sea surface topography harmonic coefficient models. *Ohio State Univ., Dept. of Geod. Sci., Report 410*, 91pp.

Rasmussen, E.B. 1991. A finite difference scheme for three dimensional modelling of fluid dynamics. *Proc. IAHR.*

Rasmussen, E.B., H.J. Vedsted, P. Justesen, and L.C. Ekebjærg, SYSTEM 3, a three dimensional hydrodynamic model, Danish Hydraulic Institute, Int. Rep., 156 pp., 1990.

Rodrígues, E., and J.M. Martin. 1994. Estimation of the electromagnetic bias from retracked TOPEX data. *J. Geophys. Res., Oceans*, 99(C12): 24971-24979.

Roman, D.R., B. Csathó, K.C. Jezek, R.H. Thomas, W.B. Krabill, R.R.B. von Frese and R. Forsberg. 1997. A comparison of geoid undulations for west central Greenland. *J. Geophys. Res., Solid Earth*, 102(B2): 2807-2814.

Sarkisyan, A.S., and F.F. Ivanov. 1971. Joint effect of baroclinicity and bottom relief as an important factor in the dynamics of the sea currents. *Investiya Academy of Sciences, USSR, Atmospheric and Oceanic Sciences*, 1: 173-188.

Schwiderski, E.W. 1980a Ocean tides, 1. Global ocean tidal equations. *Mar. Geod.*, 3: 161-217.

Schwiderski, E.W. 1980b. Ocean tides, 2. A hydrodynamical interpolation model. *Mar. Geod.*, 3: 218-257.

Scott, J.C. and A.L. McDowall. 1990. Cross-frontal cold jets near Iceland: In-water, satellite infrared, and Geosat altimeter data, *J. Geophys.Res., Oceans*, 95(C10): 18005-18014.

Seeber, G. 1993. Satellite Geodesy. *Walther de Gruyter, Berlin*, 531 pp.

Smagorinsky, J. 1963. General circulation experiments with the primitive equations. 1. The basic experiment. *Mon. Weather Rev.*, 91: 90-164.

Stefánsson, U. 1962. North Icelandic Waters. *Rit Fiskideildar*, 3: 1-269.

Stevens, D.P. 1991. A numerical ocean circulation model of the Norwegian and Greenland Seas. *Prog. Oceanog.*, 27: 365-402.

Stum, J. 1994. A comparison between TOPEX microwave radiometer, ERS 1 microwave radiometer, and European Centre for Medium-Range Weather Forecasting derived wet tropospheric correction. *J. Geophys. Res., Oceans*, 99 (C12): 24927-24939.

Swift, J.H. 1980. Seasonal processes in the Iceland Sea. *Ph.D. Thesis, University of Washington*, 296 pp.

Swift, J.H., and K. Aagaard. 1981. Seasonal transitions and water mass formation in the Iceland and Greenland Seas. *Deep-Sea Res.*, 20A(10): 1107-1129.

Sy, A., U. Schauer, and J. Meincke. 1992. The North Atlantic Current and its associated hydrographic structure above and eastward of the Mid-Atlantic Ridge. *Deep-Sea Res.*, 39A: 825-853.

Sy, A., M. Rhein, J. Lazier, K. P. Koltermann, J. Meincke. A. Putzh and M. Bersch. 1997. Surprisingly rapid spreading at newly formed intermediate water in the North Atlantic Ocean. *Nature*, 386: 675-679.

Talley, L.D. and M.S. McCartney. 1982. Distribution and circulation of Labrador Sea Water. *J. Phys. Oceanogr.*, 12: 1189-1205.

Tscherning, C.C., R. Forsberg and P. Knudsen. 1992. The GRAVSOFT package for Geoid determination. *Proc. 1st continental workshop on the geoid in Europe*, Prague, p. 327-334.

UNESCO. 1981. The practical salinity scale 1978 and the internal equation of the state of seawater 1980. *UNESCO Tech. Pap. in Mar. Sci.*, 36: 13-21.

van Aken, H.M. 1993. Current measurements in the Iceland Basin. *ICES CM 1993/C:11*.

Valdimarsson, H. 1998. Circulation in Icelandic Waters from satellite tracked drifters, altimetric and ATSR. *Department of Geophysics. Niels Bohr Institute. University of Copenhagen*, 65 pp.

Valdimarsson, H. and S.A. Malmberg. 1999. Near-surface circulation in Icelandic waters derived from satellite tracked drifters. *Rit Fiskideildar*, 16: 23-39.

Vested, H.J., P. Justesen and L. Ekebjærg. 1992. Advection-dispersion modelling in three dimension. *Appl. Math. Modelling*, 16: 506-519.

Verstraete, J.-M. and Y.-H. Park. 1995. Comparison of Topex/Poseidon altimetry and in situ sea level data at Sao Tome Island, Gulf of Guinea. *J. Geophys. Res., Oceans*, 100(C12): 25129-25134.

Wadhams, P. and V.A. Squire. 1983. An ice-water vortex at the edge of the East Greenland Current. *J. Geophys. Res., Oceans*, 88: 2770-2780, 1983.

Wegner, G. 1973 Geostrophische Oberflächenströmung im nordlichen Nordatlantischen Ozean im Internationalen Geophysikalische Jahr 1957/58. *Ber. Dt. Wiss. Komm. Meereforsch.*, 22: 411-426.

Worthington, L.V. 1970. The Norwegian Sea as a Mediterranean basin. *Deep-Sea Res.*, 17: 77-84.

Wüst, G. 1928. Der Ursprung der Atlantischen Tiefenwässer. *Zeitschr. Gefellsch. f. Erdkde.*, 506-534.

Hafrannsóknastofnun. Fjölrit
Marine Research Institute. Reports

Þessi listi er einnig á Netinu
(This list is also on the Internet)

http://www.hafro.is/Bokasafn/Timarit/fjolr.htm

1. **Kjartan Thors, Þórdís Ólafsdóttir:** Skýrsla um leit að byggingarefnum í sjó við Austfirði sumarið 1975. Reykjavík 1975. 62 s. (Ófáanlegt - Out of print).
2. **Kjartan Thors:** Skýrsla um rannsóknir hafsbotnsins í sunnanverðum Faxaflóa sumarið 1975. Reykjavík 1977. 24 s.
3. **Karl Gunnarsson, Konráð Þórisson:** Áhrif skolpmengunar á fjöruþörunga í nágrenni Reykjavíkur. Reykjavík 1977. 19 s. (Ófáanlegt - *Out of print*).
4. **Einar Jónsson:** Meingunarrannsóknir í Skerjafirði. Áhrif frárennslis á botndýralíf. Reykjavík 1976. 26 s. (Ófáanlegt - *Out of print*).
5. **Karl Gunnarsson, Konráð Þórisson:** Stórþari á Breiðafirði. Reykjavík 1979. 53 s.
6. **Karl Gunnarsson:** Rannsóknir á hrossaþara (*Laminaria digitata*) á Breiðafirði. 1. Hrossaþari við Fagurey. Reykjavík 1980. 17 s. (Ófáanlegt - *Out of print*).
7. **Einar Jónsson:** Líffræðiathuganir á beitusmokk haustið 1979. Áfangaskýrsla. Reykjavík 1980. 22 s. (Ófáanlegt - *Out of print*).
8. **Kjartan Thors:** Botngerð á nokkrum hrygningarstöðvum síldarinnar. Reykjavík 1981. 25 s. (Ófáanlegt - *Out of print*).
9. **Stefán S. Kristmannsson:** Hitastig, selta og vatns- og seltubúskapur í Hvalfirði 1947-1978. Reykjavík 1983. 27 s.
10. **Jón Ólafsson:** Þungmálmar í kræklingi við Suðvestur-land. Reykjavík 1983. 50 s.
11. Nytjastofnar sjávar og umhverfisþættir 1987. Aflahorfur 1988. *State of Marine Stocks and Environmental Conditions in Icelandic Waters 1987. Fishing Prospects 1988*. Reykjavík 1987. 68 s. (Ófáanlegt - *Out of print*).
12. Haf- og fiskirannsóknir 1988-1992. Reykjavík 1988. 17 s. (Ófáanlegt - *Out of print*).
13. **Ólafur K. Pálsson, Björn Æ. Steinarsson, Einar Jónsson, Gunnar Jónsson, Gunnar Stefánsson, Sigfús A. Schopka:** Stofnmæling botnfiska á Íslandsmiðum. Reykjavík 1988. 76 s. (Ófáanlegt - *Out of print*).
14. Nytjastofnar sjávar og umhverfisþættir 1988. Aflahorfur 1989. *State of Marine Stocks and Environmental Conditions in Icelandic Waters 1988. Fishing Prospects 1989*. Reykjavík 1988. 126 s.
15. Ástand humar- og rækjustofna 1988. Aflahorfur 1989. Reykjavík 1988. 16 s.
16. **Kjartan Thors, Jóhann Helgason:** Jarðlög við Vestmannaeyjar. Áfangaskýrsla um jarðlagagreiningu og könnun neðansjávareldvarpa með endurvarpsmælingum. Reykjavík 1988. 41 s.
17. **Stefán S. Kristmannsson:** Sjávarhitamælingar við strendur Íslands 1987-1988. Reykjavík 1989. 102 s.
18. **Stefán S. Kristmannsson, Svend-Aage Malmberg, Jóhannes Briem:** *Western Iceland Sea. Greenland Sea Project. CTD Data Report. Joint Danish-Icelandic Cruise R/V Bjarni Sæmundsson, September 1987*. Reykjavík 1989. 181 s.
19. Nytjastofnar sjávar og umhverfisþættir 1989. Aflahorfur 1990. *State of Marine Stocks and Environmental Conditions in Icelandic Waters 1989. Fishing Prospects 1990*. Reykjavík 1989. 128 s. (Ófáanlegt - *Out of print*).
20. **Sigfús A. Schopka, Björn Æ. Steinarsson, Einar Jónsson, Gunnar Jónsson, Gunnar Stefánsson, Ólafur K. Pálsson:** Stofnmæling botnfiska á Íslandsmiðum 1989. Rannsóknaskýrsla. Reykjavík 1989. 54 s.
21. Nytjastofnar sjávar og umhverfisþættir 1990. Aflahorfur 1991. *State of Marine Stocks and Environmental Conditions in Icelandic Waters 1990. Fishing prospects 1991*. Reykjavík 1990. 145 s.
22. **Gunnar Jónsson, Björn Æ. Steinarsson, Einar Jónsson, Gunnar Stefánsson, Ólafur K. Pálsson, Sigfús A. Schopka:** Stofnmæling botnfiska á Íslandsmiðum 1990. Reykjavík 1990. 53 s. (Ófáanlegt - *Out of print*).
23. **Stefán S. Kristmannsson, Svend-Aage Malmberg, Jóhannes Briem, Erik Buch:** *Western Iceland Sea - Greenland Sea Project - CTD Data Report. Joint Danish Icelandic Cruise R/V Bjarni Sæmundsson, September 1988*. Reykjavík 1991. 84 s. (Ófáanlegt - *Out of print*).
24. **Stefán S. Kristmannsson:** Sjávarhitamælingar við strendur Íslands 1989-1990. Reykjavík 1991. 105 s. (Ófáanlegt - *Out of print*).
25. Nytjastofnar sjávar og umhverfisþættir 1991. Aflahorfur fiskveiðiárið 1991/92. *State of Marine Stocks and Environmental Conditions in Icelandic Waters 1991. Prospects for the Quota Year 1991/92*. Reykjavík 1991. 153 s. (Ófáanlegt - *Out of print*).
26. **Páll Reynisson, Hjálmar Vilhjálmsson:** Mælingar á stærð loðnustofnsins 1978-1991. Aðferðir og niðurstöður. Reykjavík 1991. 108 s.
27. **Stefán S. Kristmannsson, Svend-Aage Malmberg, Jóhannes Briem, Erik Buch:** *Western Iceland Sea - Greenland Sea Project - CTD Data Report. Joint Danish Icelandic Cruise R/V Bjarni Sæmundsson, September 1989. Reykjavík 1991*. Reykjavík 1991. 93 s.
28. **Gunnar Stefánsson, Björn Æ. Steinarsson, Einar Jónsson, Gunnar Jónsson, Ólafur K. Pálsson, Sigfús A. Schopka:** Stofnmæling botnfiska á Íslandsmiðum 1991. Rannsóknaskýrsla. Reykjavík 1991. 60 s.
29. Nytjastofnar sjávar og umhverfisþættir 1992. Aflahorfur fiskveiðiárið 1992/93. *State of Marine Stocks and Environmental Conditions in Icelandic Waters 1992. Prospects for the Quota Year 1992/93*. Reykjavík 1992. 147 s. (Ófáanlegt - *Out of print*).

30. **Van Aken, Hendrik, Jóhannes Briem, Erik Buch, Stefán S. Kristmannsson, Svend-Aage Malmberg, Sven Ober:** *Western Iceland Sea. GSP Moored Current Meter Data Greenland - Jan Mayen and Denmark Strait September 1988 - September 1989*. Reykjavík 1992. 177 s.

31. **Björn Æ. Steinarsson, Einar Jónsson, Gunnar Jónsson, Gunnar Stefánsson, Ólafur K. Pálsson, Sigfús A. Schopka:** Stofnmæling botnfiska á Íslandsmiðum 1992. Reykjavík 1993. 71 s. (Ófáanlegt - *Out of print*).

32. **Guðrún Marteinsdóttir, Gunnar Jónsson, Ólafur V. Einarsson:** Útbreiðsla grálúðu við Vestur- og Norðvestur-land 1992. Reykjavík 1993. 42 s. (Ófáanlegt - *Out of print*).

33. **Ingvar Hallgrímsson:** Rækjuleit á djúpslóð við Ísland. Reykjavík 1993. 63 s.

34. Nytjastofnar sjávar 1992/93. Aflahorfur fiskveiðiárið 1993/94. *State of Marine Stocks in Icelandic Waters 1992/93. Prospects for the Quota Year 1993/94*. Reykjavík 1993. 140 s.

35. **Ólafur K. Pálsson, Björn Æ. Steinarsson, Einar Jónsson, Gunnar Jónsson, Gunnar Stefánsson, Sigfús A. Schopka:** Stofnmæling botnfiska á Íslandsmiðum 1993. Reykjavík 1994. 89 s.

36. **Jónbjörn Pálsson, Guðrún Marteinsdóttir, Gunnar Jónsson:** Könnun á útbreiðslu grálúðu fyrir Austfjörðum 1993. Reykjavík 1994. 37 s.

37. Nytjastofnar sjávar 1993/94. Aflahorfur fiskveiðiárið 1994/95. *State of Marine Stocks in Icelandic Waters 1993/94. Prospects for the Quota Year 1994/95*. Reykjavík 1994. 150 s.

38. **Stefán S. Kristmannsson, Svend-Aage Malmberg, Jóhannes Briem, Erik Buch:** *Western Iceland Sea - Greenland Sea Project - CTD Data Report. Joint Danish Icelandic Cruise R/V Bjarni Sæmundsson, September 1990*. Reykjavík 1994. 99 s.

39. **Stefán S. Kristmannsson, Svend-Aage Malmberg, Jóhannes Briem, Erik Buch:** *Western Iceland Sea - Greenland Sea Project - CTD Data Report. Joint Danish Icelandic Cruise R/V Bjarni Sæmundsson, September 1991*. Reykjavík 1994. 94 s.

40. Þættir úr vistfræði sjávar 1994. Reykjavík 1994. 50 s.

41. **John Mortensen, Jóhannes Briem, Erik Buch, Svend-Aage Malmberg:** *Western Iceland Sea - Greenland Sea Project - Moored Current Meter Data Greenland - Jan Mayen, Denmark Strait and Kolbeinsey Ridge September 1990 to September 1991*. Reykjavík 1995. 73 s.

42. **Einar Jónsson, Björn Æ. Steinarsson, Gunnar Jónsson, Gunnar Stefánsson, Ólafur K. Pálsson, Sigfús A. Schopka:** Stofnmæling botnfiska á Íslandsmiðum 1994. - Rannsóknaskýrsla. Reykjavík 1995. 107 s.

43. Nytjastofnar sjávar 1994/95. Aflahorfur fiskveiðiárið 1995/96. *State of Marine Stocks in Icelandic Waters 1994/95 - Prospects for the Quota Year 1995/96*. Reykjavík 1995. 163 s.

44. Þættir úr vistfræði sjávar 1995. *Environmental Conditions in Icelandic Waters 1995*. Reykjavík 1995. 34 s.

45. **Sigfús A. Schopka, Björn Æ. Steinarsson, Einar Jónsson, Gunnar Jónsson, Gunnar Stefánsson, Höskuldur Björnsson, Ólafur K. Pálsson:** Stofnmæling botnfiska á Íslandsmiðum 1995. Rannsóknaskýrsla. *Icelandic Groundfish Survey 1995. Survey Report*. Reykjavík 1996. 46 s.

46. Nytjastofnar sjávar 1995/96. Aflahorfur fiskveiðiárið 1996/97. *State of Marine Stocks in Icelandic Waters 1995/96. Prospects for the Quota Year 1996/97*. Reykjavík 1996. 175 s.

47. **Björn Æ. Steinarsson, Gunnar Jónsson, Hörður Andrésson, Jónbjörn Pálsson:** Könnun á flatfiski í Faxaflóa með dragnót sumarið 1995 - Rannsóknaskýrsla. *Flatfish Survey in Faxaflói with Danish Seine in Summer 1995 - Survey Report*. Reykjavík 1996. 38 s.

48. **Steingrímur Jónsson:** *Ecology of Eyjafjörður Project. Physical Parameters Measured in Eyjafjörður in the Period April 1992 - August 1993*. Reykjavík 1996. 144 s.

49. **Guðni Þorsteinsson:** Tilraunir með þorskgildrur við Ísland. Rannsóknaskýrsla. Reykjavík 1996. 28 s.

50. **Jón Ólafsson, Magnús Danielsen, Sólveig Ólafsdóttir, Þórarinn Arnarson:** Næringarefni í sjó undan Ánanaustum í nóvember 1995. Unnið fyrir Gatnamálastjórann í Reykjavík. Reykjavík 1996. 50 s.

51. **Þórunn Þórðardóttir, Agnes Eydal:** *Phytoplankton at the Ocean Quahog Harvesting Areas Off the Southwest Coast of Iceland 1994*. Svifþörungar á kúfiskmiðum út af norðvesturströnd Íslands 1994. Reykjavík 1996. 28 s.

52. **Gunnar Jónsson, Björn Æ. Steinarsson, Einar Jónsson, Gunnar Stefánsson, Höskuldur Björnsson, Ólafur K. Pálsson, Sigfús A. Schopka:** Stofnmæling botnfiska á Íslandsmiðum 1996. Rannsóknaskýrsla. *Icelandic Groundfish Survey 1996. Survey Report*. Reykjavík 1997. 46 s.

53. Þættir úr vistfræði sjávar 1996. *Environmental Conditions in Icelandic Waters 1996*. Reykjavík 1997. 29 s.

54. **Vilhjálmur Þorsteinsson, Ásta Guðmundsdóttir, Guðrún Marteinsdóttir, Guðni Þorsteinsson og Ólafur K. Pálsson:** Stofnmæling hrygningarþorsks með þorskanetum 1996. *Gill-net Survey to Establish Indices of Abundance for the Spawning Stock of Icelandic Cod in 1996*. Reykjavík 1997. 22 s.

55. Hafrannsóknastofnunin: Rannsókna- og starfsáætlun árin 1997-2001. Reykjavík 1997. 59 s. (Ófáanlegt - *Out of print*).

56. Nytjastofnar sjávar 1996/97. Aflahorfur fiskveiðiárið 1997/98. *State of Marine Stocks in Icelandic Waters 1996/97. Prospects for the Quota Year 1997/98*. Reykjavík 1997. 167 s.

57. Fjölstofnarannsóknir 1992-1995. Reykjavík 1997. 410 s.

58. **Gunnar Stefánsson, Ólafur K. Pálsson** (*editors*): *BORMICON. A Boreal Migration and Consumption Model*. Reykjavík 1997. 223 s. (Ófáanlegt - *Out of print*).

59. **Halldór Narfi Stefánsson, Hersir Sigurgeirsson**, **Höskuldur Björnsson:** *BORMICON. User's Manual*. Reykjavík 1997. 61 s. (Ófáanlegt - *Out of print*).

60. **Halldór Narfi Stefánsson, Hersir Sigurgeirsson, Höskuldur Björnsson:** *BORMICON. Programmer's Manual. Reykjavík 1997*. 215 s. (Ófáanlegt - *Out of print*).

61. **Þorsteinn Sigurðsson, Einar Hjörleifsson, Höskuldur Björnsson, Ólafur Karvel Pálsson**: Stofnmæling botnfiska á Íslandsmiðum haustið 1996. Reykjavík 1997. 34 s.

62. **Guðrún Helgadóttir:** *Paleoclimate (0 to >14 ka) of W and NW Iceland: An Iceland/USA Contribution to P.A.L.E. Cruise Report B9-97, R/V Bjarni Sæmundsson RE 30, 17th-30th July 1997*. Reykjavík 1997. 29 s.

63. **Halldóra Skarphéðinsdóttir, Karl Gunnarsson:** Lífríki sjávar í Breiðafirði: Yfirlit rannsókna. *A review of literature on marine biology in Breiðafjörður*. Reykjavík 1997. 57 s.

64. **Valdimar Ingi Gunnarsson og Anette Jarl Jörgensen:** Þorskrannsóknir við Ísland með tilliti til hafbeitar. Reykjavík 1998. 55 s.

65. **Jakob Magnússon, Vilhelmína Vilhelmsdóttir, Klara B. Jakobsdóttir:** Djúpslóð á Reykjaneshrygg: Könnunarleiðangrar 1993 og 1997. *Deep Water Area of the Reykjanes Ridge: Research Surveys in 1993 and 1997*. Reykjavík 1998. 50 s.

66. **Vilhjálmur Þorsteinsson, Ásta Guðmundsdóttir, Guðrún Marteinsdóttir:** Stofnmæling hrygningarþorsks með þorskanetum 1997. *Gill-net Survey of Spawning Cod in Icelandic Waters in 1997. Survey Report*. Reykjavík 1998. 19 s.

67. Nytjastofnar sjávar 1997/98. Aflahorfur fiskveiðiárið 1998/99. *State of Marine Stocks in Icelandic Waters 1997/98. Prospects for the Quota year 1998/99*. Reykjavík 1998. 168 s.

68. **Einar Jónsson, Hafsteinn Guðfinnsson:** Ýsurannsóknir á grunnslóð fyrir Suðurlandi 1989-1995. Reykjavík 1998. 75 s.

69. **Jónbjörn Pálsson, Björn Æ. Steinarsson, Einar Hjörleifsson, Gunnar Jónsson, Hörður Andrésson, Kristján Kristinsson:** Könnum á flatfiski í Faxaflóa með dragnót sumrin 1996 og 1997 - Rannsóknaskýrsla. *Flatfish Survey in Faxaflói with Danish Seine in Summers 1996 and 1997 - Survey Report*. Reykjavík 1998. 38 s.

70. **Kristinn Guðmundsson, Agnes Eydal:** Svifþörungar sem geta valdið skelfiskeitrun. Niðurstöður tegundagreininga og umhverfisathugana. *Phytoplankton, a Potential Risk for Shellfish Poisoning. Species Identification and Environmental Conditions*. Reykjavík 1998. 33 s.

71. **Ásta Guðmundsdóttir, Vilhjálmur Þorsteinsson, Guðrún Marteinsdóttir:** Stofnmæling hrygningarþorsks með þorskanetum 1998. *Gill-net survey of spawning cod in Icelandic waters in 1998*. Reykjavík 1998. 19 s.

72. Nytjastofnar sjávar 1998/1999. Aflahorfur fiskveiðiárið 1999/2000. *State of Marine Stocks in Icelandic Waters 1998/1999. Prospects for the Quota year 1999/2000. Reykjavík 1999*. 172 s. (Ófáanlegt - *Out of print*.)

73. Þættir úr vistfræði sjávar 1997 og 1998. *Environmental Conditions in Icelandic Waters 1997 and 1998*. Reykjavík 1999. 48 s.

74. **Matthías Oddgeirsson, Agnar Steinarsson og Björn Björnsson:** Mat á arðsemi sandhverfueldis á Íslandi. Grindavík 2000. 21 s.

75. Nytjastofnar sjávar 1999/2000. Aflahorfur fiskveiðiárið 2000/2001. *State of Marine Stocks in Icelandic Waters 1999/2000. Prospects for the Quota year 2000/2001. Reykjavík 2000*. 176 s.

76. **Jakob Magnússon, Jútta V. Magnússon, Klara B. Jakobsdóttir:** Djúpfiskarannsóknir. Framlag Íslands til rannsóknaverkefnisins EC FAIR PROJECT CT 95-0655 1996-1999. *Deep-Sea Fishes. Icelandic Contributions to the Deep Water Research Project. EC FAIR PROJECT CT 95-0655 1996-1999.* Reykjavík 2000. 164 s. (Ófáanlegt - *Out of print*).

77. Þættir úr vistfræði sjávar 1999. *Environmental Conditions in Icelandic Waters 1999.* Reykjavík 2000. 31 s.

78. *dst*^{2} *Development of Structurally Detailed Statistically Testable Models of Marine Populations. QLK5-CT1999-01609. Progress Report for 1 January to 31 December 2000*. Reykjavik 2001. 341 s. (Ófáanlegt. - *Out of print*).

79. *Tagging Methods for Stock Assessment and Research in Fisheries*. Co-ordinator: Vilhjálmur Þorsteinsson. Reykjavik 2001. 179 s.

80. Nytjastofnar sjávar 2000/2001. Aflahorfur fiskveiðiárið 2001/2002. *State of Marine Stocks in Icelandic Waters 2000/2001. Prospects for the Quota year 2001/2002.* Reykjavík 2001. 186 s.

81. **Jón Ólafsson, Sólveig R. Ólafsdóttir**: Ástand sjávar á losunarsvæði skolps undan Ánanaustum í febrúar 2000. Reykjavík 2001. 49 s.

82. **Hafsteinn G. Guðfinnsson, Karl Gunnarsson:** Sjór og sjávarnytjar í Héraðsflóa. Reykjavík 2001. 20 s.

83. Þættir úr vistfræði sjávar 2000. *Environmental Conditions in Icelandic Waters 2000.* Reykjavík 2001. 37 s.

84. **Guðrún G. Þórarinsdóttir, Hafsteinn G. Guðfinnsson, Karl Gunnarsson:** Sjávarnytjar í Hvalfirði. Reykjavík 2001. 14 s.

85. Rannsóknir á straumum, umhverfisþáttum og lífríki sjávar í Reyðarfirði frá júlí til október 2000. *Current measurements, environmental factors and biology of Reyðarfjörður in the period late July to the beginning of October 2000.* Hafsteinn Guðfinnsson (verkefnisstjóri). Reykjavík 2001. 135 s.

86. **Jón Ólafsson, Magnús Danielsen, Sólveig R. Ólafsdóttir, Jóhannes Briem:** Ferskvatnsáhrif í sjó við Norðausturland að vorlagi. Reykjavík 2002. 42 s.

87. *dst*^{2} *Development of Structurally Detailed Statistically Testable Models of Marine Populations. QLK5-CT1999-01609. Progress Report for 1 January to 31 December 2001* Reykjavik 2002. 300 s.

88. Nytjastofnar sjávar 2001/2002. Aflahorfur fiskveiðiárið 2002/2003. *State of Marine Stocks in Icelandic Waters 2001/2002. Prospects for the Quota year 2002/2003. Reykjavík 2002*. 198 s.

89. **Kristinn Guðmundsson, Ástþór Gíslason, Jón Ólafsson, Konráð Þórisson, Rannveig Björnsdóttir, Sigmar A. Steingrímsson, Sólveig R. Ólafsdóttir, Öivind Kaasa:** *Ecology of Eyjafjörður project. Chemical and biological parameters measured in Eyjafjörður in the period April 1992-August 1993*. Reykjavík 2002. 129 s.

90. **Ólafur K. Pálsson, Guðmundur Karlsson, Ari Arason, Gísli R Gíslason, Guðmundur Jóhannesson, Sigurjón Aðalsteinsson:** Mælingar á brottkasti þorsks og ýsu árið 2001. Reykjavík 2002. 17 s.

91. **Jenný Brynjarsdóttir:** *Statistical Analysis of Cod Catch Data from Icelandic Groundfish Surveys. M.Sc. Thesis*. Reykjavík 2002. xvi, 81 s.

92. Umhverfisaðstæður, svifþörungar og kræklingur í Mjóafirði. Ritstjóri: Karl Gunnarsson. Reykjavík 2003. 81 s.

93. **Guðrún Marteinsdóttir** (o.fl.): *METACOD: The role of sub-stock structure in the maintenance of cod metapopulations.* METACOD: Stofngerð þorsks, hlutverk undirstofna í viðkomu þorskstofna við Ísland og Skotland. Reykjavík 2003. vii, 110 s.

94. **Ólafur K. Pálsson, Guðmundur Karlsson, Ari Arason, Gísli R. Gíslason, Guðmundur Jóhannesson og Sigurjón Aðalsteinsson**: Mælingar á brottkasti botnfiska 2002. Reykjavík 2003. 29 s.

95. **Kristján Kristinsson**: Lúða (*Hippoglossus hippoglossus*) við Ísland og hugmyndir um aðgerðir til verndunar hennar. Reykjavík 2003. 33 s.

96. Þættir úr vistfræði sjávar 2001 og 2002. *Environmental conditions in Icelandic water 2001 and 2002*. Reykjavík 2003. 37 s.

97. Nytjastofnar sjávar 2002/2003. Aflahorfur fiskveiðiárið 2003/2004. *State of Marine Stocks in Icelandic Waters 2002/2003. Prospects for the Quota year 2003/2004.* Reykjavík 2003. 186 s.

98. *dst*^{2} *Development of Structurally Detailed Statistically Testable Models of Marine Populations. QLK5-CT1999-01609. Progress Report for 1 January to 31 December 2002*. Reykjavik 2003. 346 s.

99. **Agnes Eydal**: Áhrif næringarefna á tegundasamsetningu og fjölda svifþörunga í Hvalfirði. Reykjavík 2003. 44 s.

100. **Valdimar Ingi Gunnarsson** (o.fl.): Þorskeldiskvóti: Yfirlit yfir föngun og áframeldi þorsks á árinu 2002. Reykjavík 2004. 26 s.

101. Þættir úr vistfræði sjávar 2003. *Environmental conditions in Icelandic waters 2003*. Reykjavík 2004. 43 s.

102. Nytjastofnar sjávar 2003/2004. Aflahorfur fiskveiðiárið 2004/2005. *State of Marine Stocks in Icelandic Waters 2003/2004. Prospects for the Quota Year 2004/2005.* Reykjavík 2004. 175 s.

103. **Ólafur K. Pálsson** o.fl.: Mælingar á brottkasti 2003 og Meðafli í kolmunnaveiðum 2003. Reykjavík 2004. 37 s.

104. **Ásta Guðmundsdóttir, Þorsteinn Sigurðsson**: Veiðar og útbreiðsla íslensku sumargotssíldarinnar að haust- og vetrarlagi 1978-2003. Reykjavík 2004. 42 s.

105. **Einar Jónsson, Hafsteinn Guðfinnsson**: Ýsa á grunnslóð fyrir Suðurlandi 1994-1998. Reykjavík 2004. 44 s.

106. **Kristinn Guðmundsson, Þórunn Þórðardóttir, Gunnar Pétursson**: Computation of daily primary production in Icelandic waters; a comparison of two different approaches. Reykjavík 2004. 23 s.

107. **Kristinn Guðmundsson og Kristín J. Valsdóttir:** Frumframleiðnimælingar á Hafrannsóknastofnuninni árin 1958-1999: Umfang, aðferðir og úrvinnsla. Reykjavík 2004. 56 s.

108. **John Mortensen**: *Satellite altimetry and circulation in the Denmark Strait and adjacent seas*. Reykjavík 2004. 84 s.